Thermomechanical response of laser processed nickel-titanium shape memory alloy

by

Matthew Daly

A thesis
presented to the University of Waterloo
in fulfillment of the
thesis requirement for the degree of
Master of Applied Science
in
Mechanical Engineering

Waterloo, Ontario, Canada, 2012

Declaration

I hereby declare that I am the sole author of this thesis. This is a true copy of the thesis, including any required final revisions, as accepted by my examiners.

I understand that my thesis may be made electronically available to the public.

Abstract

The exciting thermomechanical properties of nickel-titanium shape memory alloys have sparked significant research efforts seeking to exploit their exotic capabilities. Until recently, the performance capabilities of nickel-titanium devices have been inhibited by the retention of only one thermomechanical characteristic. However, laser processing technology promises to deliver enhanced material offerings which are capable of multiple functional responses. Presented in this thesis, is an investigation of the effects of laser processing on the thermomechanical behaviour of nickel-titanium shape memory alloys. In the context of this work, laser processing refers to removal of alloy constituents, as in the case of laser ablation, or alternatively, addition of elements through laser alloying.

The effects of laser ablation on the composition, crystallography and phase transformation temperatures of a nickel-titanium strip have been studied. Application of laser energy was shown to ablate nickel constituents, induce an austenite-martensite phase change and cause an increase in phase transformation onset temperatures, which correlated well with reported findings. Laser processing of a nickel-titanium wire was shown to locally embed an additional thermomechanical response which manifested as unique shape memory and pseudoelastic properties.

Localized alloying of ternary species via laser processing of nickel-titanium strip was investigated. Synthesis of a ternary shape memory intermetallic within the laser processing region was achieved through melting of copper foils. Results from thermoanalytical testing indicated that the ternary compound possessed a higher phase transformation temperature and reduced transformation hysteresis in comparison to the reference alloy. Indentation testing was used to demonstrate the augmented thermomechanical characteristics of the laser processed shape memory alloy.

In order to demonstrate the enhanced functionality of laser processed nickel-titanium shape memory alloys, a self-positioning nickel-titanium microgripper was fabricated. The microgripper was designed to actuate through four different positions, corresponding to activation of three embedded shape memory characteristics. Thermoanalytical and tensile testing instrumentations were used to characterize the thermomechanical performance of the laser processed nickel-titanium microgripper. Results indicated that each of the laser processed microgripper components possessed unique mechanical and shape memory recovery properties.

Acknowledgements

I would like to thank my supervisor, Dr. Y. Zhou, for his advice and support during my research. He gave me an exceptional amount of academic freedom to pursue my interests which helped keep me very motivated during the course of my study.

I would also like to extend my thanks to the members of the microwelding group: Ibraheem Khan, Andrew Pequegnat, Jeff Wang, and Yongde Huang, as well as the other students and faculty of the CAMJ. Through them I learned that only with the right combination of study and fun are we able to be successful. Also, I would like to thank Ali Nasiri for his comments and advice during the preparation of this thesis.

Lastly, I would like to deeply thank my family and friends for their love and support in what have been some of the most challenging times of my life. There would be no success without them.

To my family

Table of Contents

List of Figures

List of Tables

List of Equations

Nomenclature

ϵ Tensile strain [%]

ϵ_r Retained tensile strain after mechanical loading/unloading of a martensitic nickel-titanium specimen [%]

σ Tensile stress [MPa]

σ_m Stress required to induce a martensitic transformation [MPa]

σ_r Reverse martensitic transformation stress [MPa]

σ_s Slip stress [MPa]

σ_{Dt} Stress required to detwin martensite variants [MPa].

τ Shear stress [MPa]

Δx Distance between adjacent processing spots [μm]

d_s Laser spot diameter [μm]

A_f Austenite finish phase transformation temperature [°C]

A_s Austenite start phase transformation temperature [°C]

BM   Base metal

DSC   Differential scanning calorimetry

EDX   Energy dispersive X-ray

HAZ   Heat affected zone

IMC   Intermetallic compound

LPZ   Laser processed zone

M_d Temperature at which shape memory alloy slip stress and martensitic transformation stress are equal [°C]

M_f Martensite finish phase transformation temperature [°C]

M_s Martensite start phase transformation temperature [°C]

NiTi   Nickel-titanium

OL   Spot overlap [%]

PIXE   Particle induced X-ray emission

R_o Nominal resistance of the RTD at 0 °C [Ω]

R_t Resistance of the RTD as calculated by Ohm's law [Ω]

RTD   Resistance temperature detector

SEM   Scanning electron microscope

SIM   Stress induced martensite

SMA   Shape memory alloy

TEM   Transmission electron microscopy

XRD   X-ray diffraction

Chapter 1

Introduction

Shape memory alloys (SMA)s are a subset of smart materials which are distinguished by their intrinsic ability to produce useful work which is harnessed from the thermomechanical response of the material to external stimuli. Industrial demand for increasing miniaturization has generated a significant interest in SMAs with the hopes that these functional materials can be used to create elegant design solutions to service applications on the micro- and nanoscopic scales. To date, several SMA chemistries have been discovered; however, nickel-titanium (NiTi), also known by its trade name as Nitinol, has garnered the greatest attention owing to its comparatively superior mechanical properties and excellent biocompatibility [1, 2].

As a functional material, NiTi possesses an impressive work density which makes it ideal for many microsystems applications. Given their exciting functional properties, NiTi SMAs have emerged as a leading candidate for next-generation applications in the aerospace and biomedical industries [3, 4]. Prized for their comparatively low mass and packaging volume, NiTi based actuators, grippers, and valves are emerging to replace conventional electro-mechanical systems [5]. Furthermore, NiTi implants such as arterial stents and orthodontic wires are popular biomedical applications of NiTi SMAs [6–8].

1.1 Motivation

In order to develop and expand NiTi product offerings, significant efforts have been invested to create processing techniques that can control the functional properties of NiTi [9–14]. Given that the active properties of NiTi SMAs are extremely sensitive to alloy composition and material processing history [15–19], the manufacture of application-specific NiTi alloys remains an industrial challenge. Furthermore, material functionality and performance limitations that are inherent to traditional manufacturing techniques remain unresolved.

Recent studies have shown [20–23] that laser processing technology can be used to enhance the functionality of conventional NiTi SMAs. Whereas a NiTi SMA produced from bulk manufacturing methods possesses a single set of active functional properties,

1

investigations have shown that exposure to high density laser energy can be used to locally embed independent functional material characteristics within the processed region of the NiTi alloy [24–26]. The functional properties of the processed NiTi alloy are therefore augmented by the effects of laser energy. Laser processing of NiTi SMAs promises to deliver enhanced NiTi material offerings and lead to unprecedented and novel NiTi based microsystems devices.

1.2   Thesis objectives

Before laser processing can be implemented in industrial fabrication methods, a detailed investigation of the effects of laser energy on NiTi SMA functionality and performance is required. The objective of the current thesis is to understand the changes in the thermomechanical response of NiTi resulting from laser processing operations. More specifically, the presented thesis investigates:

1. The effects of laser processing on alloy composition, crystallography, and phase transformation dynamics

2. The correlation between phase transformation dynamics and thermomechanical response within the laser processing region

3. The application of laser processing technology to NiTi based device prototypes.

1.3   Physical metallurgy of NiTi SMAs

Since their discovery in 1959 by Buehler [27], NiTi SMAs have enjoyed a significant amount of research interest from investigators seeking to better understand and exploit their exotic functional properties. Referring to an equiatomic or near-equiatomic chemistry of Ni and Ti, NiTi SMAs are considered an organized intermetallic compound (IMC) [28]. At room temperature, there is no solubility of constituent species and the SMA exists as a stoichiometric IMC. Above 630 °C, however, solution of Ni species is possible; thus allowing for the synthesis of Ni-rich SMAs by rapid quenching. Figure 1.1 provides the phase diagram of the Ni-Ti system. Although there are many other stable IMCs in the Ni-Ti alloy system, currently only the NiTi IMC is known to possess SMA properties. Precipitation of other IMCs into a NiTi matrix, however, can be used to tailor and mediate the functional response of NiTi SMAs [29].

The functional properties of NiTi SMAs are the result of a thermomechanical response to a reversible solid-state phase transformation within the alloy [1, 31, 32]. In this phase transformation, a cubic B2 austenite phase undergoes a diffusionless martensitic reorientation into a monoclinc B19' type crystal structure. The lattice constant of the austenite phase is reported to be 0.3015 nm at room temperature [33]. The lattice parameters for the monoclinc unit cell are 0.2889, 0.4120 and 0.4622 nm (a, b and c lattice
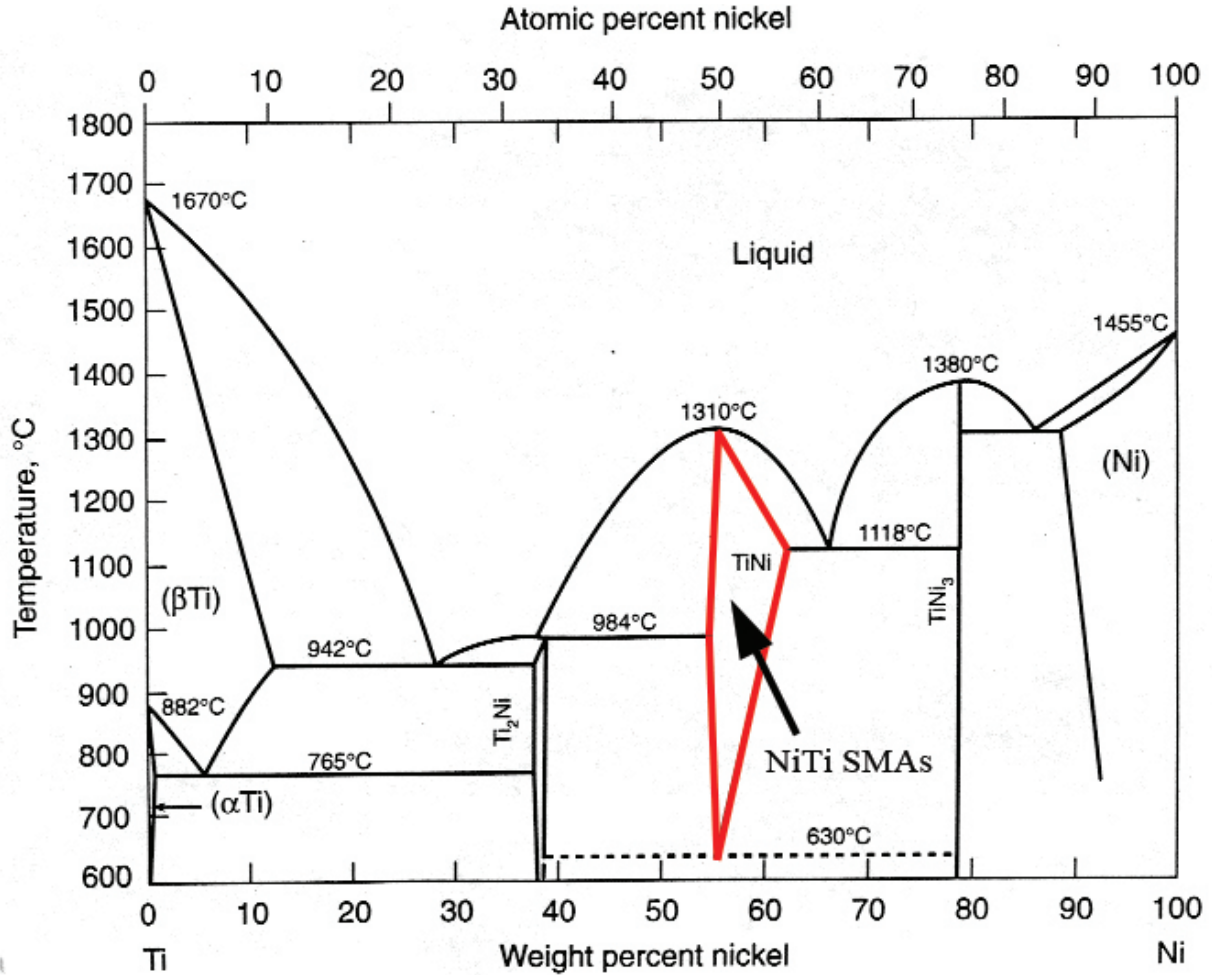
Figure 1.1: The nickel-titanium system with NiTi SMA chemistries indicated [30]. Figure reprinted with permission from ASM International.

vectors, respectively) with a monoclinic angle (β) of 96.8° [34]. Figure 1.2 provides the unit cell crystal structure of the austenite and martensite phases of NiTi. Under certain heat treatments, an intermediate trigonal structure known as R-phase can be induced in the austenite-martensite transformation pathway [35]. A detailed discussion of R-phase, however, is outside the scope of the current work and is not covered in great depth.

1.3.1 Reversible martensitic phase transformations and thermo-mechanical response

Martensitic transformations are common in many engineering materials such as metals, ceramics, and polymers. In martensitic transformations, the crystallographic lattice undergoes a shearing deformation, which can alter the volume and shape of the material on
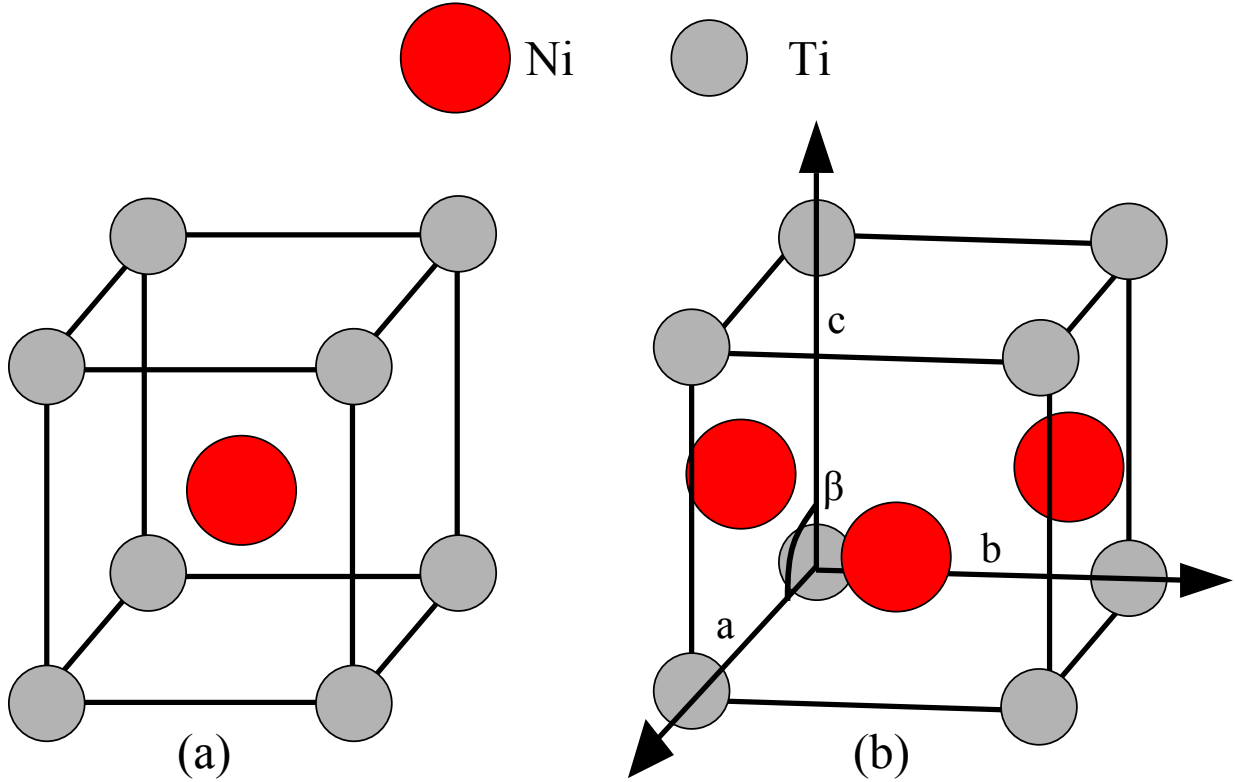
Figure 1.2: Unit cells of (a) B2 cubic austenite and (b) B19' monoclinic martensite phases in NiTi SMAs.

a macroscopic scale [36]. The manner of lattice shear can be irreversible or reversible. For example, in some metals, an irreversible martensitic transformation is accommodated by crystallographic slip within the microstructure of the alloy. In SMAs, however, reversible martensitic transformations are accommodated by twinning of the underlying microstructure [1, 31, 32]. Figure 1.3 illustrates the difference between slip and twinned martensitic transformations.

Twinned martensitic transformations of SMAs are considered reversible because the microstructures of the austenite and martensite phases can be cyclically restored with almost no accumulation of lattice defects [36, 37]. Furthermore, the twinned lattice can accommodate to an externally applied stress by undergoing a recoverable detwinning process. As shown in Figure 1.4, twinned martensite variants reorganize to accommodate a shear stress (τ) and grow along a stress-favourable orientation (detwinning) at the expense of the less-preferred variant [38, 39]. Detwinning of martensite in NiTi SMAs can be identified from an apparent low-strain yielding of the material under mechanical loading. Figure 1.5 illustrates the tensile behaviour of a typical NiTi SMA undergoing detwinning. Upon initial loading, martensitic NiTi exhibits a typical elastic response (path segment A to B in Figure 1.5). Further loading initiates lattice detwinning, which manifests as a plateau in the stress-strain curve (B to C). After the martensite lattice is completely detwinned (identified by an inflection in the tensile response), elastic deformation of the detwinned martensite begins (C to D). Unloading of the detwinned martensite progresses

Austenite

Martensitic
Transformation

Accommodation by slip   Accommodation by twinning
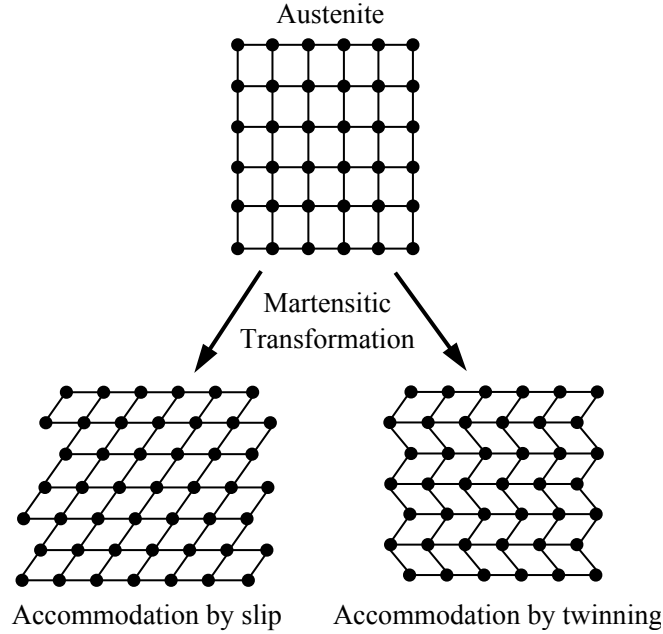
Figure 1.3: Stress accommodation of martensitic transformations. Schematic adapted from [1].

in an elastic manner (D to E). Although the mechanical strain retained after unloading appears to be plastic (ϵ_r), this strain can be recovered because of the reversible nature of martensitic transformations in NiTi SMAs. Tensile loading past the elastic limit of detwinned martensite, however, results in plastic deformation which is not recoverable.

The accommodation of martensitic variants to external stress allows for an intrinsic energy storage mechanism which can be released through an austenite-martensite phase transformation. The behaviour of SMAs such as NiTi undergoing an austenite-martensite transformation manifests itself as a thermomechanical response, which can be harnessed as useful work. The ability of SMAs such as NiTi to form a twinned martensitic structure is therefore critical to material functionality and is the distinguishing characteristic of this family of smart materials.

τ τ

τ τ

(a)   (b)   (c)
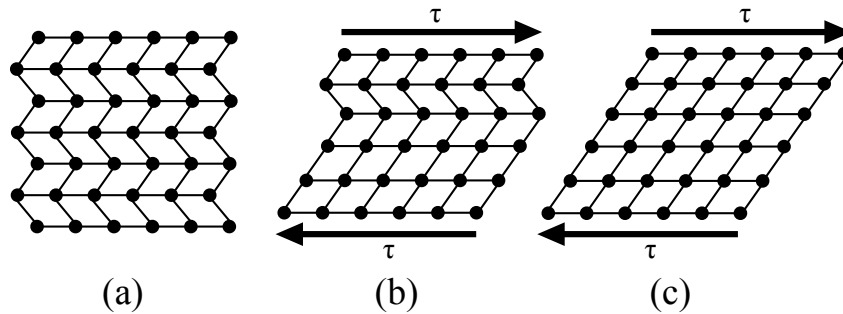
Figure 1.4: Stress accommodation in twinned martensite variants: stress-free twinned martensite (a); stress accommodation and partial detwinning (b); and complete detwinning (c).
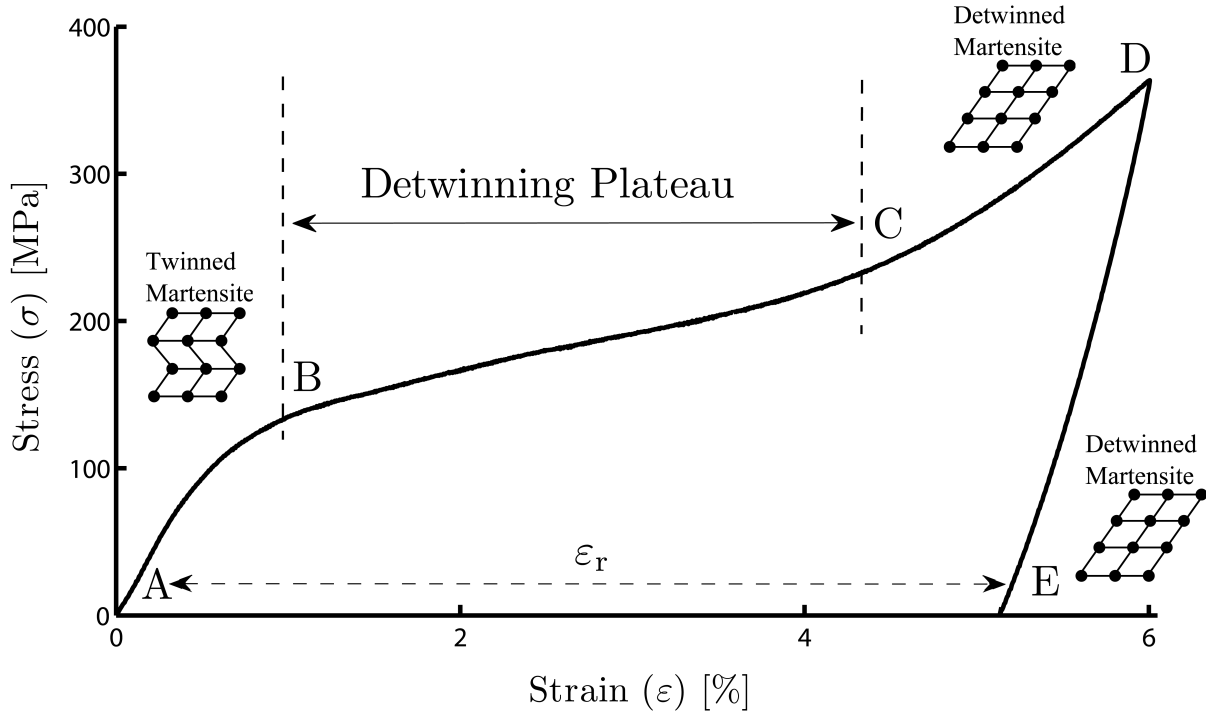
Figure 1.5: Tensile response of a typical martensitic NiTi SMA undergoing detwinning via stress accommodation. See text for description of loading path segments.

The thermomechanical response of NiTi SMAs is commonly categorized into two functional characteristics which are created by the austenite-martensite phase transformation. This reversible martensitic phase transformation can be induced thermally or via an applied stress. SMA response to a thermally induced phase transformation is known as the shape memory effect and the reaction to a stress induced transformation is classified as pseudoelasticity [1, 31, 32]. Although the term thermomechanical technically refers to both the thermally and stress induced functional properties, it is used in this work interchangeably. Context therefore infers correct interpretation of the term to refer to either the shape memory effect or pseudoelasticity.

1.3.2 Thermally induced transformations and the shape memory effect

In the case of a thermally induced martensitic phase transformations, material response is typically identified using thermoanalytical techniques such as differential scanning calorimetry (DSC) and is characterized by four temperatures: martensite start (M_s), martensite finish (M_f), austenite start (A_s) and austenite finish (A_f), according to the ASTM F2004–05 standard. A typical DSC response of a solutionized NiTi SMA is provided in Figure 1.6. As illustrated in the provided figure, the transformation onset and finish temperatures are defined as the intersection of peak and baseline heat flow tangents.
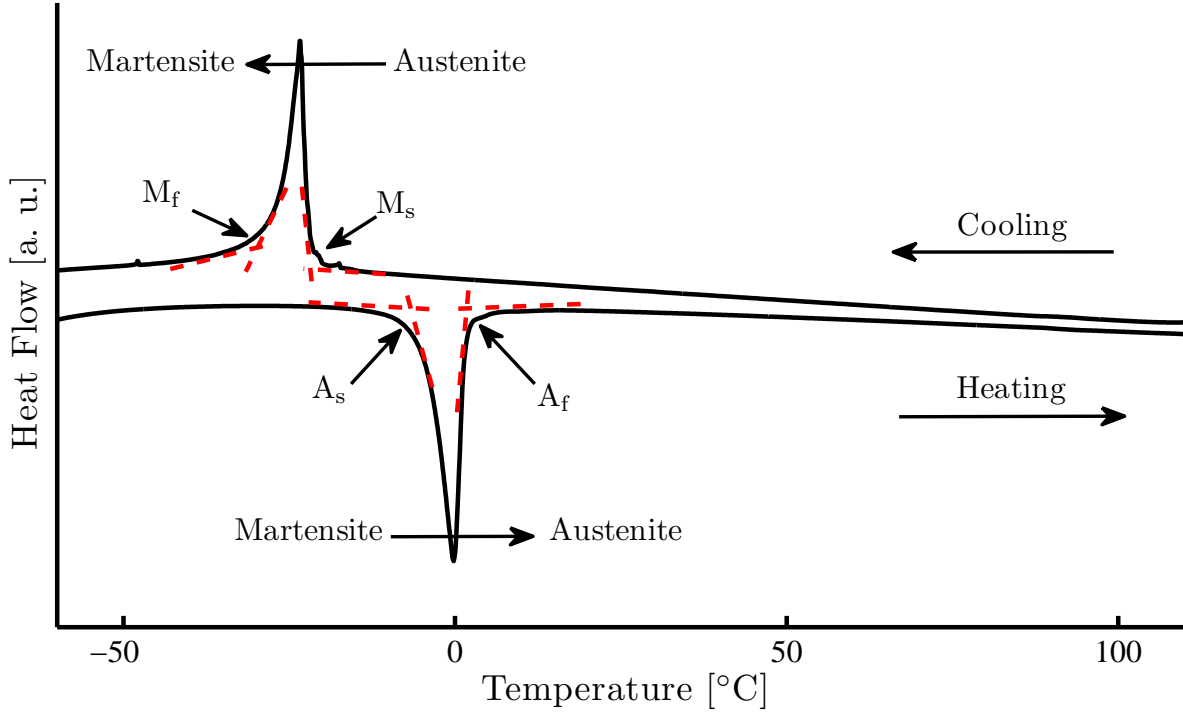
Figure 1.6: DSC scan of a solution treated NiTi SMA. Austenite-martensite phase transformations are characterized by peaks in the heat flow traces. A thermal hysteresis of 30 °C between endothermic and exothermic phase transformations is typical in NiTi SMAs.

In NiTi, a transformation hysteresis of up to 50 °C [1] is known to exist and is the result from interfacial friction and defects within the lattice. The magnitude of hysteresis is closely related to the composition, processing history, and stress-state of the specific NiTi SMA [40].

The shape memory effect is an intrinsic property of SMAs and it refers to the ability of a material to remember a specific geometry which can be recovered even after apparent plastic deformation of the alloy (ϵ_r, in Figure 1.5). In a process known as shape training, SMAs such as NiTi are programmed with a specific geometry through a constrained heat treatment protocol. A schematic of the shape memory effect is provided in Figure 1.7. Upon cooling the austenite NiTi structure below M_f (path segment A to B in Figure 1.7b), plastic strain energy can be stored through the stress-accommodation and detwinning of martensite variants in the alloy microstructure [41] (B to C). Subsequent heating of NiTi to above A_f releases the stored plastic strain and recovers the programmed geometry (C to A). Thus, a cyclic recovery of stored strain energy is possible. In NiTi SMAs, strains as high as 10% can be recovered in single crystals through the shape memory effect, however, typical polycrystal NiTi SMAs operate well under this threshold to avoid the accumulation of damage in the microstructure [42]. Under normal conditions, SMAs such as NiTi exhibit a one-way shape memory effect, where a restorative shape change can only be achieved by heating a deformed alloy above A_f. However, with NiTi SMAs a number of thermomechanical processing regimens exist whereby a reversible or two-way

shape memory recovery is possible [9, 43–45]. In each of these processes, lattice defects are introduced along specific crystallographic planes in order to favour a specific martensitic variant. The effect of preferred variant selection manifests macroscopically as a shape change. Thermal cycling between M_f and A_f temperatures therefore permits the recovery of two programmed shapes. SMAs conditioned with two-way shape memory, however, only exhibit approximately 2% recoverable strain due to stress fields associated with lattice defects [45]. A comparison of the one-way and two-way shape memory effects are provided in Figure 1.8. While the one-way memory effect requires a deformation mechanism (path segments B to C in Figure 1.8a) in its operational cycle, the two-way memory effect can be activated solely through thermal cycling (path segments A to B in Figure 1.8b).

While the two-way shape memory effect expands the number of viable applications for NiTi SMAs, there are significant design challenges associated with its implementation. Given that the deployment of a two-way SMA relies heavily on the texture of the microstructure and orientation of lattice defects, it is extremely difficult to synthesize SMA devices with reliable and predictable performance dynamics. The majority of NiTi applications therefore implement the one-way shape memory effect with an external biasing mechanism [5]. Under this arrangement, elastic deformation of a biasing device is achieved during shape memory actuation. Upon cooling of the SMA below M_f, the stored elastic energy is used to detwin the microstructure of the SMA; thus allowing for cyclic operation. This strategy is often advantageous compared to the two-way shape memory effect because it allows for conventional materials, which require less demanding processing constraints, to be implemented in the design.

1.3.3 Stress induced transformations and pseudoelasticity

In addition to thermally induced transformations, NiTi SMAs can be conditioned to undergo stress induced austenite-martensite phase transformations at temperatures above A_f. In order to form stress induced martensite (SIM), the NiTi SMA must be strengthened such that the slip stress (σ_s) exceeds the stress required to form SIM (σ_m). Typical strain hardening protocols involve cold work on the order of 25% [18] as well as a heat treatment designed to precipitation harden the NiTi lattice with the matrix coherent Ti_3Ni_4 IMC [46].

Stress induced transformations in NiTi can be identified using tensile testing methods. While the mechanical response of solutionized NiTi exhibits normal elastic-plastic behaviour, as shown in Figure 1.9, under a stress induced martensitic transformation the tensile response of NiTi displays unique mechanical properties. The serrated appearance of the stress strain curve presented is typical for NiTi SMAs and is caused by the nucleation of SIM along shear bands which propagate across the loaded specimen [47–50]. Upon initial loading, the NiTi SMA exhibits a typical linear-elastic tensile response (path segment A to B in Figure 1.9b). Initiation of the stress induced transformation begins when loading of the heat treated NiTi specimen reaches σ_m, which represents the energy threshold at which the cubic austenite lattice shears into a detwinned martensite structure. Once σ_m is reached, the transformation progresses and SIM grows at an isostress condition in a phenomenon known as pseudoelasticity (B to C). As with thermally induced transformations,
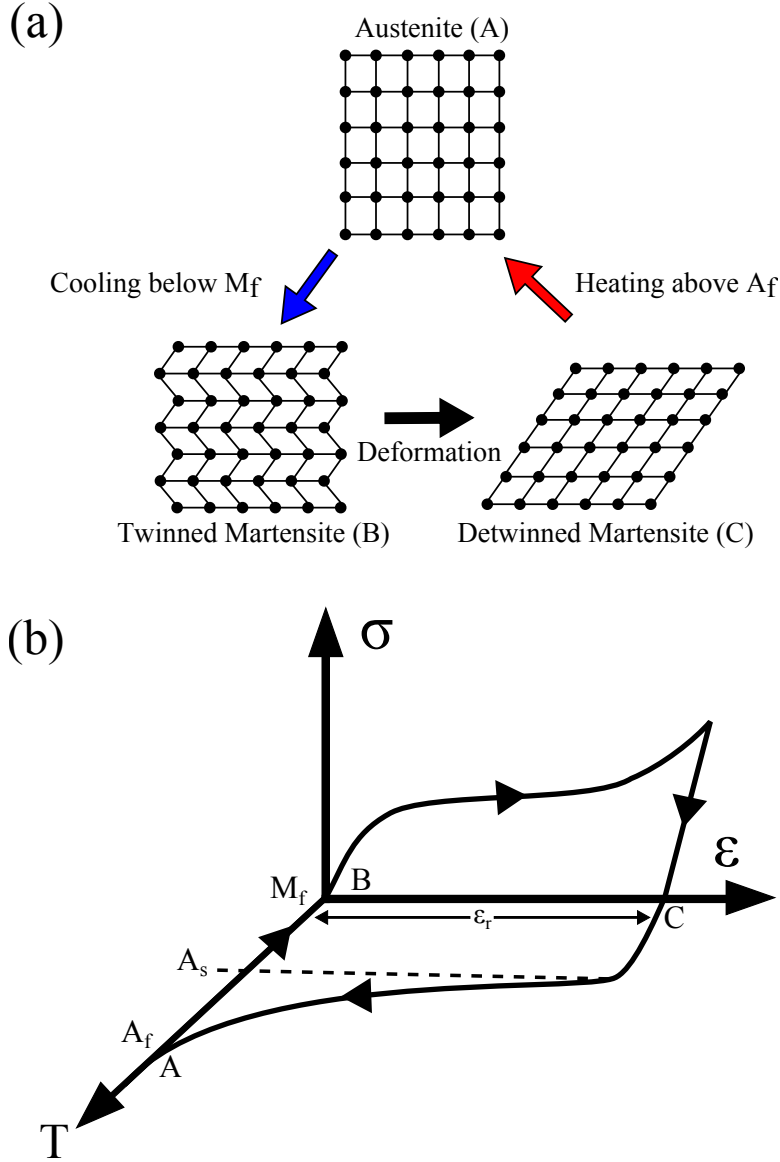
Figure 1.7: Schematic representation of the shape memory effect: NiTi SMA crystallographic response to external heating/cooling and deformation (a); stress-strain-temperature space for loading/thermal protocol implementing the shape memory effect (b), adapted from [32]. See text for description of path segments.

SIM transformations are reversible which allows for the recovery of pseudoelastic strain. During unloading, the material recovers strain energy stored by the SIM (C to D). The reverse SIM transformation progresses at a lower stress plateau (σ_r), which is analogous to the hysteresis associated with thermally induced transformations. Depending on the texture of the pseudoelastic NiTi specimen, a perfect pseudoelastic response (ie. 100% recovery) may not be possible because of local yielding of unfavourably oriented grains in the microstructure [51]. Mechanical cycling above 20 cycles, however, can usually stabilize SIM variants and establish a perfect pseudoelastic response [32]. Typical pseudoelastic responses of NiTi SMAs approach 8% strain [52]. If mechanical loading is allowed to exceed

8% strain, plastic loading of the SIM can occur, resulting in permanent damage of the NiTi specimen.

As the temperature of NiTi rises above A_f, the thermodynamic stability of the austenite phase increases, which causes a corresponding increase in the stress needed to form SIM. The increase in σ_m is linear with temperature and is known to follow the Clausius-Clapeyron relation [19, 53]. Given the increase in thermodynamic stability of austenite with temperature, there exists a maximum temperature (M_d), whereby pseudoelasticity is no longer possible. At temperatures above M_d, the σ_m stress exceeds the σ_s of the specimen and therefore the specimen begins to fail before onset of pseudoelasticity. Figure 1.10 illustrates the stress-temperature space conditions for the shape memory effect and pseudoelasticity in NiTi.
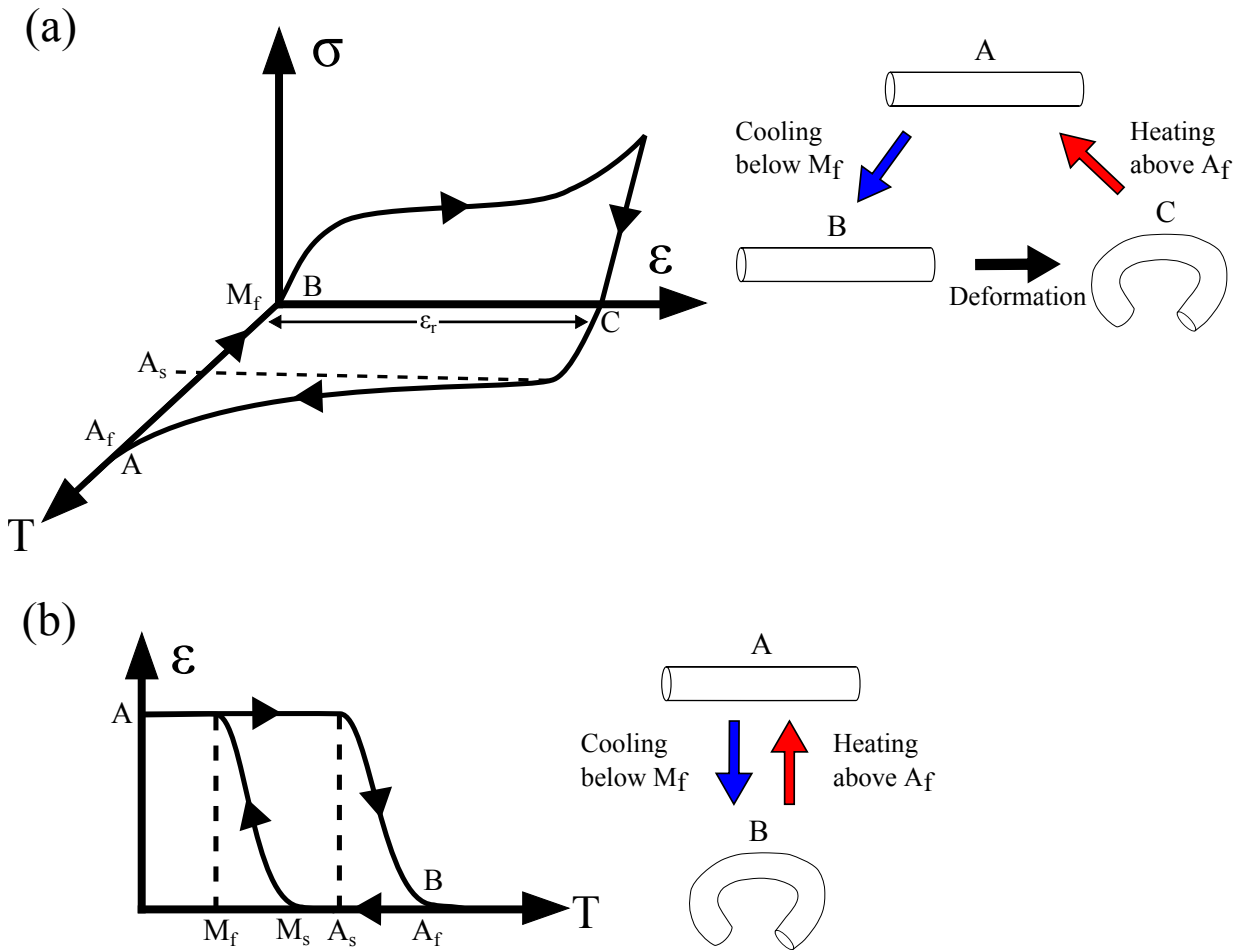
Figure 1.8: Illustration of the shape memory effect exhibiting a one-way response (a) and a two-way response (b). See text for description of path segments.
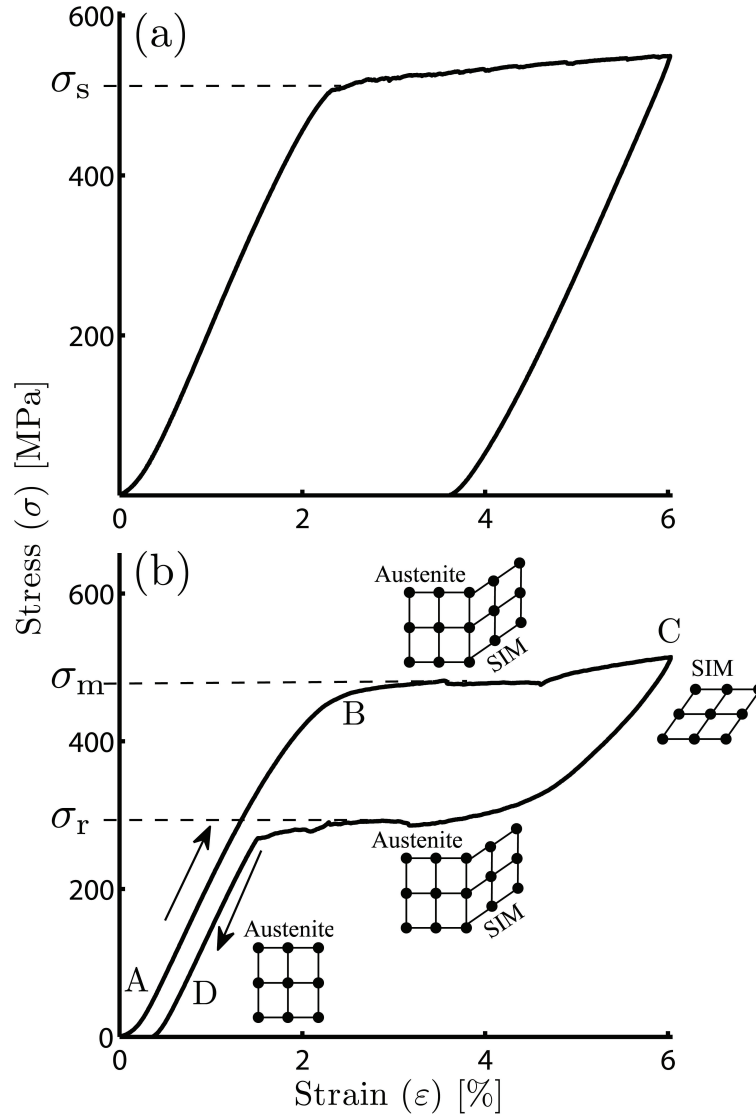
Figure 1.9: Tensile response of solutionized NiTi (a) and NiTi conditioned for pseudoelasticity (b). The solution treated NiTi ($\sigma_s < \sigma_m$) exhibits a typical elastic-plastic response whereas the pseudoelastic NiTi ($\sigma_m < \sigma_s$) forms SIM such that much of the seemingly plastic deformation is recovered upon unloading. See text for description of loading path segments.

1.3.4 Effects of composition and processing on the thermome-chanical behaviour of NiTi

The thermomechanical behaviour of NiTi is known to be very sensitive to both alloy composition and processing history. From the experimental data collected in Figure 1.11, studies show that the M_s temperature of NiTi can vary by over 100 K with a composition change of only 1 at.% [15]. At an equiatomic chemistry, the M_s temperature stabilizes at approximately 65 °C, since excess Ti cannot be held in solution as per the Ni-Ti phase
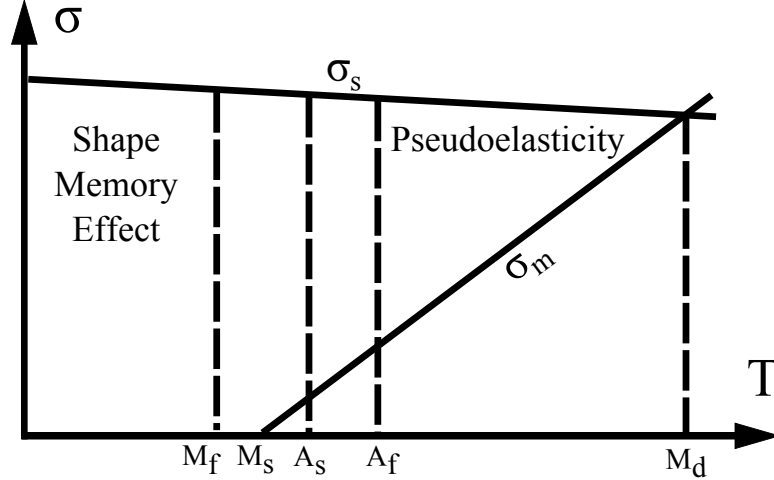
Figure 1.10: Stress-temperature space conditions for NiTi SMAs exhibiting the shape memory effect and pseudoelasticity. Schematic adapted from [54].

diagram (Figure 1.1). Small changes in NiTi SMA composition therefore drastically alter its phase transformation temperatures and subsequent shape memory recovery characteristics. In addition to changes in the shape memory effect, NiTi composition indirectly determines the σ_m required for SIM. NiTi alloys with a lower A_f possess a larger σ_m because of the comparatively higher thermodynamic stability of their austenite phases [19].

Although thermomechanical processing is critical to pseudoelastic training of NiTi SMAs, protocols must be carefully designed as strain hardening of the NiTi lattice causes drastic changes in phase transformation dynamics. The effects of strain hardening mechanisms can stabilize intermediate phases in NiTi and induce the R-phase reaction [35]. Furthermore, strain hardening also has a diffusing effect on phase transformation reactions, as shown in Figure 1.12. Identification of R-phase transformations in both the heating and cooling paths is not always possible due to overlapping heat flows with martensite or austenite phase transformations [55].

1.3.5   Ternary NiTiX SMAs

In terms of practical SMA applications, the wide hysteresis associated with the thermomechanical response of NiTi SMAs is problematic and necessitates the development of complex non-linear control schemes [56–59]. The addition of ternary species to the NiTi has been shown in several investigations to beneficially alter the thermomechanical properties [60–62]. For example, ternary NiTi based IMCs containing chromium, cobalt, manganese and iron have been shown to act as austenite stabilizers. NiTi SMAs alloyed with austenite stabilizers exhibit a much lower martensite start transformation temperature. On the other hand, ternary species containing hafnium, gold, zirconium or palladium serve as martensite stabilizers by significantly increasing austenite phase transformation onset temperatures. Perhaps the most useful of the ternary additives, copper has demonstrated an ability to narrow the thermal transformation hysteresis in NiTi; thereby facilitating a more robust
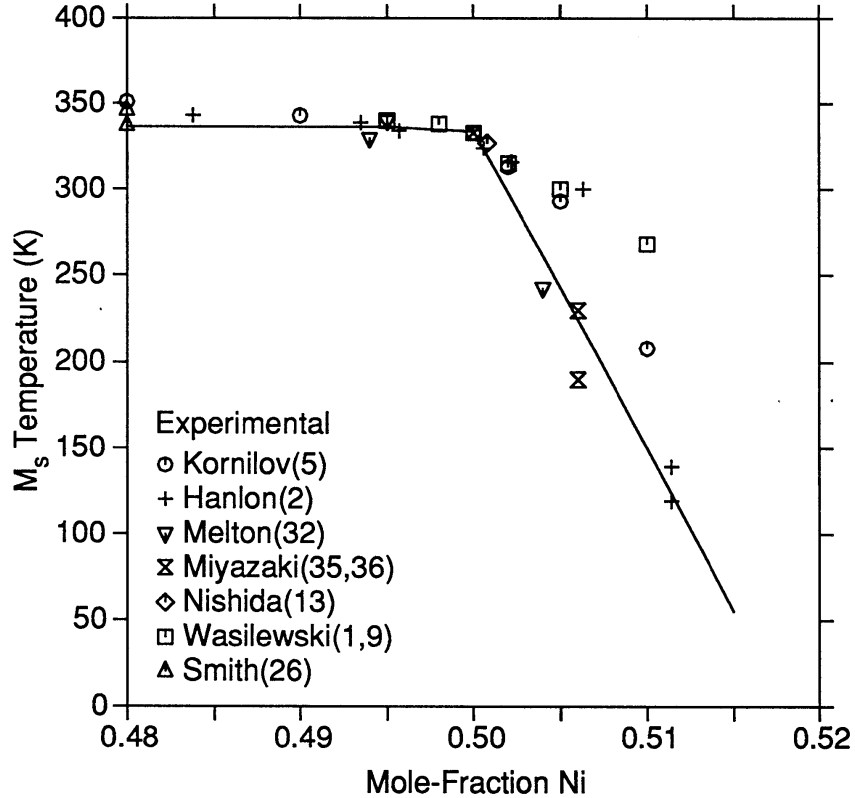
Figure 1.11: Theoretical (solid line) and experimental (markers) comparison of M_s temperatures in relation to NiTi SMA chemistry [15]. Figure reprinted with permission of Springer.

functionality in NiTi alloy offerings [63, 64]. The synthesis of ternary NiTi SMAs is common in industrial applications where a tailored thermomechanical response is required.

1.4   Thesis organization

The present work studies the effects of laser processing on the thermomechanical response of NiTi SMAs. Chapter two provides a detailed review of the existing literature pertaining to current NiTi SMA fabrication technologies and their limitations, advances in laser processing of NiTi, and existing NiTi based devices. The remainder of this thesis is separated into three studies. An investigation of the effects of laser ablation on the thermomechanical response of two NiTi SMAs is presented in Chapter three. The metallurgy and thermomechanical responses of laser processed the NiTi SMAs are examined using electron microscopy, thermoanalytical and tensile instrumentations. Chapter four examines the changes in thermomechanical behaviour associated with the addition of copper to an conventional NiTi SMA via laser processing. Thermoanalytical and indentation testing as well as surface profilometry are used to qualify and compare thermomechanical properties. Practical applications of laser processing technology are provided in chapter five, where the enhanced thermomechanical responses and deployment characteristics of a
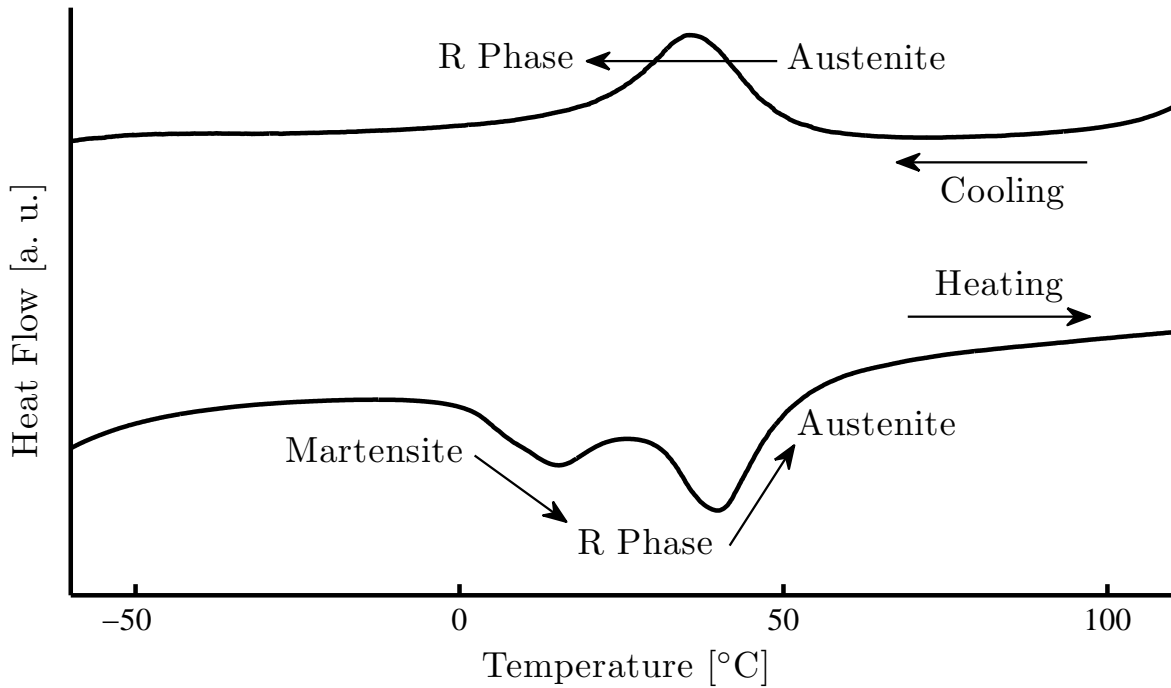
Figure 1.12: DSC scan of a NiTi sample exhibiting the intermediate R-phase transformation after thermomechanical processing. Detection of a distinct martensite to R-phase transformation is not always possible with DSC testing.

laser processed NiTi device is showcased. Finally, chapter six provides concluding remarks and recommended future work.

1.5 Contributions

1.5.1 Journal publications

1. **Daly, M.**, Pequegnat, A., Zhou, Y. and Khan, M.I. (2012) "Enhanced thermomechanical functionality of a laser processed NiTi shape memory alloy", (In preparation, Chapter 3)

2. **Daly, M.**, Pequegnat, A., Zhou, Y. and Khan, M.I. (2012) "Enhanced thermomechanical functionality of a laser processed hybrid NiTi-NiTiCu shape memory alloy", Smart Materials and Structures. Submission Number: SMS/414239/PAP (In Press, Chapter 4)

3. **Daly, M.**, Pequegnat, A., Zhou, Y. and Khan, M.I. (2012) "Fabrication of a novel laser processed NiTi shape memory microgripper with enhanced thermomechanical functionality", Special Issue: Journal of Intelligent Material Systems and Structures. **Invited paper**. Submission Number: JIM-11-347 (In Press, Chapter 5)

4. Pequegnat, A., **Daly, M.**, Wang, J., Khan, M.I. and Zhou, Y. (2012) "Dynamic actuation of a novel laser processed NiTi linear actuator", Special Issue: Smart Materials and Structures. **Invited paper**. Submission Number: SMS/418887/SPE (Under Review)

1.5.2   Refereed conference proceedings

1. **Daly, M.**, Pequegnat, A., Khan, M.I., Zhou, Y. (2011) "Fabrication of a novel monolithic NiTi based shape memory microgripper via Multiple Memory Material processing", Proceedings of the ASME 2011 Conference on Smart Materials, Adaptive Structures and Intelligent Systems (SMASIS), Scottsdale, AZ, USA, September 18 - 21, 2011.[1]

2. Pequegnat, A., Vlascov, M., **Daly, M.**, Khan, M.I., Zhou, Y. (2011) "Dynamic actuation of a Multiple Memory Material processed Nitinol linear actuator", Proceedings of the ASME 2011 Conference on Smart Materials, Adaptive Structures and Intelligent Systems (SMASIS), Scottsdale, AZ, USA, September 18 - 21, 2011.

3. **Daly, M.**, Salehian, A., Doosthoseini, A. (2010) "Thermal robustness assessment of a rigidized space inflatable boom via experimental modal analysis and finite element modeling", Proceedings of the ASME 2010 Conference on Smart Materials, Adaptive Structures and Intelligent Systems (SMASIS), Philadelphia, USA, September 28 - October 1, 2010. doi:10.1115/SMASIS2010-3677

4. Doosthoseini, A., Salehian, A., **Daly, M.** (2010) "Analysis of wrinkled membranes bounded with Macro-fiber Composite (MFC) actuators", Proceedings of the ASME 2010 Conference on Smart Materials, Adaptive Structures and Intelligent Systems (SMASIS), Philadelphia, USA, September 28 - October 1, 2010. doi:10.1115/SMASIS2010-3782

1.5.3   Non-refereed publications

1. **Daly, M.**, Salehian, A. (2010) "Inflatable space structures: The future of satellite design", ME Today, Volume 11, American Society of Mechanical Engineers.

---

[1]Selected as the winner of the **Best Student Paper Award**

Chapter 2

Fabrication of NiTi SMAs

Given modern trends towards miniaturization and lean-design philosophies, there is a strong desire within industry to exploit the exotic functional properties of NiTi SMAs in order to develop novel and innovative device offerings. Since the thermomechanical response of NiTi is extremely sensitive to alloy processing history, it is very difficult to produce application-specific NiTi SMAs using traditional bulk manufacturing techniques. Russell provides an excellent review of current ingot casting and rolling technologies implemented in NiTi SMA manufacture [65]. Although many NiTi alloy formats (ie. sheet, wire, tube, ribbon) are available using conventional manufacturing methods, Russell notes that their functional property offerings are generally limited to very few formulations. In a similar study, Wu reports the tight compositional tolerances required to control the phase transformation temperatures of NiTi SMAs to within 5 °C [66]. Furthermore, Wu indicates that development of advanced material processing techniques is necessary to manufacture stringent NiTi SMA chemistries.

A number of advanced manufacturing techniques have been developed to produce NiTi SMAs with comparatively better control over functional properties. Development of NiTi thin film fabrication techniques, for example, has generated significant interest for applications in microsystems technologies. A number of investigators have therefore made significant contributions to the development of NiTi SMA thin film fabrication techniques [67–71]. In particular, a study by Busch et al. [69] is fundamental because the authors documented the first observed case of shape memory response in a NiTi thin film. Developments in NiTi thin films processing have led to the development of a number of novel microsystems devices [72, 73].

Although fabrication of NiTi thin films has led to a number of impressive microsystems applications, according results published in studies by, Gyobu et al., and Grummon and LaGrange [74, 75], uniformity of film composition depends heavily on substrate positioning. Given the sensitive relationship between composition and thermomechanical properties in NiTi SMAs, a more robust processing technology is therefore required for the development of next-generation technologies.

In addition to thin films processing, powder metallurgy and sintering is another advanced manufacturing technology that has been extensively developed for the fabrication

of high quality NiTi SMAs. Powder metallurgy is particularly attractive for forming porous NiTi structures which have found many niche biomedical applications. NiTi SMAs are considered an ideal candidate material for biocompatible bone implants because of their comparatively high recovery strain, low-density and excellent cell adhesion capabilities [76, 77].

Traditional NiTi powder metallurgy sintering techniques rely on inert atmosphere or vacuum sintering synthesis protocols [78, 79]. In order to produce high porosity NiTi specimens, exothermic processes such as thermal explosion sintering are employed [80, 81]. The primary limitation of powder metallurgy sintering is the incomplete formation of NiTi resulting from unreacted Ni species and the growth of competing IMCs. To explain this phenomenon, Whitney et al. [82] completed a thorough investigation of the reaction mechanisms and microstructural evolution during thermal explosion sintering. The authors note that while Ni readily reacts with β-Ti the diffusion of Ti into Ni is relatively slow, leaving almost pure Ni precipitates inside the NiTi matrix. Furthermore, the authors identified a eutectoid reaction upon cooling which nucleates undesirable Ti_2Ni precipitates. These inhomogeneous structures are a troublesome consequence of powder metallurgy sintering because they indirectly alter the thermomechanical behaviour of the NiTi matrix and serve as crack initiation sites. While reactive sintering is advantageous for producing low-density NiTi structures, the inherent implications on thermomechanical response make powder metallurgy manufacturing techniques less desirable for producing NiTi SMAs in performance-critical applications.

2.1   Laser processing of NiTi SMAs

While significant effort has been invested to develop exotic manufacturing techniques, research into processing technologies has shown that perhaps less complex methods may be employed to tailor thermomechanical behaviour. In recent years, laser processing has developed as a reliable method to modify the thermomechanical response of bulk manufactured NiTi SMAs. Although laser processing has shown promise to deliver a precise mechanism for controlling thermomechanical behaviour in NiTi SMAs, relatively little and often conflicting literature is published on the subject.

2.1.1   Thermomechanical response of laser processed NiTi

The first investigation of laser processing on the thermomechanical behaviour of NiTi SMAs was completed by Araki et al. [83]. In this work, the authors stated the preservation of thermomechanical properties after joining $NiTi_{49.3at.\%}$ alloys using laser beam welding, although they failed to provide experimental evidence of shape memory recovery or pseudoelasticity. In a related study, Hirose et al. [84] reported similar findings, again failing to provide direct evidence of thermomechanical response in the joined NiTi SMAs. Schloßmacher et al. [85–87] performed a more rigorous investigation of laser processing effects on the thermomechanical behaviour in NiTi SMAs. Using a $NiTi_{50.6at.\%}$ alloy, the

authors reported a slight increase in phase transformation temperatures after laser beam welding operations [85]. The investigators provided tensile and DSC evidence for shape memory and pseudoelastic properties but failed to identify the underlying cause for the discrepancy in phase transformation onset temperatures between laser processed and base material samples. Similarly, Falvo et al. [88] showed comparable changes in phase transformation onset temperatures but again failed to provide an explanation for this effect. In a separate study, Schloßmacher et al. [87] reported on the effects of laser processing on a $NiTi_{48.4at.\%}$ alloy. In this work, the investigators noted a sharp decrease in hardness of the NiTi specimen in the laser melted zone, although, they failed to provide an explanation or interpretation for this phenomenon. Furthermore, the authors noticed a sharp drop in the pseudoelastic plateau stress which was stated, without evidence in a separate study by Schüßler [89], as being caused by recovery during laser melting.

In a 1999 study by Tuissi et al. [90], the effects of Nd:YAG laser processing on a $NiTi_{49.6at.\%}$ alloy were investigated. Similar to Schloßmacher et al. and Falvo et al. [85, 88], the authors reported a change in phase transformation temperatures after application of laser energy, as shown in Figure 2.1. The authors attributed disturbances in the DSC scans to changes in microstructure as a result of laser welding operations, however, they failed to provide micrographs of the laser melted region nor cited works to support this conclusion. In contrast to trends reported by Schloßmacher et al. and Schüßler [87, 89], Tuissi et al. [90] did not detect a significant drop in pseudoelastic stress. This discrepancy is likely due to differences in laser processing dimensions between the NiTi tensile specimens studied. In the Schloßmacher et al. [87] study, the laser was passed over much of the gauge length of the tensile specimen, such that the majority of the loaded material had been laser melted. On the other hand, Tuissi et al. [90] performed only a single bead pass on the tensile specimens before loading. Changes in the pseudoelastic response of the laser processed NiTi specimen were likely not detectable due to the small volume fraction of laser melted material within the tensile gauge length. This discrepancy in the literature was addressed, in detail, by a recent study from Khan et al. [91]. In this work, the authors performed a single bead pass on an NiTi tensile specimen. Through high precision micro-tensile testing, the authors identified the subtle presence of a lower pseudoelastic plateau, as shown in Figure 2.2.

The first evidence of an underlying mechanism responsible for the changes in thermomechanical behaviour is found in a 2001 study by Man et al. [92]. In this work, the investigators examined the effects of laser surface melting on the corrosion properties of a $NiTi_{49.2at.\%}$ alloy. Upon application of laser energy, the authors discovered a localized increase in the Ti/Ni ratio within the processing region. Although, this particular alloy is normally in the austenite phase at room temperature ($A_f = 0\ °C$), using X-ray diffraction (XRD) instrumentation, the authors detected the presence of martensite within the processing region. These findings were further confirmed in separate studies by Khan and Zhou, and Tam et al. [20, 22]. Using DSC and XRD analysis, Khan and Zhou [20] demonstrated a shift in phase transformation onset temperatures resulting from the application of laser power. As shown in Figure 2.3, the laser processed NiTi specimens exhibit two sets of austenite-martensite phase transformations: the subzero temperature set corresponding to the base metal and the higher temperature set representing the laser melted material. Using transmission electron microscopy (TEM), Khan and Zhou [20] were able to reveal a
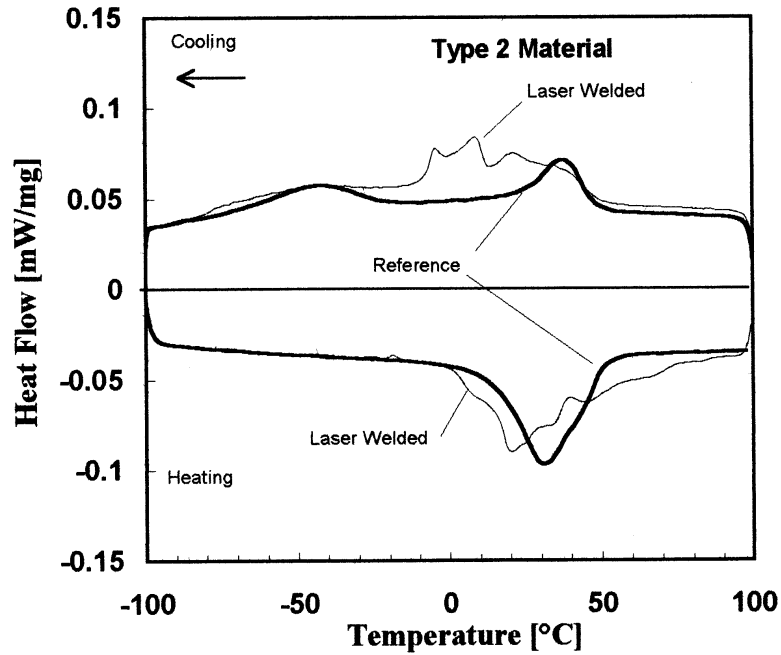
Figure 2.1: DSC scan of a laser processed NiTi specimen after Tuissi et al. [90]. The authors' explanation for the changes in phase transformation dynamics after laser processing is not supported with experimental evidence or cited works. Figure reprinted with permission from Elsevier.
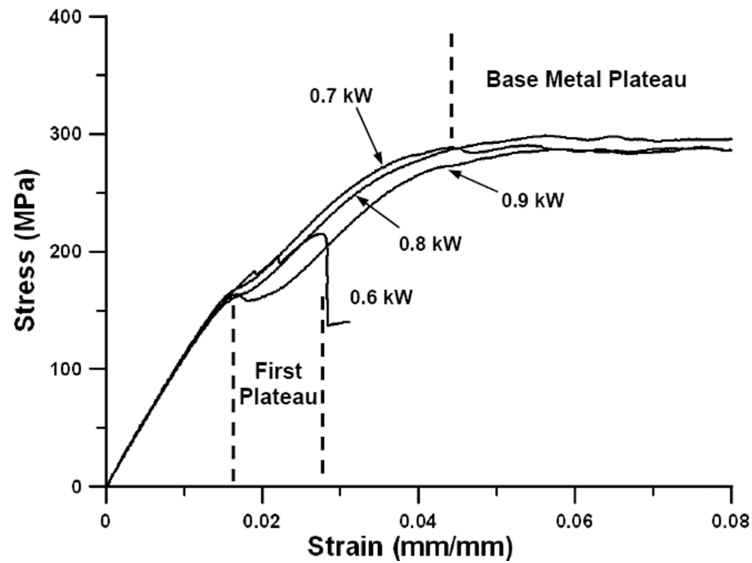
Figure 2.2: A laser processed NiTi specimen exhibiting two pseudoelastic plateau stresses after Khan et al. [91]. These results resolve the existing literature discrepancy between works by Tuissi et al. [90], and Schüßler and Schloßmacher et al. [87, 89]. Figure reprinted with permission from the Japanese Institute of Metals

19
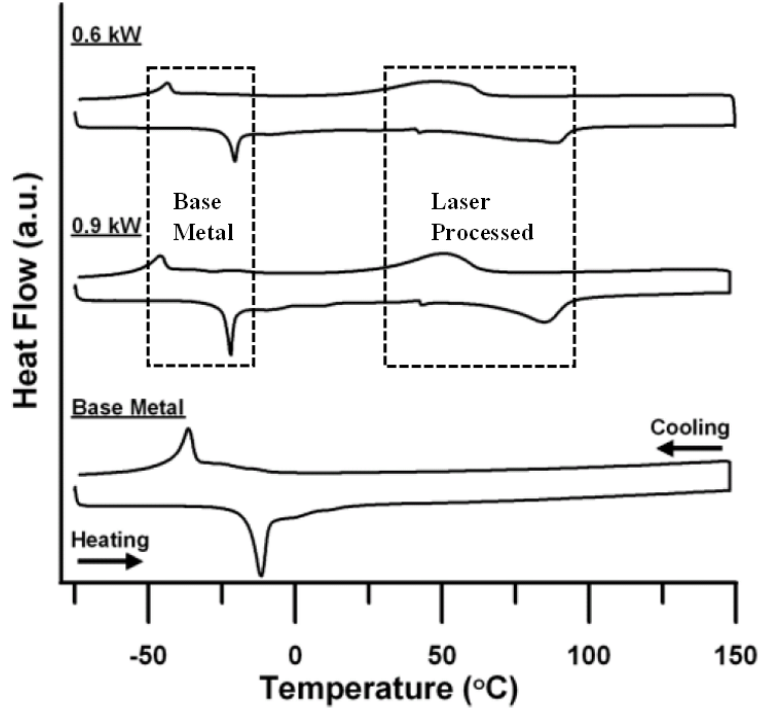
Figure 2.3: A laser processed NiTi specimen exhibiting two phase transformation dynamics after Khan and Zhou [20]. Phase transformation responses from the base metal and laser processed NiTi are annotated. Figure reprinted with permission from Elsevier.

martensitic relief pattern within the laser melted NiTi at room temperature. Figures 2.4 and 2.5 provide TEM images of both the base metal and laser processed NiTi samples at temperatures below M_f and above A_f, respectively. Using similar laser processing parameters to Khan and Zhou [20], Tam et al. [22] were able to explain the changes in hardness reported by Schloßmacher et al. [87] as the result of a localized phase change within the laser processing region.

2.1.2 Effects of laser processing on NiTi composition

The key factor to understanding the underlying mechanism behind localized phase changes in NiTi has only recently been identified. In a 2011 study, Khan [21] was able to establish that incident laser energy caused a preferential ablation of Ni species due to its comparatively lower partial pressure. Consequently, the localized Ti/Ni ratio within the laser processing region was found to increase in laser processed NiTi SMAs. Given the sensitive relationship between composition and thermomechanical response, a localized enrichment of Ti chemistry caused a subsequent increase in phase transformation onset temperatures with the processing region.

Using pulsed Nd:YAG laser processing technology, Khan [21] further investigated the effects of laser parameters on the thermomechanical behaviour of NiTi strip. In this study,

20
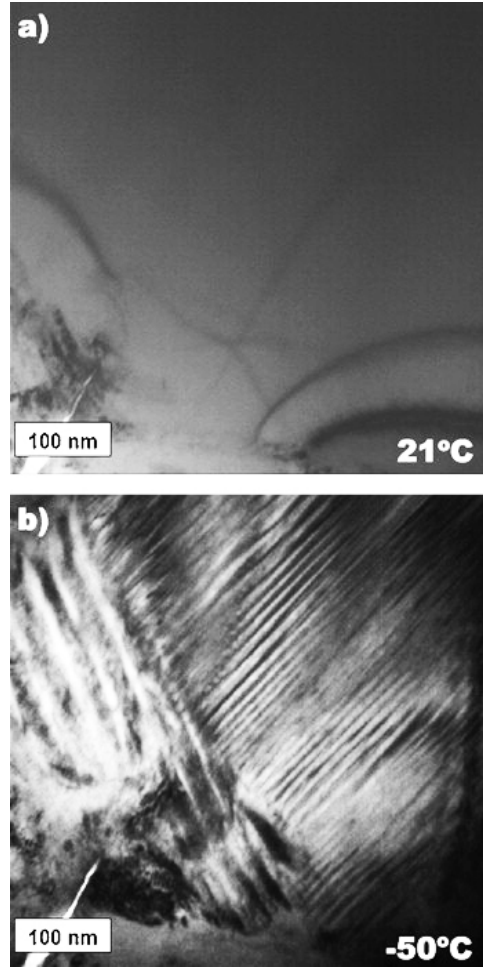
Figure 2.4: Base metal TEM images of a NiTi alloy with the austenite phase visible at 21 °C (a) and the twinned martensite structure apparent at -50 °C (b) [20]. Figure reprinted with permission from Elsevier.

the author identified the number of laser pulses as the key parameter to influencing shifts in local phase transformation temperatures. Khan [21] found that parameters such as peak power and processing time were less critical in effecting changes in thermomechanical response. These findings correlated well with a study completed by Jandagh et al. [93], who examined the rate of vapourization in pulsed Nd:YAG stainless steel alloy. Furthermore, Khan [21] established a saturation limit for the effects of laser processing. Given the solubility limitations in the Ni-Ti system, the author found that pulsed laser processing caused only a marginal change in transformation temperatures after 5 laser pulses. After 5 pulses, a stable M_s temperature of approximately 65 °C was reported, which corresponded well with the collected experimental data and thermodynamic analysis completed by Tang [15]. According to TEM analysis, after 5 pulses the local Ti/Ni ratio of the processed NiTi sample has reached saturation. Further pulsing induces precipitation of Ti_2Ni IMCs into the base material (Figure 2.6).

Although Khan [21] has demonstrated the effects of laser processing on composition and subsequent phase transformation dynamics in NiTi, an assessment of the changes in

21
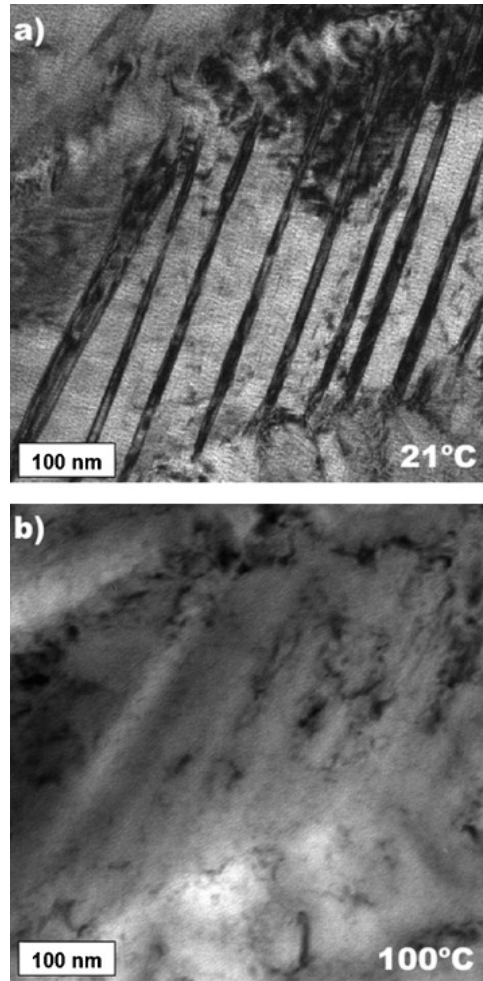
Figure 2.5: TEM image of a laser processed region from the NiTi SMA in Figure 2.4. The twinned martensite phase is visible at 21 °C (a) and the austenite structure is apparent at 100 °C (b) [20]. Figure reprinted with permission from Elsevier.

thermomechanical response is still absent from the literature. Further study of the effects of laser processing on the functional properties of NiTi SMAs such as the shape memory effect and pseudoelasticity is therefore required.

2.2 NiTi devices and applications

From an application's perspective, laser processing promises to remove many of the performance limitations inherent to NiTi SMAs. Laser processing technology has been shown to deliver NiTi SMAs which possess multiple phase transformation temperatures; allowing for an unprecedented functionality. Whereas a traditional NiTi SMA possess a single shape memory and pseudoelastic characteristic, laser processed NiTi SMAs can be programmed to remember multiple shape memory geometries or trained to exhibit several embedded pseudoelastic responses. The performance potential for laser processed NiTi
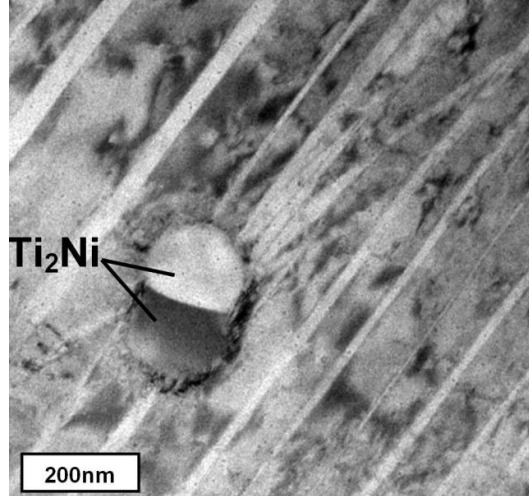
Figure 2.6: TEM image of a laser processed NiTi SMA. The NiTi matrix is Ti saturated from laser pulsing which induces precipitation of the Ti_2Ni IMC [21].

applications is therefore anticipated to be very high. However, as laser processing is only now emerging as a leading NiTi processing technology, the number of laser processed NiTi device publications is limited. To the authors knowledge, two recent studies of laser processed NiTi linear actuators by Pequegnat et al. [25, 26] represent the sole contributions to this research.

While there are a large number of diverse microsystems NiTi products available, the scope of this thesis is narrowed to discussion of a shape memory microgripper. Given the complicated path trajectories demanded from smart material microsystems technologies, monolithic fabrication of NiTi devices is usually not practical and SMA components are often integrated into hybrid packages [5]. For example, several hybrid designs exist for NiTi microgripper heads. Lee et al. [94] have developed a passively biased SMA microgripper by sputtering a NiTi film onto a silicon substrate and Kohl et al. [95] created an integrated antagonistic SMA microgripper by laser micromachining a NiTi thin sheet. Although in each of these designs gripper actuation is achieved through SMA response, device performance is inherently limited by their reliance on external systems which position the microgripper head prior to, and after, gripping operations.

Chapter 3

Effects of laser ablation on the phase transformation temperatures and thermomechanical behaviour of NiTi SMAs

The current literature regarding the effects of laser processing on the thermomechanical behaviour of NiTi SMAs is insufficient. Although laser processing is now understood to cause drastic changes in the functional properties of NiTi SMAs [20–23] further investigation is required to experimentally identify and quantify changes in thermomechanical response. An in-depth study of the effects of laser processing on both shape memory and pseudoelastic responses is therefore necessary in order to understand the performance and functionality of laser processed NiTi SMAs.

In the context of the present work, laser processing is considered to be the application of laser energy to effect a compositional and microstructure change in NiTi SMAs. Application of laser processing can remove chemical species, as in the case of surface ablation, or additionally, locally alloy other elements (Chapter 4). The purpose of the current chapter is to examine the effects of laser ablation on the thermomechanical behaviour of NiTi SMAs.

Given the significant lack of literature reported on laser processing of NiTi SMAs, it is prudent to first verify the laser pulsing study presented by Khan [21]. For this purpose, NiTi strip identical to the material used in Khan's work has been obtained for study. The first section of the current chapter replicates the study completed by Khan [21] to ensure the robustness of laser processing technology.

Building upon initial work by Tam [23], the second portion of this chapter examines the changes in thermomechanical response resulting from laser processing operations. Thermoanalytical and tensile instrumentations are used to assess the shape memory and pseudoelastic responses of a laser processed NiTi wire. Given the poor machinability of NiTi [96], the preparation of NiTi dog-bone samples is not practical and therefore NiTi wire was chosen because of its direct application in tensile testing. A detailed investigation

of the mechanical strength and fractography of laser processed NiTi has already been completed in previous works by Khan et al. and Tam et al. [22, 91] and therefore is omitted from the current study.

3.1   Pulsed Nd:YAG laser processing

Laser processing of the NiTi SMA base metal (BM) was achieved using a Miyachi Unitek model LW50-A pulsed Nd:YAG laser source with a 1.06 μm wavelength beam and a nominal post-optic spot size of 600 μm. Figure 3.1 provides a photograph of the Miyachi Nd:YAG laser system. In order to ensure uniform application of laser power across the processing spot, the laser system was equipped with a stepped index optical fibre. The energy distribution of the stepped index fibre is provided in Figure 3.2.
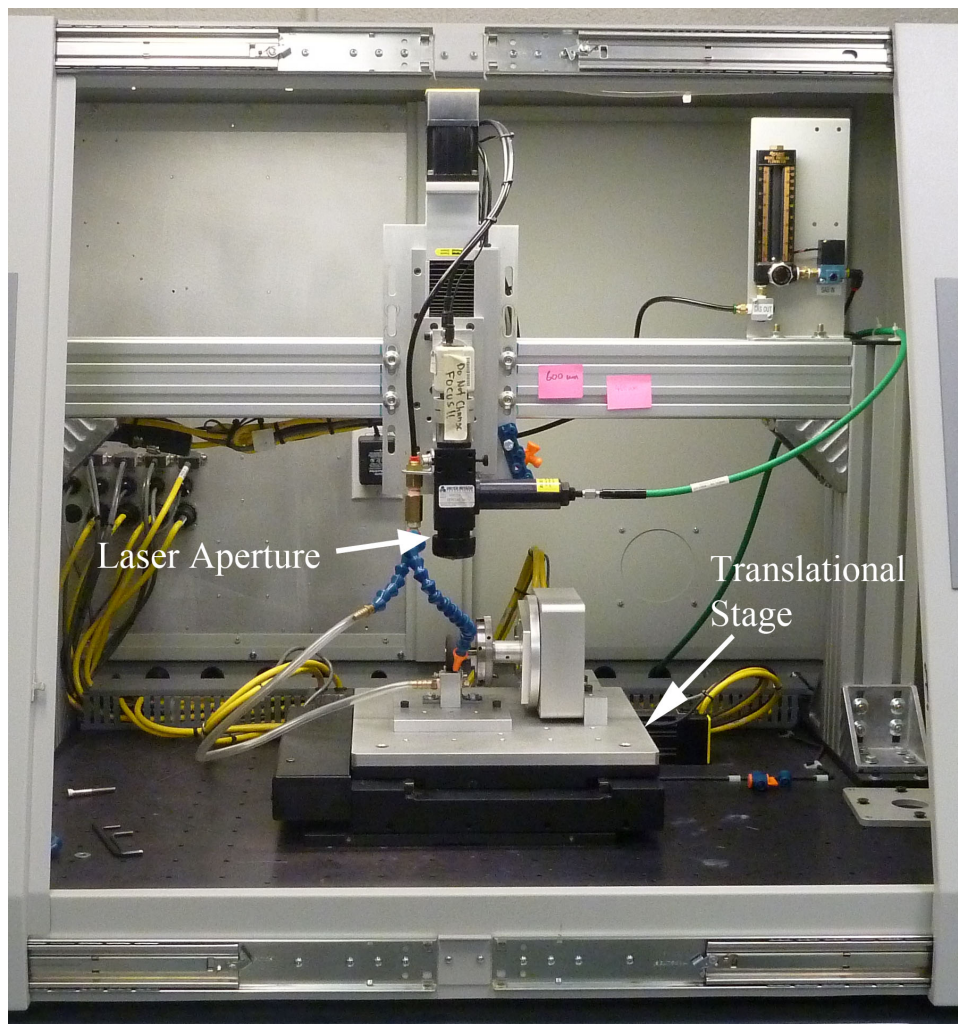
Figure 3.1: The Miyachi Unitek Nd:YAG laser system equipped with translational stage for path programming.
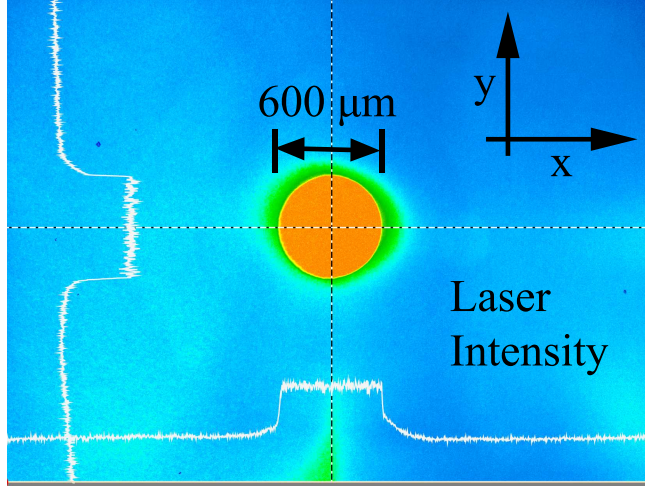
Figure 3.2: Spatial power profile of the stepped index fibre-optic cable implemented with the Nd:YAG laser system.

In addition to the laser optics, the Miyachi laser system was equipped with a programmable gantry, capable of translation and rotation in three dimensions. A custom program was written to interface with the gantry controller, allowing for automation of laser processing. Customized fixturing was manufactured to provide clamping pressure and deliver a shielding atmosphere to the laser processed zone (LPZ) during operation. Photographs of the NiTi strip and wire laser processing fixtures are provided in Figure 3.3. Argon shielding gas was provided to the processing region of the NiTi SMA strip and wire at rates of 0.84 m^3/hr (30 CFH) and 0.42 m^3/hr (15 CFH) respectively.

In order to process large regions of NiTi, a laser spot overlapping (OL) protocol was incorporated into the automation program. Overlapping is typically defined as an offset in terms of percentage of the spot diameter (d_s). Figure 3.4 illustrates laser processing procedure of a NiTi strip using OL. In strip processing, d_s is used to determine the movement (Δx) of the laser head required to achieve the desired OL by the following relation:

$$\Delta x = d_s(1 - OL) \qquad (3.1)$$

Given the circular geometry of the LPZ, Δx is defined as the distance between centres of adjacent processing spots. In NiTi wire processing, however, the laser head remains stationary and spot overlapping is achieved via spindle feed (Figure 3.3b). d_s is therefore used to determine the angular rotation of the spindle which is required to obtain the programmed OL. Optical micrographs of NiTi wire specimens processed at different overlaps are provided in Figure 3.5. When processing at OLs less than 50%, the cross-section of the wire is superficially distorted by the terminal solidification front during freezing.

Laser power and beam duration parameters were determined through qualitative assessment. Parameter schedules were chosen through iterative testing based on the following criteria: laser penetration depth; cracking within solidification structure; and evidence of
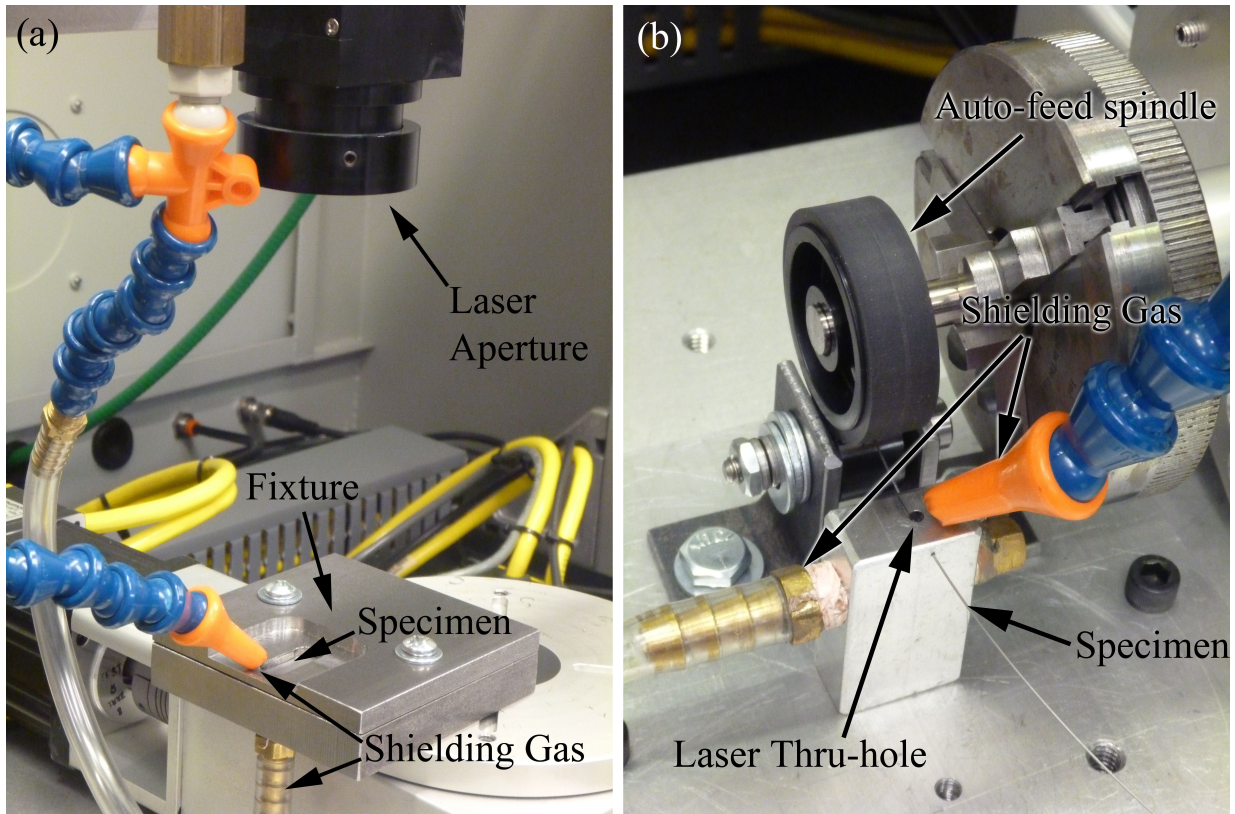
Figure 3.3: Fixturing and argon shielding lines for laser processing operations of the strip (a) and wire (b) NiTi SMAs.
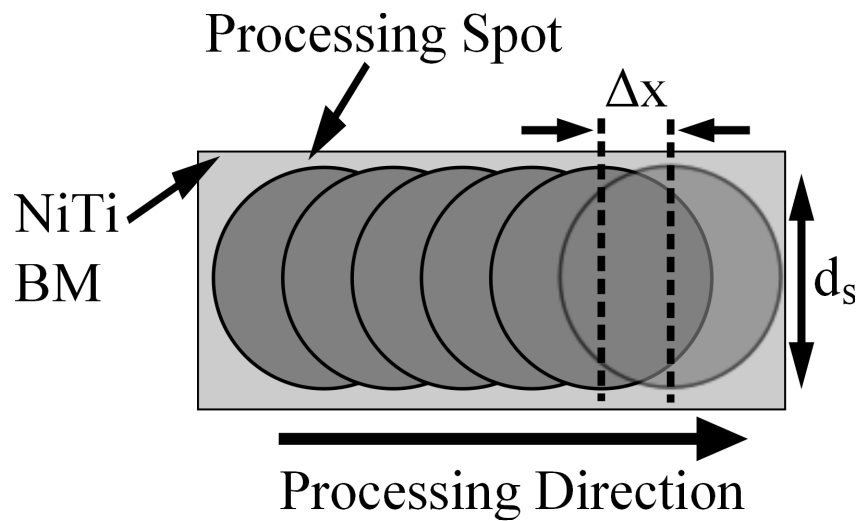
Figure 3.4: Pulsed laser processing of a NiTi strip using OL. The d_s parameter is used to determine the movement of the laser head (NiTi strip) or angular rotation of the auto-feed spindle (NiTi wire) to achieve the desired OL.

Figure 3.5: NiTi SMA wires processed at -55% OL (a) and 75% OL (b). Superficial bulging of the wire cross-section is evident along the terminal solidification front in (a).

oxidation. Unsuitable laser parameters produced incomplete penetration, terminal solidification cracks and showed evidence of surface oxidation; whereas ideal schedules achieved full penetration with a crack-free solidification structure and clean surface condition. The selected parameter schedules and pulse profiles for the NiTi strip and wire are provided in Figure 3.6.

3.2   Effects of laser ablation on NiTi SMA strip

In order to verify the robustness of laser processing technology, a pulsed Nd:YAG study of NiTi strip, similar to the investigation completed by Khan [21], has been undertaken. NiTi strip specimens, with laser processing schedules ranging from 1 to 10 pulses, were prepared for examination. The purpose of this investigation is to confirm the composition, crystallographic, and phase transformation kinetic changes resulting from the implementation of laser processing protocols. Furthermore, the shifts in phase transformation onset temperatures are compared to results obtained by Khan [21] to verify the robustness of laser processing technology and the proposed Ti saturation limit.

3.2.1   Experimental

3.2.1.1   NiTi SMA strip material selection

Commercially available cold-rolled 400 μm NiTi strip with a nominal composition of 50.8 at.% Ni and 49.2 at.% Ti was used for laser processing validation. In its wrought condition, the NiTi SMA exhibited a very poor thermomechanical response. The as-received material was therefore solution treated in a vacuum furnace at 800 °C for 3.6 ks followed
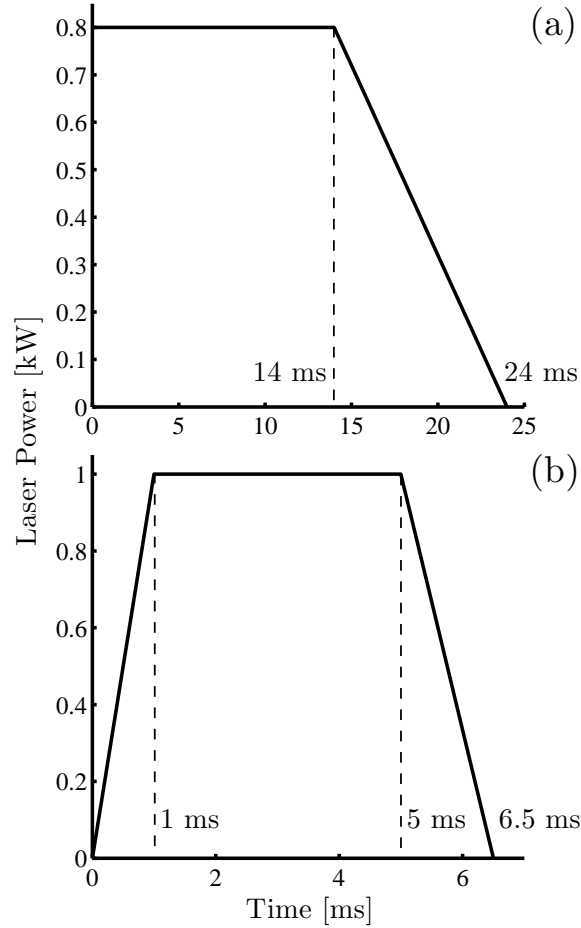
Figure 3.6: Laser pulse profile for the NiTi SMAs. Strip specimens were processed at 0.8 kW peak power for 14 ms with a 10 ms downslope (a), and wire samples were processed at 1 kW peak power with a 1 ms upslope, 4 ms hold and 1.5 ms downslope (b).

by an argon gas quench to restore its functional properties. Prior to laser processing operations, the NiTi strip was chemically cleaned with a hydrofluoric-nitric acid etching solution to remove surface oxides and contaminants. The etching solution contained 7.5 mL HF, 20 mL HNO_3 and 72.5 mL H_2O by volume. NiTi SMA samples were immersed in the acid solution for 240 s under ultrasonic agitation. The post-etched NiTi strip samples possessed a uniform thickness of 370 μm.

3.2.1.2   Optical Microscopy

In order to assess the effects of heat treatment on alloy microstructure, samples for optical microscopy examination were prepared. Microscopy specimens were ground sequentially with silicon-carbide paper to a 1200 fine grit and then polished with 1 μm and 0.25 μm microid diamond suspensions. Final polishing was conducted using colloidal silica suspension. NiTi samples were then ultrasonically cleaned in ethanol for 300 s prior to etching.

Chemical etching was performed using a dilute hydrofluoric-nitric acid solution containing: 3mL HF, 14 mL HNO_3 and 82 mL H_2O by volume. Samples were immersed in the etchant for 25-30 s and subsequently ultrasonically cleaned in ethanol prior to examination. Optical microscopy examination was performed using an Olympus BX51M Metallurgical Microscope under Differential Interference Contrast polarization. Micrographs of the as-received and solutionized NiTi strip microstructures are provided in Figure 3.7. The effects of heat treatment have relaxed internal stresses from rolling operations and formed an equiaxed microstructure with grains diameters varying from 20-40 μm. The intra-granular surface distortions evident in the micrographs were not a result of metallographic preparation and are common in the microstructure of NiTi [36, 97]. White surface structures, such as those in Figure 3.7b, are localized pits formed by fluoric-based etchant artifacts [98]. They are not secondary phases and their identity has been confirmed by chemical analysis.

3.2.1.3 Electron microscopy and chemical analysis

In order to assess composition changes in pulsed NiTi SMA strip samples, a Jeol JSM-6460 scanning electron microscope (SEM) equipped with an INCA X-Sight 350 energy dispersive X-ray (EDX) analysis aperture was used for microscopy and chemical analysis. SEM micrographs and EDX chemical measurements were collected at a 20 keV acquisition energy and nominal 1 μm interaction spot. NiTi SMA samples were polished and etched following the same procedure outlined for optical microscopy analysis. Prior to SEM analysis, the samples were carbon coated to improve conductivity.

3.2.1.4 Phase analysis

Crystallographic phases in the laser processed NiTi strip specimens were identified using XRD analysis. Room temperature XRD patterns were captured using a Rigaku SA-HF3 (1.54 Å Copper-Kα) X-ray source equipped with an 800 μm collimator operating at an excitation voltage of 50 kV. Samples examined by XRD analysis were ground to a 1200 fine grit. Further polishing or chemical etching of specimens was not required.

3.2.1.5 Thermoanalytical testing

Changes in phase transformation temperatures of the laser processed NiTi strip specimens were analyzed via DSC instrumentation using a Thermal Analysis Q2000 acquisition system equipped with a refrigerated cooling unit. DSC scans were collected using a modified ASTM F2004-05 testing standard. Heat flow was measured at a controlled heating and cooling rate of 5 °C/min ranging from -75 °C to 120 °C. Austenite and martensite onset and finish temperatures were defined according to the ASTM standard outlined in Section 1.3.2.
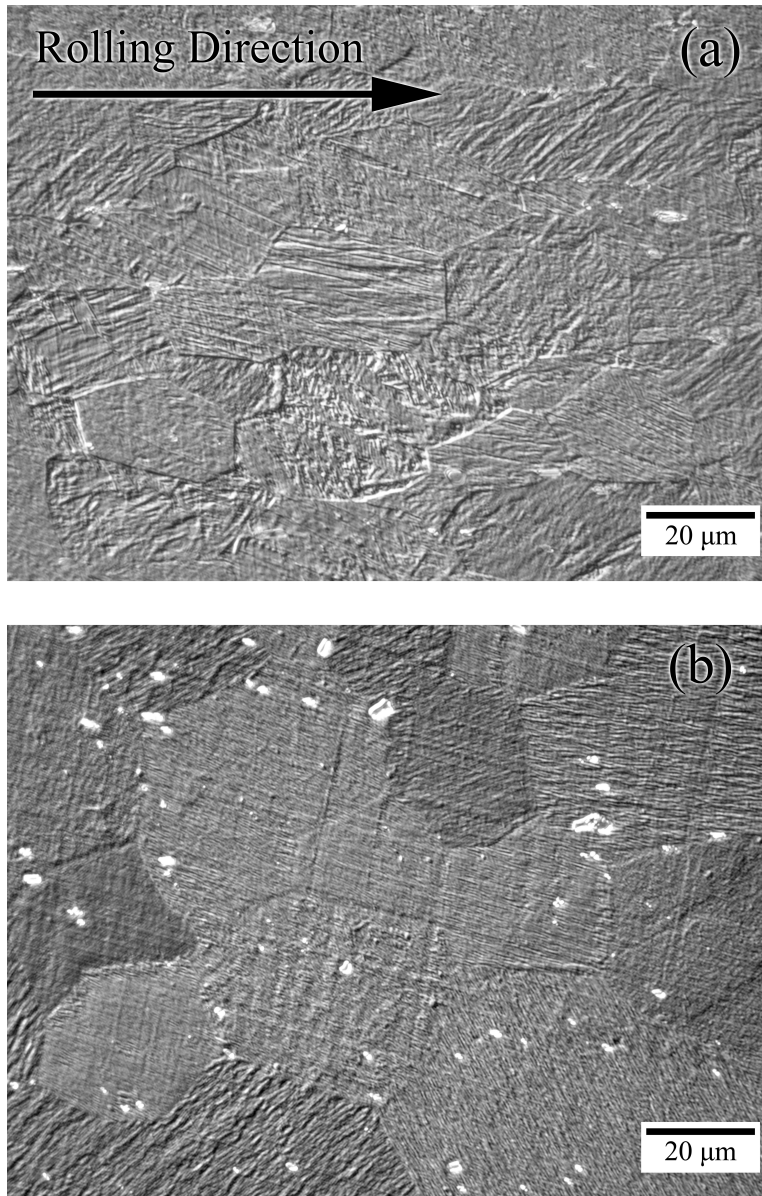
Figure 3.7: Optical micrographs of as-received (a) and solutionized (b) NiTi SMA strip. The intragranular surface distortions are typical in NiTi microstructures and the white surface pits are artifacts from hydrofluoric acid etching agents.

3.2.2 Results and discussion

3.2.2.1 Compositional changes in laser processed NiTi Strip

Results from electron microscopy and chemical analysis indicate an abrupt change in SMA composition upon crossing the LPZ-BM interface. As shown in Figure 3.8, EDX results indicate that SMA composition shifted to a Ti rich chemistry within microns of the processing boundary. Due to the high cooling rates associated with laser processing,

only a very minor heat affected zone (HAZ) was formed between material domains. The equiaxed BM and dendritic LPZ microstructures therefore formed a readily visible and well-established processing boundary between the two regions. Although EDX results are generally only accurate to $\pm$ 1 at.%, the differences in chemistries between the BM and LPZ are clear from the collected emission spectra. Given the inaccuracies of EDX technology and the extreme sensitivity of NiTi physical metallurgy to composition, it was impractical to assess incremental changes in SMA chemistry with respect to pulsing protocol. Further study using a more precise chemical analysis method such as particle induced X-ray emission (PIXE) spectroscopy is therefore recommended to accurately quantify composition changes in laser processed NiTi SMAs.

3.2.2.2 Crystallographic changes in laser processed NiTi strip

In addition to ablation of Ni species, laser processing has been reported by Khan [20] to cause a related crystallographic change in pulsed NiTi strip. Figure 3.9 provides the collected XRD patterns for the BM and LPZ material domains of a processed NiTi
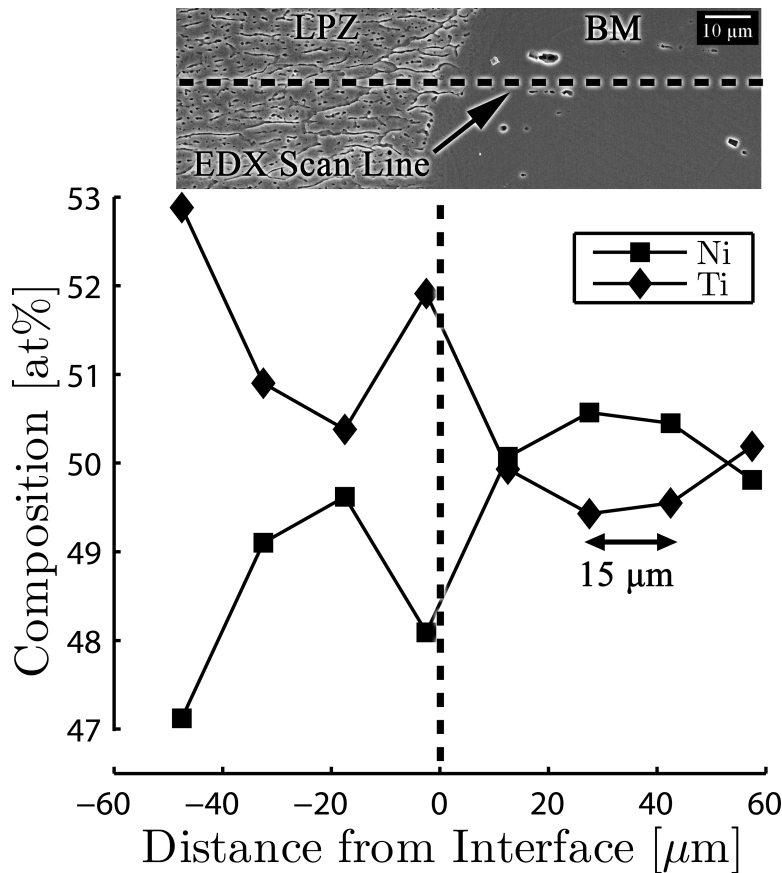
Figure 3.8: SEM micrograph and EDX trace of a NiTi SMA strip processed for 3 pulses at 0% OL. SMA chemistry is Ti rich in the LPZ. EDX measurements were collected at 15 μm intervals across the BM-LPZ interface.
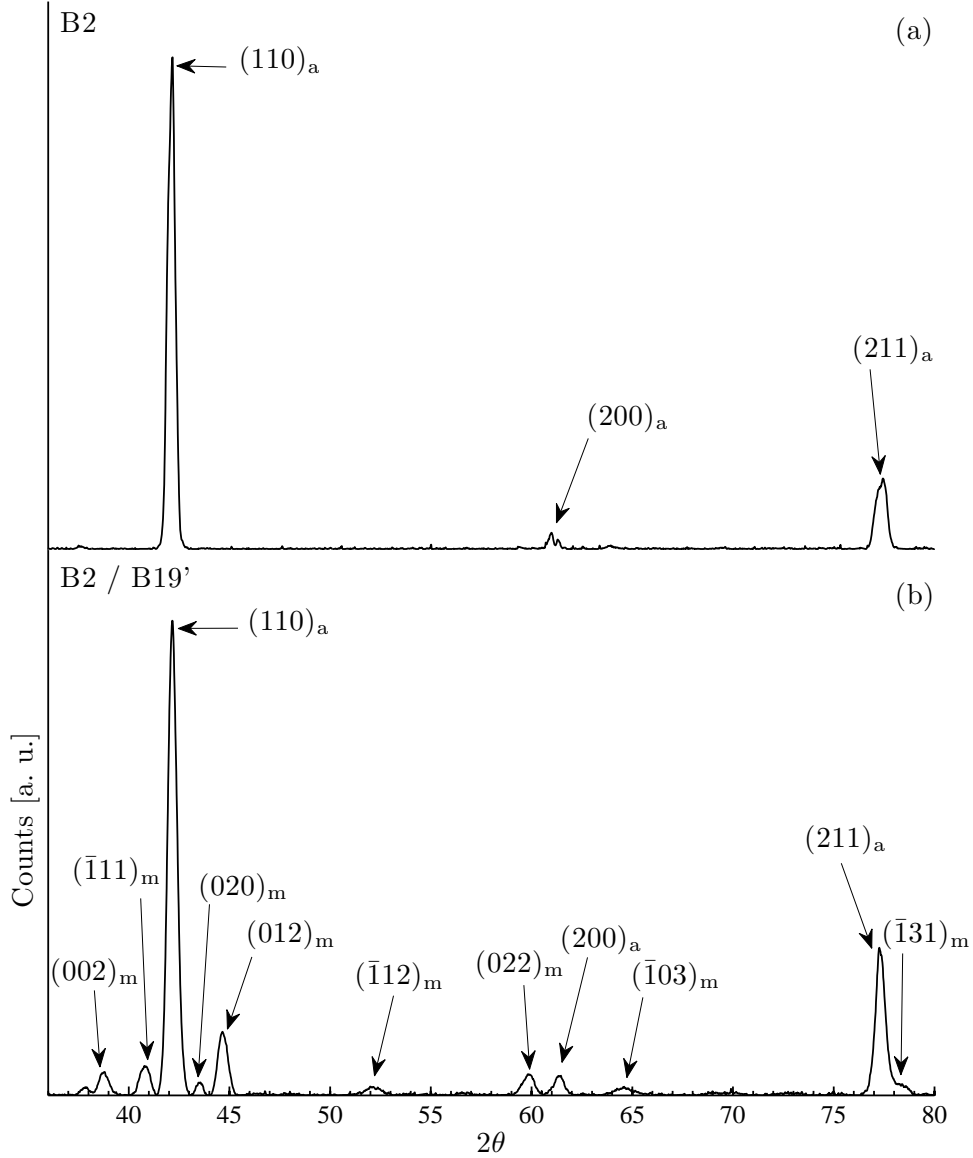
Figure 3.9: Indexed XRD patterns for the BM (a) and LPZ (b) material domains. The LPZ was processed for 3 pulses at 0% OL. Detection of the B2 cubic phase in (b) was likely due to retained BM within the sampling volume. All diffraction patterns were collected at 22 °C.

strip. As anticipated, crystallographic analysis of the BM revealed three diffraction peaks at the 42, 61 and 77 Bragg angles, which agreed well with reference patterns for the B2 austenite lattice (indexed with subscript a)[99]. Results from the LPZ, however, indicate the presence of an additional phase within the solidification structure. The additional diffraction peaks correlated well with reference patterns for B19' martensite (indexed with subscript m) [100]. The effects of laser ablation have therefore caused a localized phase conversion within the LPZ. Since the specimen was prepared at 0% OL, the detection of B2 austenite can be explained by the presence of retained BM between processing spots of the LPZ.

3.2.2.3 Changes in phase transformation dynamics of laser processed NiTi strip

The crystallographic changes induced by laser processing were anticipated to cause corresponding shifts in phase transformation onsets. Results from thermoanalytical testing indicated that phase transformation temperatures in the 3 pulse sample were shifted approximately 50 °C in the LPZ. Figure 3.10 provides DSC scans of the BM and LPZ material domains of the NiTi SMA strip. The increase in width of transformation peaks was believed to be caused by slight inhomogeneities within the LPZ [101]. Retained BM was detected in the collected DSC data, which corroborated the presence of the B2 cubic phase in the XRD analysis of the LPZ.

3.2.2.4 Effects of pulsing on phase transformation dynamics

In order to verify the Ti saturation limit for laser processed NiTi strip, DSC scans were collected for SMA samples which were processed for 1 to 10 pulses. The phase transformation onset temperatures are provided in Table 3.1 and a plot of the M_s onsets with respect to pulsing is provided in Figure 3.11. A statistical analysis of NiTi strip processed under different laser parameters found that the standard deviation of M_s onset tempera-
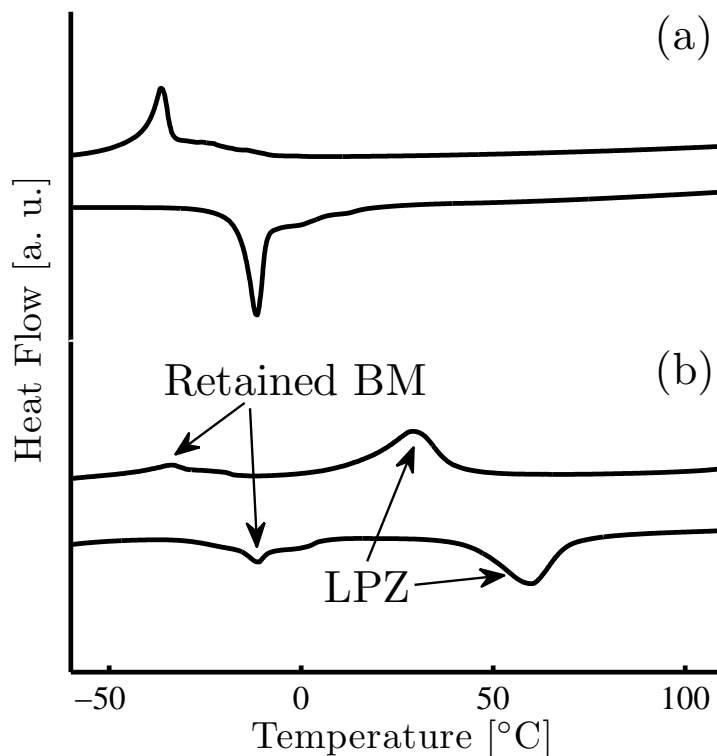
Figure 3.10: DSC scans of the NiTi BM (a) and LPZ (b) material domains. The LPZ was processed for 3 pulses at 0% OL. Retained BM in (b) corroborated the presence of B2 cubic martensite in the XRD analysis of the LPZ.

tures was less than 2 °C. Examination of the DSC data indicated that M_s temperatures stabilized after 5 pulses between 335 K and 340 K, which agreed well with findings reported by Khan [21]. The thermodynamic analysis completed by Tang is provided as an inset in Figure 3.11 to correlate changes in composition, M_s temperatures, and laser pulsing [15]. A comparative analysis using PIXE instrumentation that directly correlates laser pulsing and SMA composition with shifts in phase transformation onsets is recommended for future work.

Table 3.1: Phase transformation temperatures (°C) for NiTi SMA strip samples processed at 1 to 10 pulses (P).

Temp.	BM	1 P	2 P	3 P	4 P	5 P	6 P	7 P	8 P	9 P	10 P
								Sample			
M_s	-16.1	13.0	25.1	43.0	53.2	63.5	64.4	66.3	64.0	64.0	66.9
M_f	-41.3	-10.8	-7.6	2.4	15.3	16.2	20.9	22.7	24.4	34.0	36.7
A_s	-16.1	9.4	22.4	40.0	47.1	52.1	57.9	61.9	63.3	68.9	70.9
A_f	-8.6	35.3	54.0	71.5	83.9	90.6	94.7	96.4	92.0	93.9	95.8
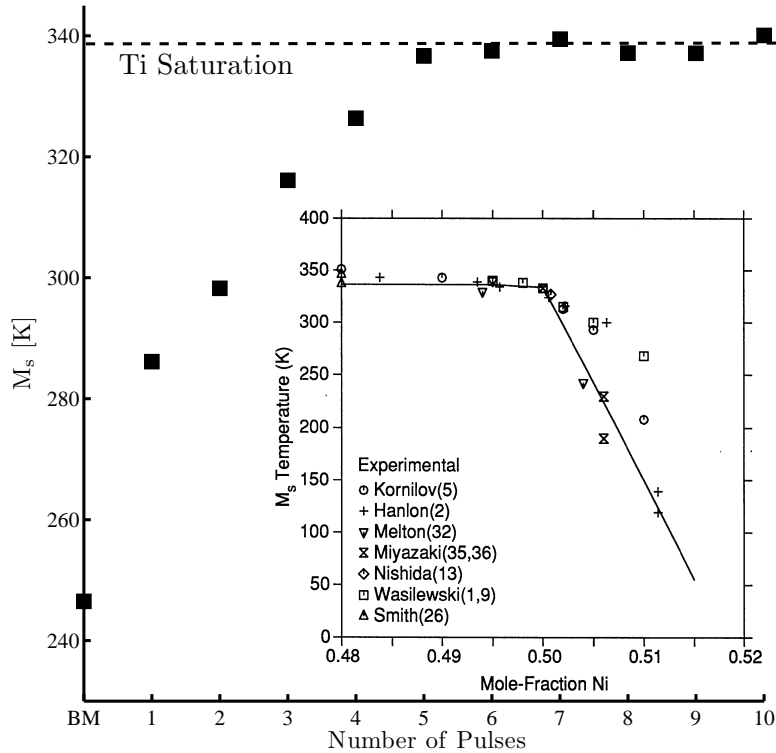
Figure 3.11: M_s temperatures of NiTi SMA strip samples processed for 1 to 10 pulses. For comparison purposes, onsets are reported in Kelvin. Figure inset was obtained from [15] and reprinted with permission from Springer.

3.3 Effects of laser ablation on the thermomechanical response of NiTi SMA wire

Although it is now understood that laser processing can alter the functional properties of NiTi SMAs, an investigation which quantifies changes in their thermomechanical behaviour is currently absent from the literature. The current section therefore examines changes in both the shape memory effect and pseudoelastic response of a laser processed NiTi SMA wire. For the purposes of this study, NiTi wire samples were laser processed at 2 pulses using the parameters defined in Figure 3.6b. Optical micrographs of a laser processed NiTi SMA wire specimen are provided in Figure 3.12. Optical micrographs were prepared as specified in Section 3.2.1.2. The surface quality of the processing spot was excellent, with only minor distortion of the cross-section due to bulging along the solidification terminus. Evidence of directional solidification, terminal solidification fronts and martensite relief patterns were visible in the microstructure of the laser processed specimen. Unlike the NiTi SMA strip specimens, the NiTi wires possessed a considerable HAZ of approximately 100 μm in width.

3.3.1 Experimental

3.3.1.1 NiTi SMA wire material selection

Commercially available cold-drawn 410 μm NiTi wire with a nominal composition of 50.8 at.% Ni and 49.2 at.% Ti was used for laser processing. Prior to laser processing operations, the NiTi wire was chemically cleaned with a hydrofluoric-nitric acid etching solution to remove surface oxides and contaminants. The etching solution contained 15 mL HF, 40 mL HNO_3 and 55 mL H_2O by volume. NiTi SMA samples were immersed in the acid solution for 15-20 seconds. The post-etched NiTi wire samples possessed a uniform thickness of 380 μm.

3.3.1.2 Shape memory recovery assessment

In its cold worked condition, the as-received NiTi SMA wire exhibited a very poor shape memory recovery. The as-received material (also referred to as BM) was therefore annealed at 800 °C for 300 s to restore its functional properties. Laser processed NiTi samples prepared at 0% OL were also fabricated for shape memory assessment. Given their relatively stress-free microstructures, an annealing protocol was not required. Table 3.2 provides a test matrix for heat treatment and processing protocols of the NiTi SMA wires used for shape memory assessment.

In order to characterize the effects of heat treatment on the microstructure and shape memory recovery of the NiTi SMA wire, optical micrographs and DSC scans of the as-received and annealed BM wire samples were prepared and are provided in Figures 3.13 and 3.14 respectively. DSC testing was conducted under the ASTM standard as specified in Section 3.2.1.5. The effects of heat treatment have significantly annealed the
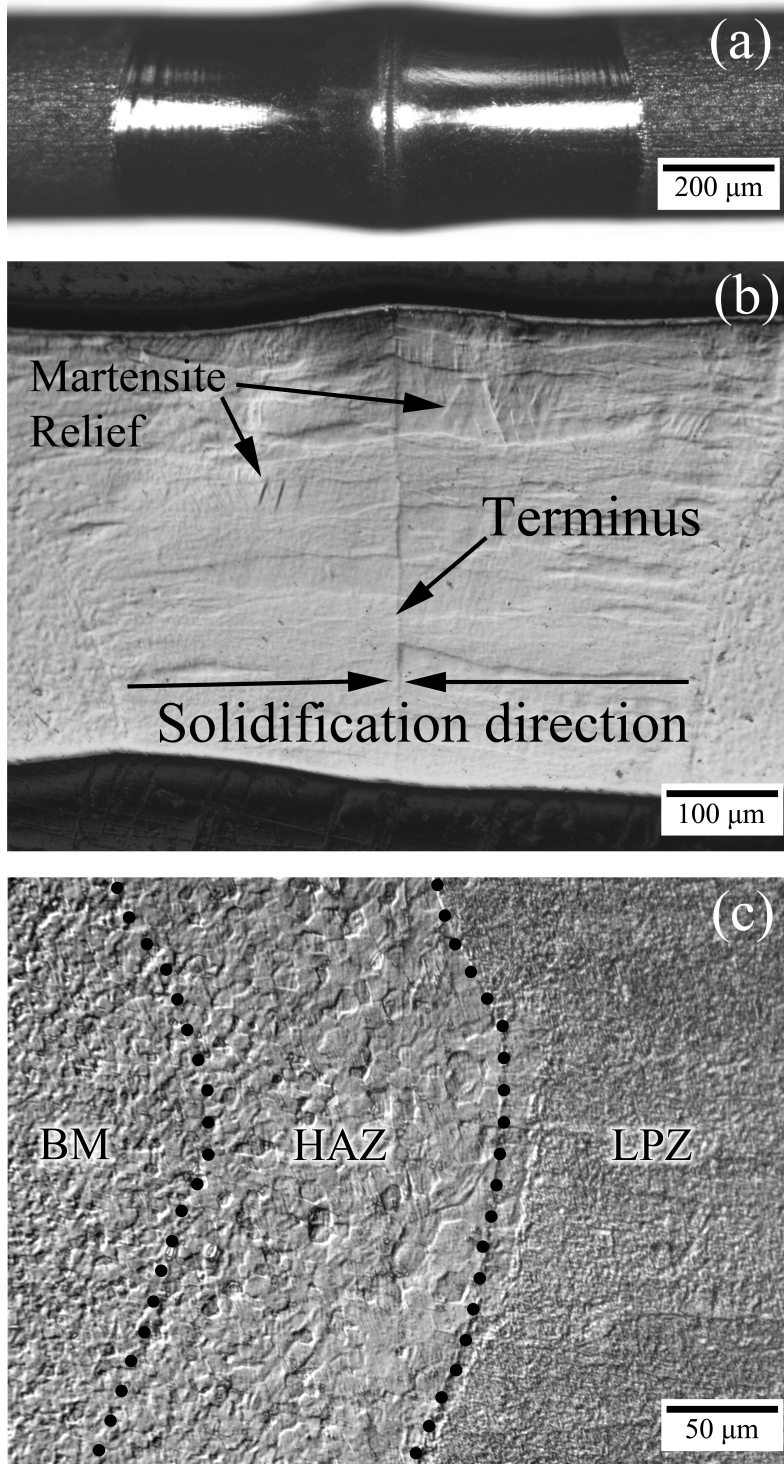
Figure 3.12: Optical micrographs of a NiTi SMA wire laser processing spot: exterior wire surface (a); solidification structure of a processing spot (b); and high magnification image of laser processing interface (c).

Table 3.2: Heat treatment and laser processing protocols for shape memory assessment of NiTi SMA wire specimens

Identifier	Heat treatment (800 °C 300 s)	Laser processing (0% OL)
as-received BM		
annealed BM	✓	
laser processed		✓

microstructure of the NiTi wire. Grain structures were recrystallized from a cold-drawn geometry to an equiaxed morphology. The intra-granular surface distortions and white surface artifacts visible in the micrographs were caused by the same phenomena as with the NiTi SMA strip. In addition to microstructure relaxation, the effects of heat treatment have restored shape memory functionality to the NiTi SMA wire. The collected DSC data revealed clear evidence of a phase transformation in the annealed sample which was absent from the as-received BM.

An Instron model 5548 micro-tensile testing machine equipped with an environmental chamber was used to assess shape memory recovery of the NiTi SMA wire samples. Specimens were cooled in the chamber to below M_f of the annealed BM and loaded under an ASTM F2516–07 testing protocol at a rate of 1.0 mm/min. Tensile specimens were loaded to 6% strain and then subsequently relaxed. Upon complete unloading, the laser processed samples were environmentally heated at approximately 15 °C/ min to above A_f of the laser processed wire, in order to trigger shape memory recovery. A zero load condition was maintained at the crossheads and displacement feedback was continuously recorded. The measured displacement was then normalized against the final length of the NiTi SMA wire and then correlated with collected temperature data to measure and track shape memory response. Temperature measurements were recorded using a thin film resistance temperature detector (RTD) with an uncertainty of $\pm$ 0.3 °C. Appendix A provides an uncertainty analysis of the reported temperature measurements. A photograph of the test setup is provided in Figure 3.15. In order to eliminate high frequency signal noise, the collected displacement and temperature data sets were filtered using a low-pass Butterworth algorithm [102].

3.3.1.3 Pseudoelasticity training and testing

In its as-received condition, the NiTi SMA wire had undergone significant cold work and due to the large degree of lattice strain in the microstructure, was unable to achieve a stress induced phase transformation. Additionally, the yield stress of the laser processed NiTi SMA wire samples was beneath the pseudoelastic threshold and therefore tensile loading induced failure by slip mechanisms. The laser processed samples were therefore strain hardened under a thermomechanical processing protocol involving cold work (> 25% [18]) and aging at 400 °C for 3.6 ks. For consistency purposes, the as-received wire was also cold worked and aged using this protocol. Table 3.3 provides a test matrix for

thermomechanical training of NiTi SMA wire specimens strengthened for pseudoelasticity.

An Instron model 5548 micro-tensile testing machine equipped with an environmental chamber was used to assess pseudoelastic response of the NiTi SMA wire samples. Specimens were heated in the chamber to above A_f of the laser processed NiTi wire and loaded under a modified ASTM F2516–07 testing protocol at a rate of 1.0 mm/min. Tensile
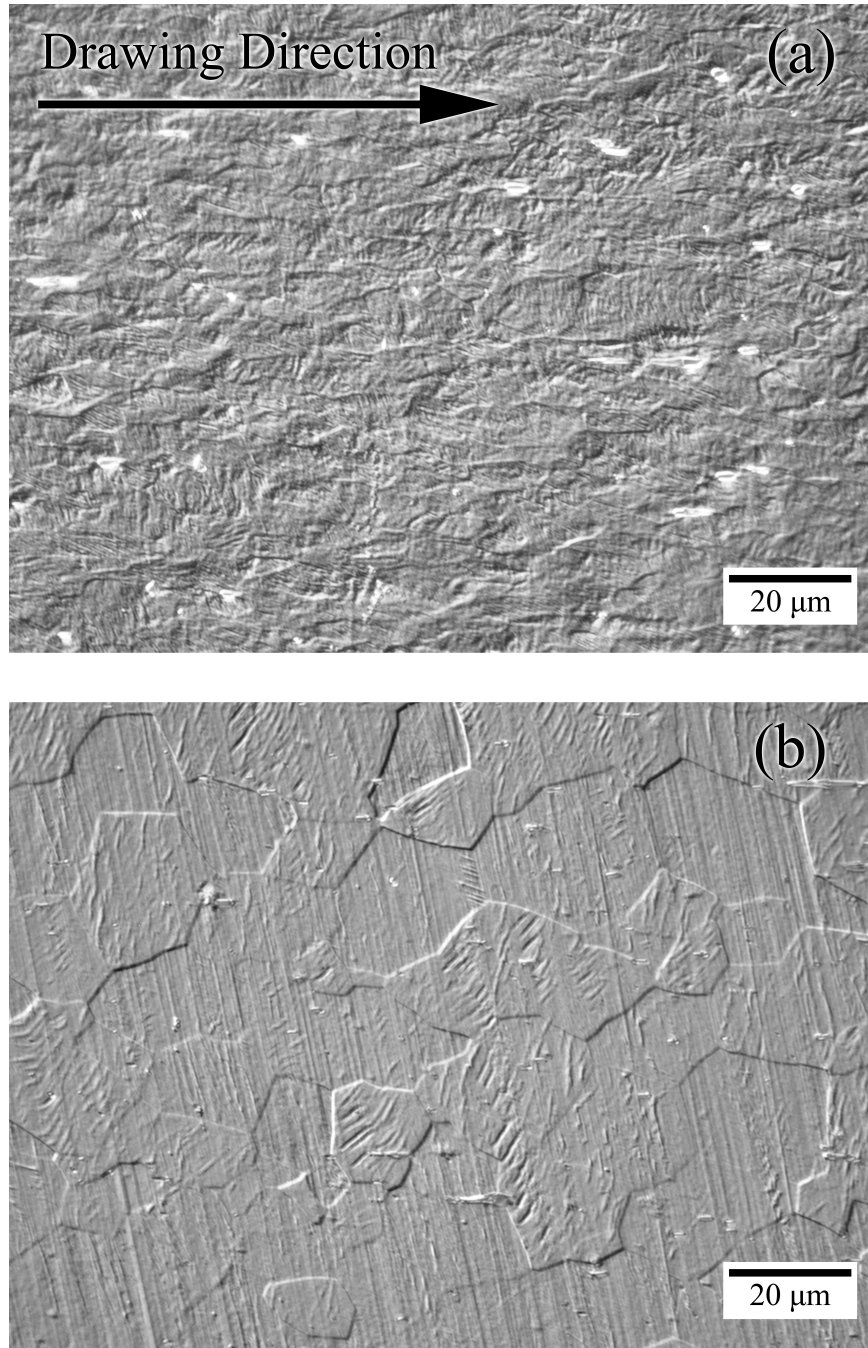
Figure 3.13: Optical micrographs of the as-received (a) and annealed BM (b). The effects of heat treatment have induced recovery and recrystallization in the NiTi SMA wire.
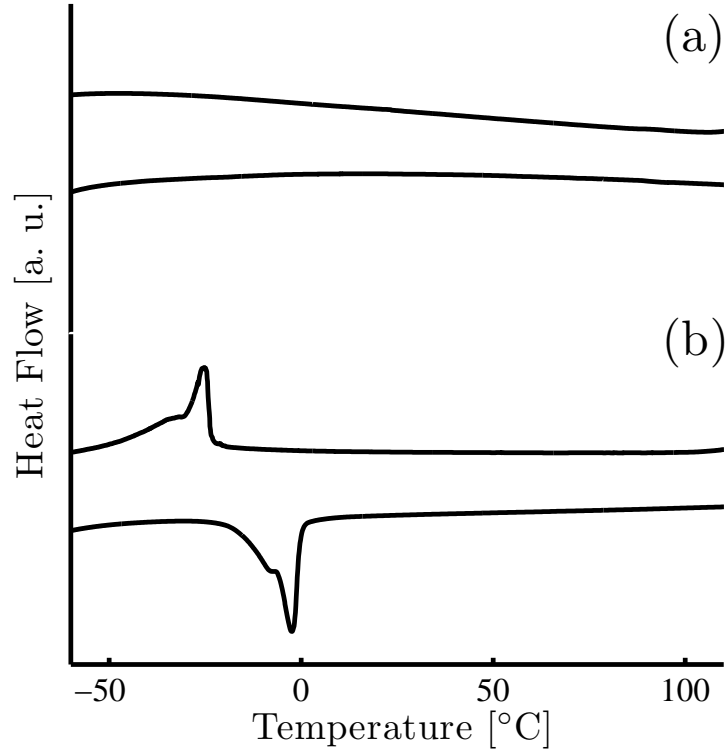
Figure 3.14: DSC scans of the as-received (a) and annealed BM (b). The effects of heat treatment have restored the shape memory effect in (b).

specimens were loaded to 10% strain and then subsequently relaxed.

3.3.2 Results and discussion

3.3.2.1 Changes in phase transformation temperatures

Figure 3.16 provides DSC scans of the annealed BM and laser processed NiTi SMA wire samples. The phase transformation onset temperatures of each specimen are provided in Table 3.4. Examination of the collected DSC data revealed a new set of phase transformation peaks with A_s and M_s temperatures at approximately 40 °C higher than the

Table 3.3: Thermomechanical training and laser processing protocols for pseudoelasticity assessment of NiTi SMA wire specimens

Identifier	Laser processing (0% OL)	Cold working (> 25%)	Heat treatment (400 °C 3.6 ks)
as-received BM			
aged BM		✓	✓
laser processed	✓	✓	✓
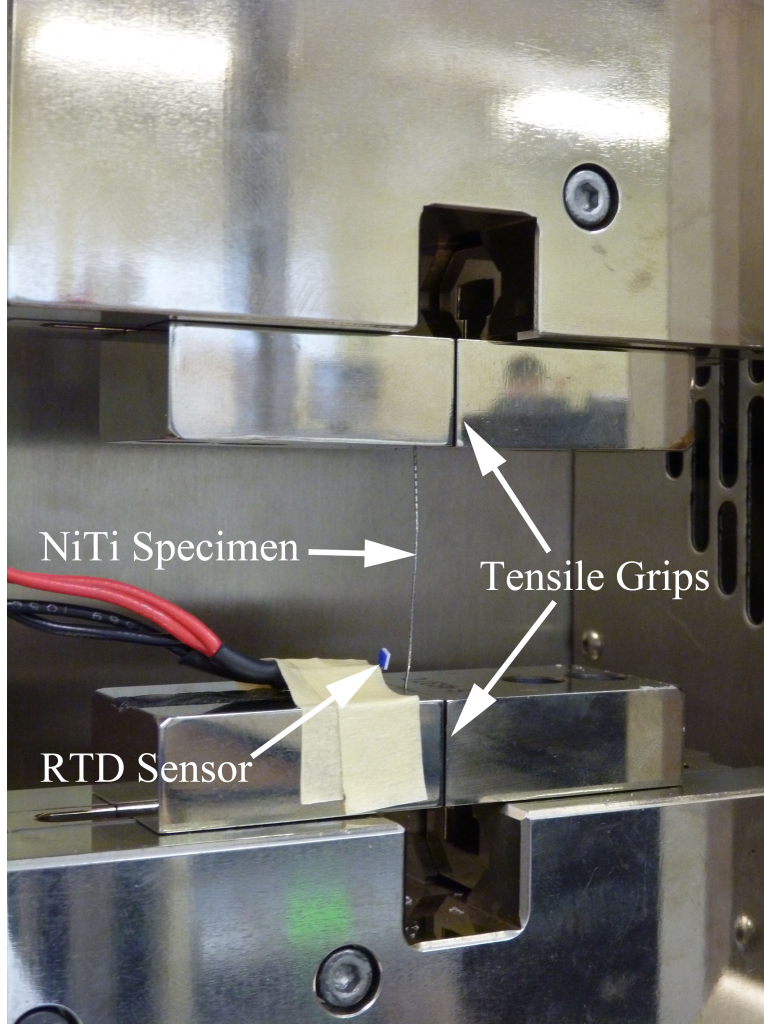
Figure 3.15: Tensile testing configuration for shape memory recovery assessment of the NiTi SMA wire samples.

Table 3.4: Phase transformation temperatures (°C) for the NiTi SMA wire samples.

Identifier	M_s	M_f	A_s	A_f
as-received BM	-	-	-	-
annealed BM	-23.5	-32.6	-16.0	0.7
laser processed	23.3	4.3	30.8	50.5

subzero onsets of the annealed BM. DSC scans also detected phase transformations from retained BM in the laser processed sample. As shown in Figure 3.17, some BM is retained between laser spots, due to the conical geometry of the laser processing volume.
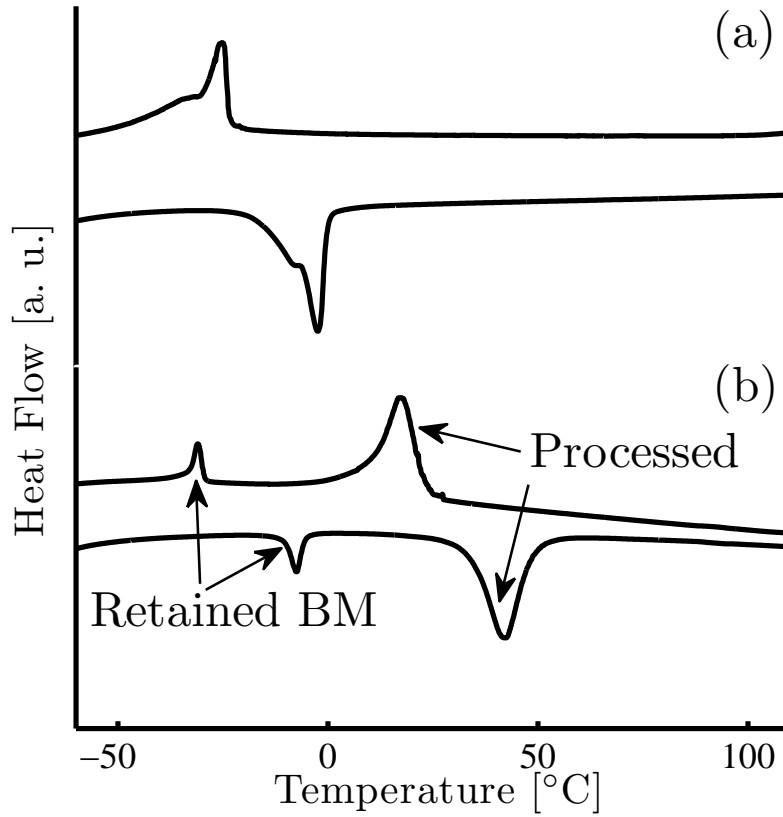
Figure 3.16: DSC scans of the annealed BM (a) and laser processed (b) NiTi SMA wires. Due to the conical geometry of the laser processing volume, some retained BM was sampled together with the laser processed NiTi wire.
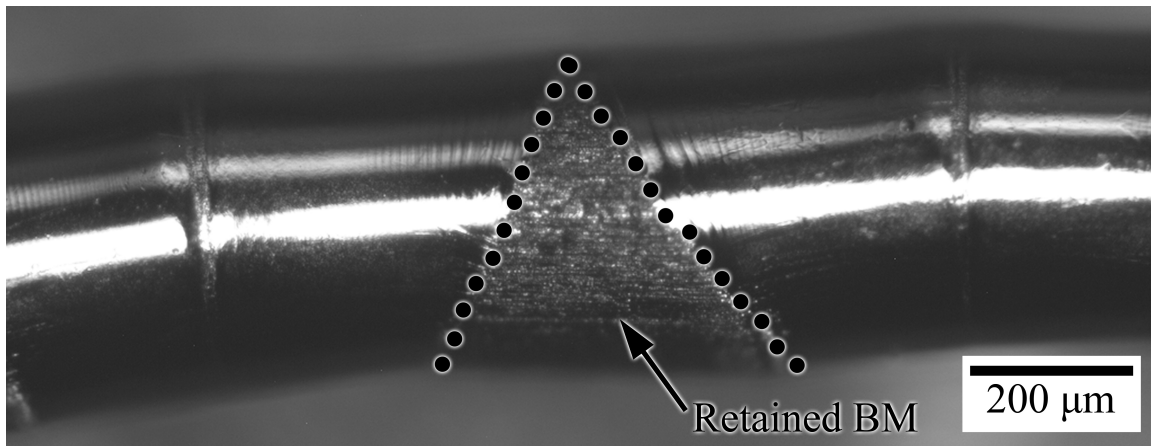
Figure 3.17: Optical micrograph of a NiTi SMA wire surface processed at 0% OL. This micrograph was captured perpendicular to the processing axis. Up to 200 μm of BM was retained between processing spots because of the conical melt geometry.
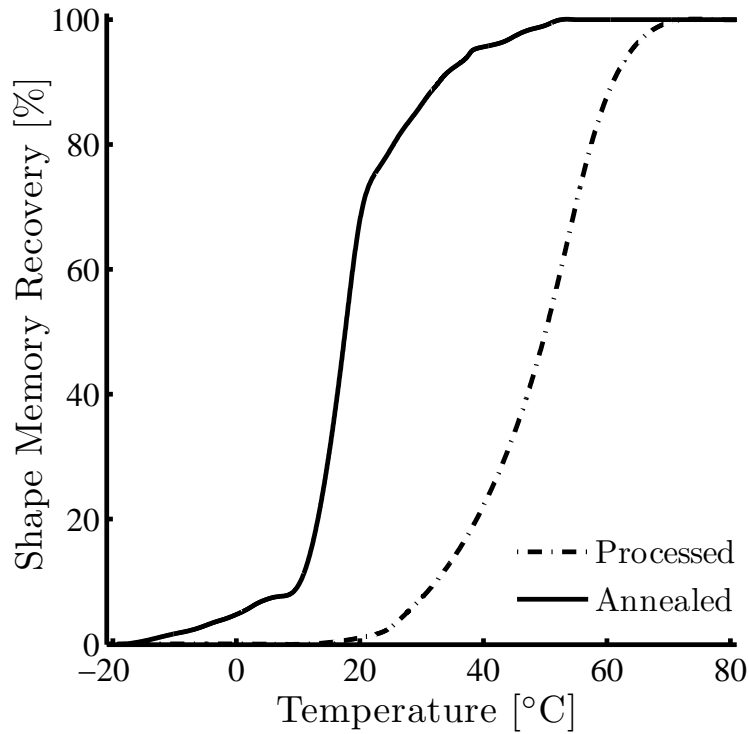
Figure 3.18: Shape memory recoveries of annealed BM and laser processed NiTi SMA wire specimens.

3.3.2.2 Changes in shape memory recovery

Figure 3.18 provides the captured data for the shape memory recoveries of the annealed BM and laser processed NiTi SMA wire samples. As anticipated from the DSC results, each NiTi wire exhibited a unique shape memory recovery. Temperatures corresponding with the onset of shape memory recovery (A_s) correlated well with phase transformation onset temperatures determined from DSC instrumentation. However, shape memory recovery progressed at temperatures above A_f for both the annealed BM and laser processed NiTi SMA wire specimens. This discrepancy can be explained by thermal sinking to the tensile grips and the relatively aggressive heating profile used during testing. Shape memory recovery was therefore slightly hindered in portions of the NiTi SMA wires which were adjacent to the gripping points.

3.3.2.3 Changes in pseudoelastic response

The tensile responses of the NiTi SMA wire specimens are provided in Figure 3.19. For stress calculations, optical micrographs and image processing software were used to determine the cross-sectional areas of the cold worked NiTi SMA wire specimens. Due to a large degree of prior cold working during manufacture, the as-received NiTi SMA was incapable of a stress induced phase transformation. Tensile loading therefore caused plastic deformation via dislocation movement and slip [1]. The aged NiTi SMA wire, however,

43

exhibited a pseudoelastic response with σ_m and σ_r loads of approximately 730 and 440 MPa respectively. As shown in Figure 3.19c, the laser processed NiTi SMA wire also exhibited pseudoelasticity, but at lower plateau stresses than the aged NiTi wire. Differences between pseudoelastic responses of the aged and laser processed NiTi SMA wire specimens were a result of the different phase transformation temperatures of the two specimens. In the case of the laser processed NiTi SMA wire, the austenite finish temperature was much higher, causing the austenite phase to be thermodynamically less stable [103]. A lower stress was therefore required to shear the cubic lattice to form SIM. The effects of laser processing have also caused a change in microstructure, which was likely the cause of the change in slope of the pseudoelastic plateau [26]. Both the aged BM and laser processed NiTi SMA wire specimens retained some plastic strain after unloading, which was attributed to localized yielding of unfavourably oriented grains in the microstructure [51]. Mechanical cycling of NiTi SMA wire specimens is required to stabilize their functional responses.

3.3.2.4 Augmented pseudoelastic response

In order to assess functionality enhancements which can be achieved with laser processing, an additional NiTi SMA wire sample, processed at -100% OL, was prepared and thermomechanically trained. Figure 3.20 provides the tensile response of the laser processed NiTi SMA wire. A two-stage pseudoelastic recovery can be identified from examination of the collected tensile data. The first loading plateau (σ_{m_1}, at approximately 400 MPa) corresponded to the laser processed volume of the sample and the second loading plateau (σ_{m_2}, at approximately 550 MPa) represented the pseudoelastic response of the aged NiTi retained in unprocessed segments of the wire. The plateau decrease and modulus change in the response of the aged NiTi SMA wire volume was likely due to recrystallization of the BM during laser processing operations (Figure 3.12c). To the author's knowledge, this represents the first example of a NiTi SMA wire capable of two independent pseudoelastic responses as the result of localized ablation of alloy species. Although the sample retained a small amount of plastic strain, mechanical cycling proved effective in producing a perfect pseudoelastic response. Cyclic decreases in pseudoelastic plateau stresses are a known phenomenon in NiTi SMAs and were likely caused by the development of internal stresses within the microstructure [104].

While this study has focussed on the thermomechanical properties of NiTi SMAs processed at 2 pulses, it is expected that similar enhancements in material functionality can be achieved using different pulsing protocols. Future work is therefore planned to further explore the functionality augmentations which can be achieved using laser processing.

3.3.3 Chapter summary

In the first section of this chapter, changes in the crystallographic, composition, and phase transformation dynamics of laser processed NiTi SMA strip were investigated in order to validate preliminary reports on laser processing technology. Results indicated that laser processing altered the localized Ti/Ni ratio, which induced a martensitic phase

transformation within the LPZ. DSC results confirmed a shift in phase transformation onset temperatures within the LPZ. NiTi samples processed for more than 5 pulses exhibited a stable M_s temperature ranging between 335 and 340K. These findings agreed well with reported results and therefore served as validation of laser processing technology.

Upon verifying the robustness of laser processing technology, induced changes in material functionality were examined. In the second section of this chapter, the effects of laser
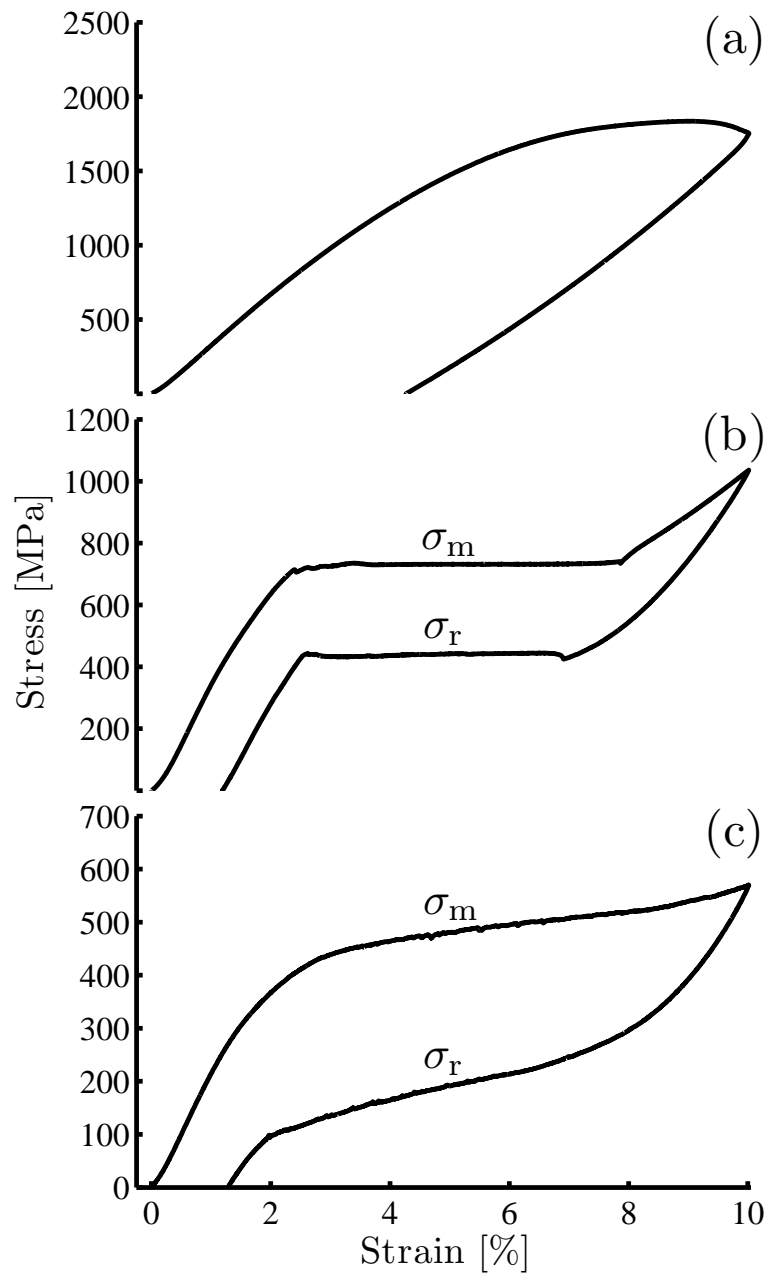
Figure 3.19: Tensile responses of as-received (a) and aged BM (b), and laser processed at 0% OL (c) NiTi SMA wire specimens. Testing was conducted at 60 °C.

ablation on the thermomechanical properties of a NiTi SMA wire processed at 2 pulses and 0% OL were investigated. DSC results showed a drastic increase in the phase transformation temperatures of laser processed NiTi SMA wire samples, which was anticipated from previous studies. As a result, the laser processed NiTi SMA wire was capable of recovering shape memory at temperatures approximately 40 °C higher than the reference material. Furthermore, pseudoelastic laser processed samples exhibited a stress induced transformation at approximately 300 MPa lower than the aged NiTi SMA wire. Tensile testing of a wire processed at -100% OL revealed two pseudoelastic plateaus and mechanical cycling of the processed specimen achieved a perfect pseudoelastic response. The vaporizing effects of
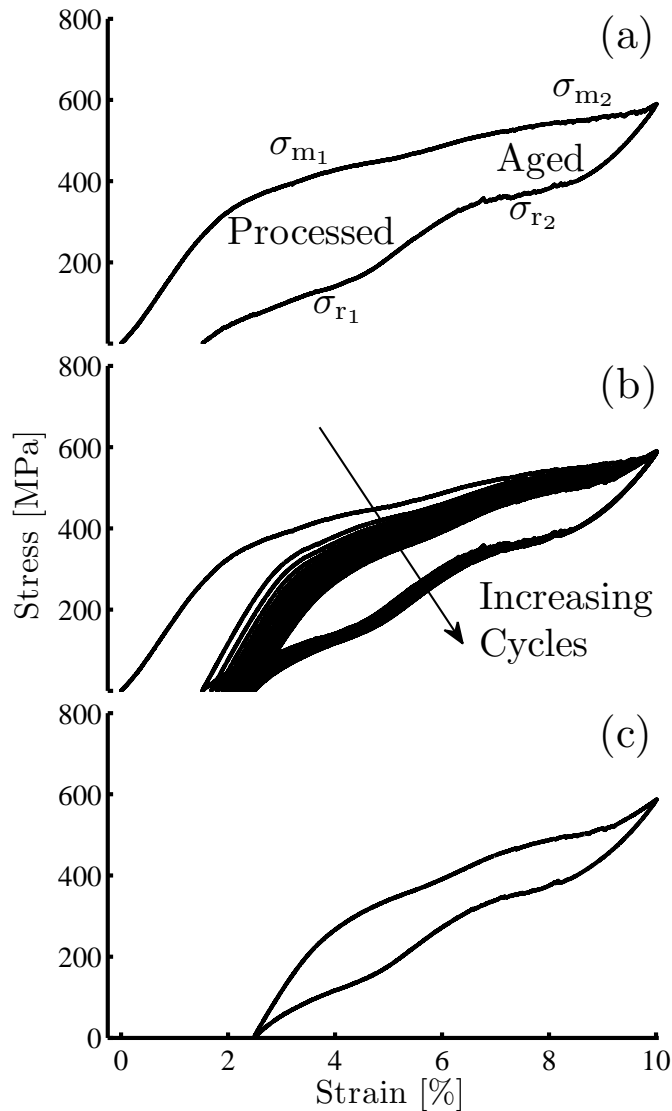
Figure 3.20: Pseudoelastic response of a NiTi SMA wire laser processed at -100% OL (a). The specimen exhibited an augmented response combining the individual behaviours of the aged and laser processed (0% OL) NiTi SMA wires. Mechanical cycling (b) of the sample produced a perfect pseudoelasticity after 20 cycles (c).

laser processing have therefore embedded an additional thermomechanical response within the NiTi SMA wire.

Laser processing technology has demonstrated the capability to augment the functionality of conventional NiTi SMAs by locally altering phase transformation dynamics within processed material domains. Through localized ablation of alloy species, laser processed NiTi SMAs can be exploited to unlock additional thermomechanical characteristics. Laser processed NiTi SMAs are therefore capable of augmented functional responses which manifest as additional shape memory recoveries and pseudoelastic responses. Implementation of laser processing protocols is therefore expected to lead to unprecedented NiTi SMA offerings and novel applications.

Chapter 4

Effects of laser alloying on the thermomechanical behaviour of NiTi SMAs

While NiTi SMAs have enjoyed relative success in many applications, next generation technologies require more precise control over their active thermomechanical properties. Furthermore, the controllability of conventional NTi devices remains inhibited due to a well-known hysteresis associated with its functional response [105]. One established method to improve thermomechanical behaviour in NiTi is through the introduction of copper (Cu) into the binary system which results in the formation of the ternary NiTiCu IMC [106, 107]. Acting as a nickel substitutional, investigations have shown that relatively small amounts of Cu reduce friction in the NiTi lattice and can therefore significantly narrow the transformation hysteresis loop [63, 71]. Furthermore, the addition of Cu to NiTi simultaneously modifies thermomechanical behaviour in the SMA by altering the Ti:(Ni, Cu) ratio. The purpose of the present chapter is to expand the functional properties of a conventional NiTi SMA by implementing laser processing to locally alloy Cu into the BM. The resulting hybrid structure represents the first combination of binary NiTi and ternary NiTiCu SMA species within a monolithic alloy. Through laser processing operations, the functional properties of the conventional NiTi are augmented with a localized set of NiTiCu shape memory characteristics; therefore permitting a multi-stage SMA recovery with improved hysteresis.

4.1 Experimental

Commercially available cold-rolled 400 μm NiTi strip with a nominal composition of 50.8 at.% Ni and 49.2 at.% Ti was used as the reference alloy for this investigation. The as-received material was solution treated in a vacuum furnace at 800 °C for 3.6 ks followed by an argon gas quench. This heat treatment protocol was designed to achieve an annealed condition and remove any prior thermomechanical training. Prior to processing,
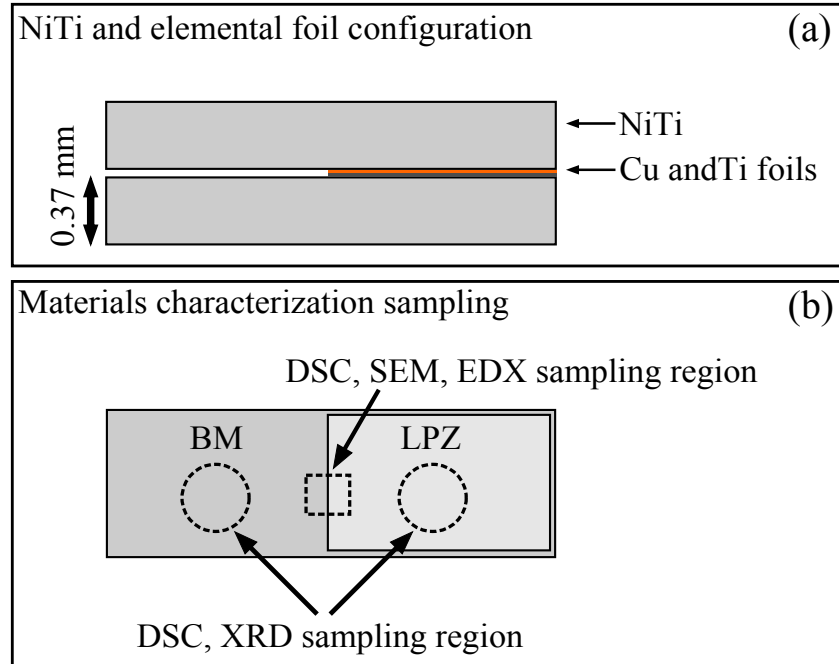
Figure 4.1: Cross-sectional view (not to scale) of the laser processing configuration for the NiTi-NiTiCu SMA (a). Top view of laser processed specimen outlining the BM-LPZ interface and bulk regions sampled for materials characterization testing (b). Figure reprinted from [108] with permission from the Institute of Physics.

the solutionized NiTi was chemically etched with a hydrofluoric-nitric acid solution to remove surface oxides; uniformly reducing the strip thickness to 370 μm.

Localized alloying of the as-received NiTi BM was achieved using a Miyachi Unitek model LW50-A pulsed Nd:YAG laser source with a nominal post-optic spot size of 600 μm. In this study, laser energy was used to locally melt elemental constituents into the parent NiTi matrix. Chemically cleaned, high purity foils were used as elemental sources for laser processing operations. Given that solutionized NiTi exhibits shape memory characteristics in only the near-equiatomic range, a stoichiometric ratio of Ti was alloyed along with Cu in order to maintain Ti solubility, ensure substitutional competition of Ni and Cu, and eliminate the precipitation of unwanted Ni or Cu rich IMCs. In order to protect the LPZ from atmospheric contaminants, argon shielding was provided at a rate of 0.85 m^3/hr (30 ft^3/hr). An illustration of the laser processing configuration and areas sampled for materials characterization is provided in Figure 4.1. A sample region measuring approximately 1 cm by 1 cm was laser processed for this study. Samples were laser processed at 1.5 kW power for 10 ms (rectangular pulse under a 50% OL pulsing profile. Full laser penetration through the sample cross-section was achieved to ensure proper melting. In its molten state, the LPZ was expected to rapidly homogenize due to Marangoni convection effects.

In order to confirm the presence of the NiTiCu IMC within the LPZ, sample composition and crystal structure were investigated. A Jeol JSM-6460 SEM equipped with an INCA X-Sight 350 EDX analysis aperture were used for microscopy and chemical analysis

of the BM-LPZ interface. As per a recent study by Undisz et al. [98], a dilute HF etchant was used for microstructure analysis to limit surface pitting and avoid the formation of surface artifacts. Crystallographic data was collected from the BM and LPZ structures using XRD analysis. XRD patterns were captured using a Rigaku SA-HF3 (1.54 Å Copper-Kα) X-ray source equipped with an 800 μm collimator, operating at an excitation voltage of 50 kV. Specimens were carefully extracted from the LPZ bulk to prevent inadvertent sampling of the BM.

Changes in phase transformation temperatures and thermal hysteresis in the hybrid NiTi-NiTiCu specimen were quantified via DSC testing using a Thermal Analysis Q2000 acquisition system equipped with a refrigerated cooling unit. For data collection, a modified ASTM F2004–05 testing standard was followed. Heat flow was measured at a controlled heating and cooling rate of 5 °C/min in a range from -75 °C to 120 °C. Austenite and martensite start and finish temperatures (A_s and A_f, M_s and M_f respectively) were defined according to the ASTM standard and thermal hysteresis was calculated as the difference in temperature between peak heat flows in the heating and cooling curves.

Shape memory recovery of the NiTi-NiTiCu hybrid SMA was evaluated using an Instron model 5548 micro-tensile tester capable of a $\pm$ 0.02 μm position resolution and $\pm$ 0.5 μm measurement accuracy. In order to assess the shape memory response of the BM and LPZ, samples were cooled to below M_f of the BM inside an environmental chamber and indented to a load of 100 N with a 1.6 mm (1/16 in.") diameter spherical tip positioned in the tensile gripper jaws. A photograph of the indentor setup is provided in Figure 4.2. After indentation, the samples were environmentally heated with a monotonic profile at a rate of 15 °C/min to above A_f of the LPZ. During heating, a zero load condition was maintained on the crossheads and indentation depth was continually monitored. The measured depth was then normalized against the final indentation depth and correlated with the collected temperature data to provide an in situ assessment of shape memory recovery. Specimen temperature was measured using a RTD. The collected temperature measurements were digitally filtered using a low pass Butterworth algorithm to eliminate high frequency noise originating from input AC line voltages [102]. In order to visualize the changes in surface topography from deformation and heating operations, a Veeco model WYKO NT1100 optical profiler with a depth resolution of 3 nm was used to image the indentation site of the LPZ at each stage of testing.

4.2 Results and discussion

4.2.1 Detection of the NiTiCu IMC

Results from chemical analysis indicate that the Cu was well dispersed throughout the LPZ solidification structure. Due to the rapid cooling rates associated with laser processing, a distinct change in microstructure was observed between the LPZ solidification structure and equiaxed NiTi BM grains. As shown in Figure 4.3, SEM imaging revealed dendritic grain growth and a typical solidification structure at the BM-LPZ interface which
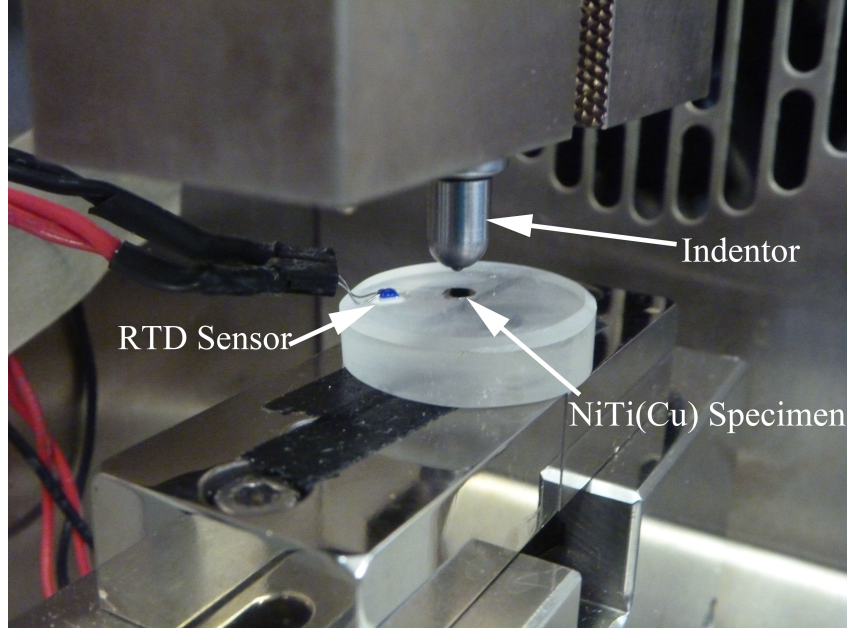
Figure 4.2: Indentor configuration for shape memory recovery assessment of the NiTi(Cu) SMA samples.

formed a well-defined boundary between material domains. An EDX line scan captured at the processing boundary showed a drastic rise in Cu content upon crossing the BM-LPZ processing line; quickly reaching bulk concentrations within a few μm of the interface. From further EDX analysis of the LPZ, the averaged bulk composition of the LPZ was determined to be $Ni_{31.9}Ti_{52.1}Cu_{16}$ with a measurement standard deviation of 2 at.%. Although EDX results are expected to be accurate to $\pm$ 1at.%, incomplete Marangoni mixing was likely the cause of minor inhomogeneities within the LPZ solidification structure.

While the results of chemical analysis have detected Cu within the LPZ, it was necessary to verify the crystal structure of the NiTiCu IMC using XRD techniques. Results of the room temperature XRD analysis collected from the BM and LPZ are provided in Figure 4.4. In order to clearly illustrate the subtle differences in crystal structures, a narrow 2θ range is presented. The obtained data agreed well with reference diffraction patterns for the NiTi and NiTiCu structures. Results indicated that the BM possessed the expected cubic B2 austenite diffraction pattern, whereas the LPZ exhibited an orthorhombic B19 martensite structure [109]. It is well understood that Cu content drives competing orthorhombic and monoclinic martensite transformations in the NiTiCu system and therefore detection of a B19 orthorhombic structure as opposed to the typical B19' monoclinic crystal was not unexpected [63]. Furthermore, diffraction patterns from elemental Cu or Ti, common NiCu and TiCu compounds, nor the parent NiTi alloy were detected in the LPZ.
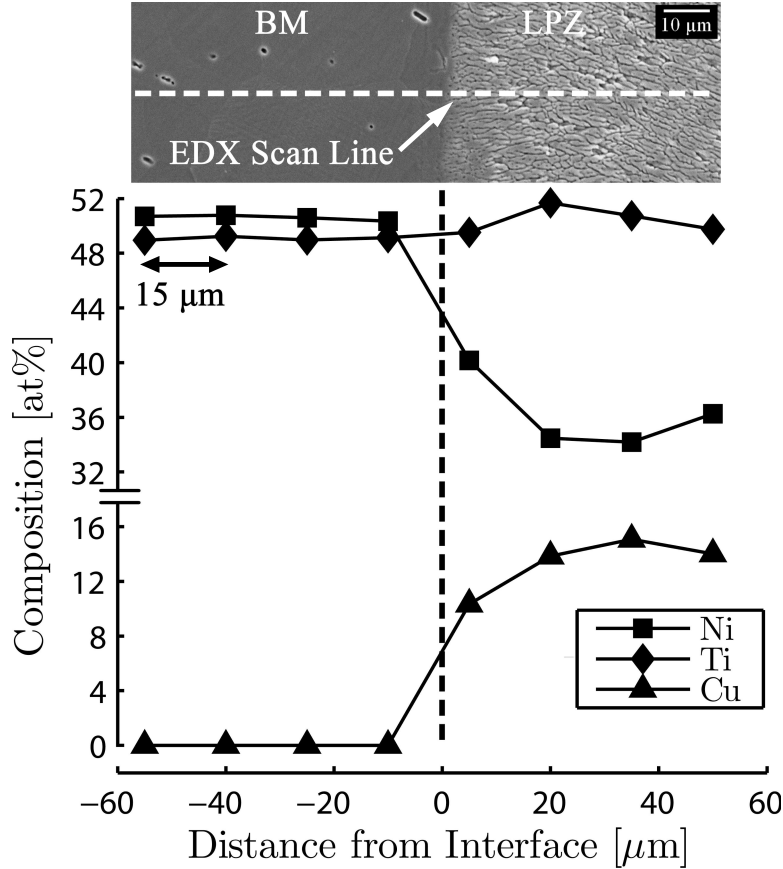
Figure 4.3: EDX line profile and microstructure cross-section along the BM-LPZ interface. Figure reprinted from [108] with permission from the Institute of Physics.

4.2.2 Effects of laser processing on phase transformation temperatures and thermal hysteresis

The collected DSC scans for the NiTi BM and NiTiCu LPZ bulk are shown in Figures 4.5a and 4.5b, with the extrapolated transformation onset and finish temperatures and hysteresis provided in Table 4.1. A considerable shift in phase transformation onsets was detected for the LPZ material domain, which increased well above the subzero temperatures observed in the BM. For example, M_s was found to increase by approximately 100 °C in the NiTiCu domain when compared to the unprocessed NiTi. Furthermore, results showed a significant reduction in transformation hysteresis of nearly 50% between the BM and LPZ material domains, which is desirable for controls applications. This drastic reduction of transformation hysteresis agreed very well with trends reported by Miyazaki and Ishida [71], who established a lower threshold for hysteresis in the NiTiCu system at approximately 12 °C in chemistries greater than 10 at.% Cu. Increases in DSC peak widths in the LPZ bulk were attributed to the minor inhomogeneity within the solidification structure. Since onset temperatures in NiTi SMA systems are extremely sensitive to composition [15], minute variations within the LPZ created a wider thermal range in which the austenite-
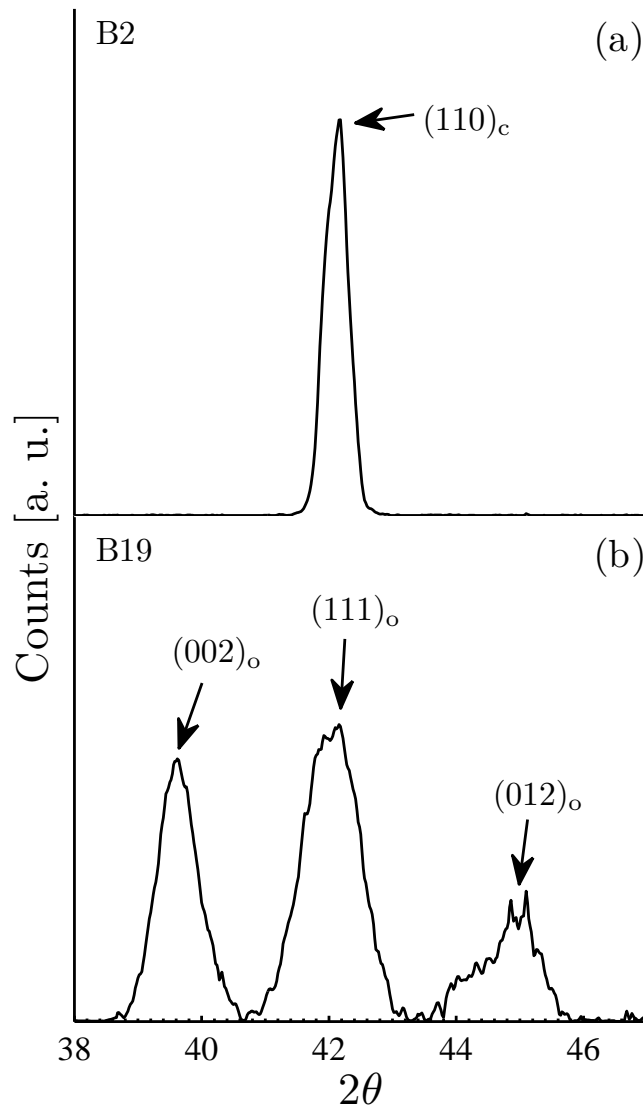
Figure 4.4: Room temperature XRD patterns of B2 cubic BM austenite (a) and B19 orthorhombic LPZ martensite crystal structures (b). Figure reprinted from [108] with permission from the Institute of Physics.

martensite phase transformation progressed [101]. In order to provide further evidence of hybrid functionality, a DSC scan of the BM-LPZ interface, illustrating both transformation characteristics, is provided in Figure 4.5c. Distortion of transformation peaks are believed to be the result of internal stresses at the material interface.
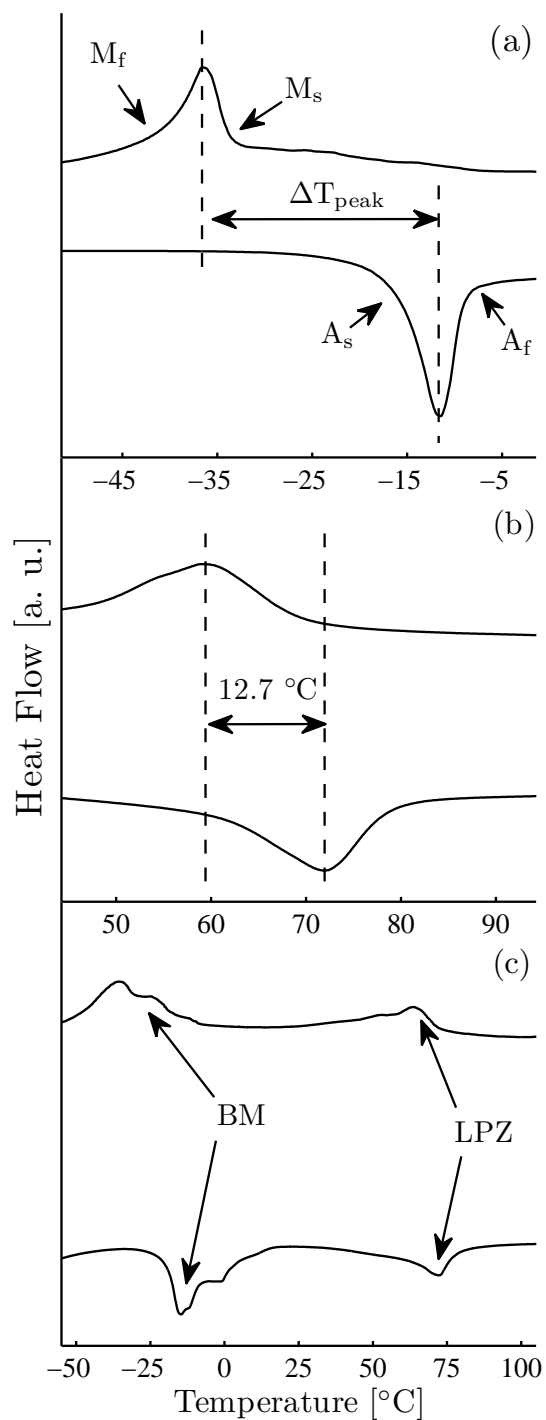
Figure 4.5: DSC scans of the BM (a) and LPZ (b) bulk, and BM-LPZ interface (c) showing altered hysteresis and shifted onset temperatures. Abscissae are offset in (a) and (b) to illustrate hysteresis narrowing. Figure reprinted from [108] with permission from the Institute of Physics.

Table 4.1: Phase transformation temperatures and hystereses (°C) for the BM and LPZ bulk.

Material Domain	A_s	A_f	M_s	M_f	ΔT_{peak}
BM	-16.1	-8.6	-33.0	-41.3	24.9
LPZ	59.5	79.3	69.9	44.7	12.7

4.2.3   Shape memory response of the NiTi-NiTiCu hybrid

The effects of laser processing have locally embedded a unique thermal response within the as-received NiTi BM. Prior to processing operations, the NiTi BM was capable of only a single thermomechanical response which is dependent on its fabrication history. Introduction of Cu has altered the phase transformation temperatures and thermal hysteresis properties of the BM. A complementary change in thermomechanical response was therefore expected. Results from indentation testing confirmed the presence of two independent thermomechanical domains within the NiTi-NiTiCu SMA. Provided in Figure 4.6, the collected data shows independent recoveries of the BM and LPZ as they are heated through their respective phase transformation ranges (A_{s_1}, A_{f_1} and A_{s_2}, A_{f_2}). The specific onset and finish temperatures observed in indentation testing differed slightly from the extrapolated DSC measurements due to thermal sinking to the indentation head. Despite the relatively aggressive heating profile used during thermal cycling of indented specimens, differences in transformation ranges between the BM and LPZ were well represented by the collected data and agreed well transformation peak widths observed in DSC data.

In order to better visualize the recovery of indented specimens, surface topological profiles were collected at each stage of indentation testing for the LPZ. Given that the measurement range of the surface profilometer was limited to an area measuring 300 μm by 225 μm, a less aggressive indentation load of 15 N was used to ensure that surface distortion was isolated to the measurement window. As shown in Figure 4.7, the initially flat LPZ specimen was indented to a relative depth of approximately 2 μm. Upon heating the LPZ above its A_f temperature, the surface distortion directly beneath and periphery to the indentation site recovered. As reported by Ni et al. [110], a complete recovery of the pristine surface was not expected due to the complex strain distribution and material pile-up developed during indentation operations.

4.2.4   Enhanced functionality of the NiTi-NiTiCu hybrid alloy

Comparison of the collected materials characterization analyses revealed that the binary parent NiTi structure has been reorganized into a ternary NiTiCu IMC within the LPZ. As shown in Figures 4.5 and 4.6, laser alloying of Cu has created a new material domain with shifted phase transformation temperatures; therefore embedding a unique shape memory response within the LPZ. Furthermore, transformation hysteresis was reduced in the LPZ, leading to improved SMA controllability. To the author's knowledge, this study represents the first example of a NiTi based SMA that possesses an enhanced thermomechanical functionality as the result of a locally embedded NiTiCu ternary system.
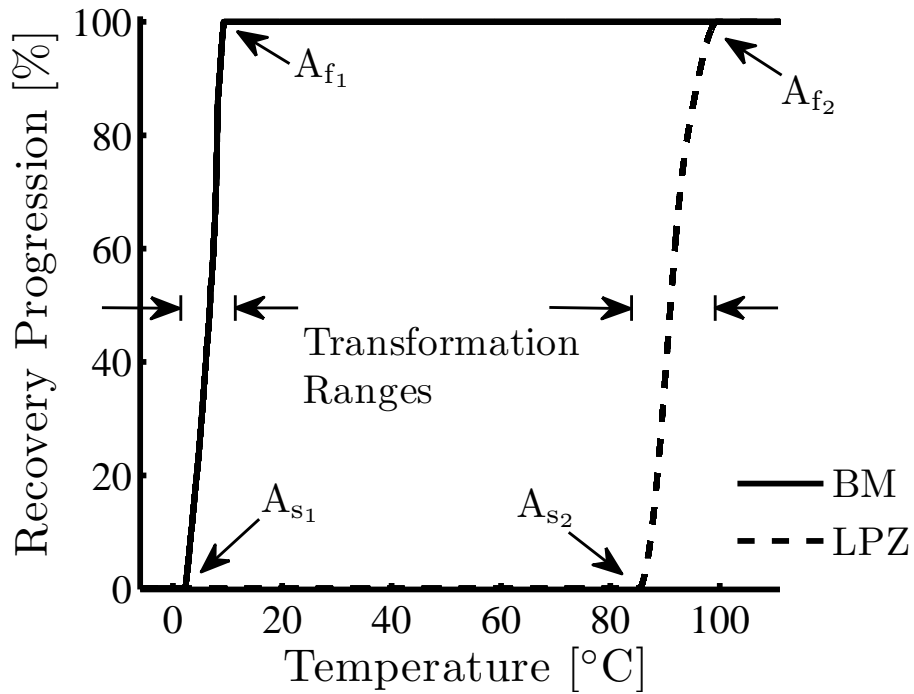
Figure 4.6: Shape memory recovery of the BM and LPZ as determined by indentation testing. BM and LPZ samples were each indented below M_f of the BM and then heated monotonically to above A_f of the LPZ. Figure reprinted from [108] with permission from the Institute of Physics.

Laser processing of the as-received NiTi BM has created a hybrid SMA which possesses a customizable set of shape memory responses. From a device functionality perspective, unique shape memories can be triggered by progressively heating the NiTi-NiTiCu hybrid through its active thermal range. Unprecedented novel applications can therefore be realized by exploiting the multi-functional capabilities of this monolithic NiTi-NiTiCu SMA.

This study has focused on the enhanced thermomechanical behaviour that was achieved through localized alloying of Cu into a parent NiTi alloy. However, the extent to which the laser alloying process can be used to enhance the functionality of conventional NiTi requires further investigation. Furthermore, mechanical interactions between processing domains and BM are not fully understood. Future work will focus on understanding micro-mechanical dynamics along processing interfaces and characterization of complementary changes in pseudoelastic behaviour. Investigation of other known ternary NiTi intermetallic species such as Pd, Hf, Zr, Cr, and Co is also planned in order to exploit other performance enhancing chemistries.
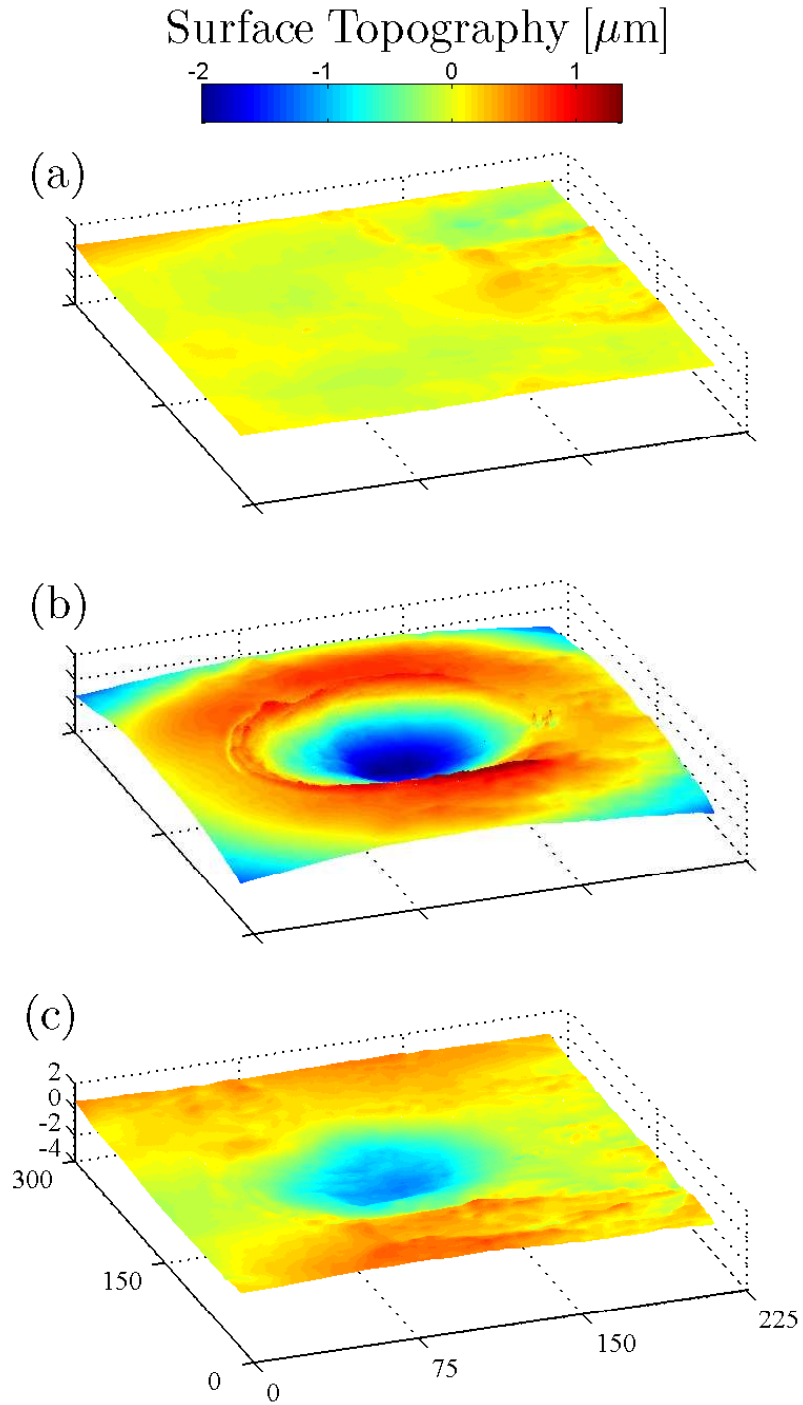
Figure 4.7: Surface topography of the indentation site of the LPZ at each stage of shape memory testing: prior to indentation (a); after indentation (b); and after heating above A_f (c). Axis labels are all in units of μm. Figure reprinted from [108] with permission from the Institute of Physics.

4.3 Chapter summary

Laser processing technology has been used to locally alloy Cu into a NiTi SMA. The localized synthesis of a NiTiCu IMC was confirmed through chemical and crystallographic analyses. Results from DSC instrumentation showed that the NiTiCu material domain possessed a unique thermal behaviour in comparison to the NiTi BM. Phase transformations in the LPZ were detected at over 50 °C above the sub-ambient austenite finish temperatures of the BM. Furthermore, the transformation hysteresis in the LPZ was found to be significantly reduced to 12.7 °C, which represented a significant improvement in SMA controllability. Data captured from indentation testing indicated that the NiTi-NiTiCu hybrid SMA possessed two unique shape memory recoveries, whose independent responses were a result of the composition differences between the BM and LPZ material domains. The combined thermomechanical responses of the NiTi-NiTiCu SMA hybrid represent a significant augmentation of traditional NiTi SMA capabilities and permit an enhanced functional material offering.

Chapter 5

Enhanced thermomechanical functionality of a novel laser processed NiTi shape memory microgripper

With the surging demand for microsystems technology in the aerospace and biomedical industries, a significant need has developed for elegant smart material mechanisms to replace conventional electro-mechanical systems. NiTi SMAs are considered a top candidate for a variety of next generation smart materials applications because of their excellent combination of mechanical properties and biocompatibility [3, 4, 111]. While NiTi has enjoyed relative success in many microsystems devices, future technologies demand more precise control over its functional thermomechanical properties; namely the shape memory effect.

Recent investigations have shown that exposure to high density laser energy can alter thermomechanical behaviour in NiTi by shifting phase transformation onset temperatures within the processing region [20, 25, 26, 108, 112]. This technique can be used to locally tune the thermomechanical response of conventional NiTi SMAs [24, 113]. Laser processing therefore permits the localized embedment of unique shape memory responses within a monolithic NiTi structure; thus enhancing the functionality of NiTi by augmenting its thermomechanical characteristics. The purpose of the present work is to implement laser processing to fabricate a novel NiTi based microsystems device with enhanced thermomechanical functionality.

Given the complicated path trajectories demanded from smart material microsystems technologies, monolithic fabrication of NiTi devices is usually not practical and SMA components are often integrated into hybrid packages [5]. For example, several hybrid designs exist for NiTi microgripper heads. Lee et al. [94] have developed a passively biased SMA microgripper by sputtering a NiTi film onto a silicon substrate and Kohl et al. [95] created an integrated antagonistic SMA microgripper through laser micromachining of a NiTi thin sheet. Although each of these designs achieves gripper actuation through

exploitation of the shape memory effect, device performance is inherently limited by their reliance on external systems to position the microgripper head during gripping operations. In order to eliminate the need for external positioning systems, presented in this work is a monolithic laser processed NiTi microgripper capable of self-positioning. Actuation of positioning segments and the device gripper head is achieved through the sequential activation of unique thermomechanical regimes. The added thermomechanical functionality of the laser processed NiTi eliminates the need for external positioning systems and greatly reduces the complexity of the NiTi microsystems device. To the authors knowledge, this study represents the first example of a monolithic NiTi microgripper that possesses multiple recoverable thermomechanical characteristics.

5.1 Experimental

Commercially available 410 μm diameter NiTi wire with a nominal composition of 50.8 at.% Ni and 49.2 at.% Ti was used for microgripper construction (referred to as BM). Prior to laser processing, the surface oxides were removed using a hydrofluoric-nitric acid etching agent; uniformly reducing the wire diameter to 380 μm.

Laser processing was achieved using a Miyachi Unitek pulsed Nd:YAG laser system (Model LW50 A) which produced a 1.06 μm wavelength beam and possessed a nominal post-optic spot size of 600 μm. In order to process larger lengths of NiTi wire, a custom fixture was designed to advance the wire between laser pulses. Processing parameters were selected to locally embed three unique thermomechanical responses within the as-received NiTi alloy. NiTi samples were processed at 0% OL using the parameters from Figure 3.6. Pulsing protocols of 2, 4 and 10 pulses were implemented in fabrication of the microgripper components. In each laser processing schedule, full melting of the BM was achieved. The two lower temperature thermomechanical material domains were designed to actuate the positioning segments of the microgripper and the higher temperature shape memory was used to close the microgripper head. In order to avoid contamination during laser processing operations, argon shielding was provided to the processing region at a flow rate of 0.42 m^3/hr (15 ft^3/hr). After laser processing operations, the wire was resistively shape trained using a Sorensen XG series 33-25 programmable DC power supply. Figure 5.1 illustrates the processing dimensions of the NiTi wire and microgripper shape-set geometry.

In order to confirm the embedment of independent thermomechanical material domains within the laser processed NiTi microgripper, DSC analysis was used to capture changes in phase transformation onset temperatures in the NiTi samples. DSC scans were performed using a Thermal Analysis Q2000 system equipped with a refrigerated cooling system. As-received and laser processed samples were prepared for comparison. Given the high power densities associated with laser processing, a heat treated wire specimen was also analyzed to ensure that changes in phase transformation onsets were not the result of localized annealing of the as-received material. Sample data were collected using a modified ASTM F2004-05 testing protocol. Heat flow was measured at a controlled heating and cooling rate of 5 °C/min and austenite and martensite start and finish temperatures (A_s and A_f, M_s and M_f respectively) were defined following the ASTM standard.
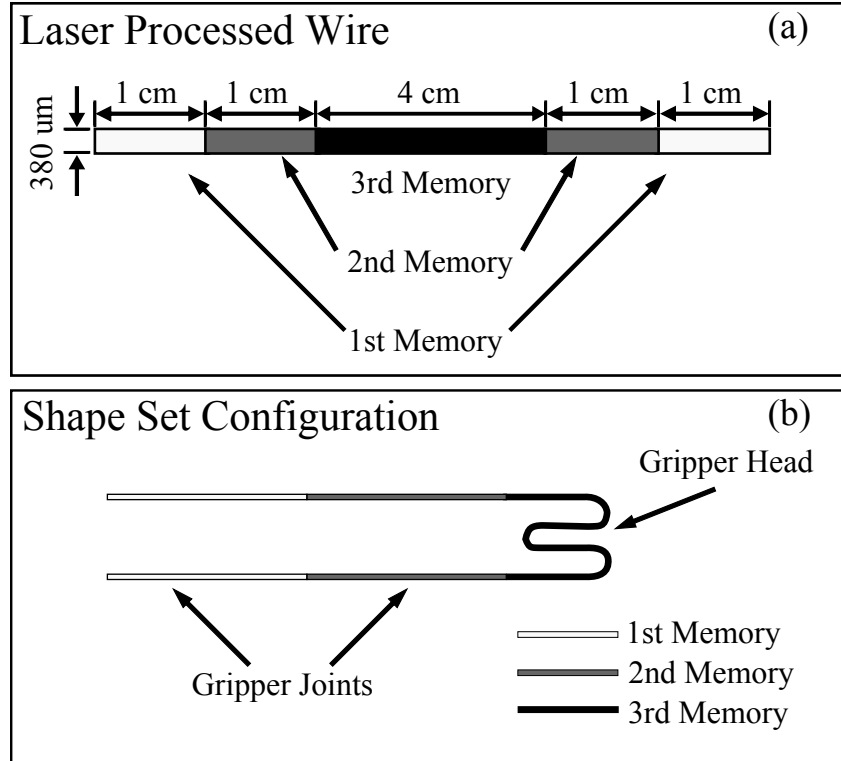
Figure 5.1: Processing dimensions of the NiTi microgripper (not to scale). Dimensions of the laser processed NiTi wire (a). Configuration of the laser processed regions after resistive shape setting (b). Figure reprinted from [114] with permission from Sage Publications.

Shape memory recovery of the laser processed NiTi samples was assessed using an Instron model 5548 micro-tensile machine with a $\pm$ 0.5 μm measurement accuracy (Figure 3.15). Tensile samples were loaded at room temperature (20 °C) under an ASTM F2516–07 testing protocol at a rate of 1.0 mm/min to 6% strain and then subsequently relaxed. Upon complete unloading, laser processed samples were heated in situ to above A_f in an environmental chamber in order to activate each embedded thermomechanical response. A zero load condition was maintained at the crossheads and displacement feedback was continuously recorded in order to assess material recovery. The measured displacement was then normalized against the final length of the NiTi SMA wire and then correlated with collected temperature data to track shape memory recovery. Temperature measurements were recorded using a thin film RTD.

Actuation of the laser processed NiTi microgripper was achieved by resistive heating methods that were controlled using a National Instruments PXI-1031 data acquisition module equipped with a RTD. In order to assess phase transformations in situ, online resistivity measurements were captured by monitoring applied voltage and current loads during microgripper actuation. The uncertainty in resistance measurements was $\pm$ 0.013 Ω (95%), as specified by the manufacturer of the power supply implemented for resistive heating. In order to eliminate high frequency signal noise from AC line voltages, the collected thermomechanical and resistivity data were filtered using a low-pass Butterworth

algorithm [102].

5.2 Results and discussion

5.2.1 Detection of embedded thermomechanical behaviour

The collected DSC scans and corresponding phase transformation onset temperatures are provided in Table 5.1 and Figure 5.2, respectively. Examination of the as-received sample showed a single diffuse sub-ambient phase transformation. The broad transformation range and low hysteresis were typical of trained NiTi and are commonplace in commercially available material [23]. As shown in Figure 5.2b, the effects of heat treatment on the as-received material have destroyed prior material training and re-established a thermal response consistent with solutionized NiTi [12]. DSC scans of the microgripper components (Figures 5.2c-e) revealed sub-ambient heat flow peaks which were attributed to transformations from retained BM. As shown in Figure 5.3a, a portion of the NiTi samples was not melted during laser pulsing operations due to the conical geometry of the processing region. Optical microscopy of an isolated laser pulse revealed a recrystallized zone approximately 100 - 200 μm in width (Figure 5.3b). A thermal response typical of annealed NiTi was therefore not unexpected in the laser processed samples. The slight distortions detected in the BM phase transformation dynamics were likely due to the relatively small volume fraction of retained BM in the DSC sample.

In addition to transformation peaks from retained BM, results from DSC testing captured three additional thermal responses which were absent in the as-received and heat treated NiTi samples. The effects of laser processing therefore embedded three unique thermal behaviours within the single NiTi wire - allowing for independent shape memories to be recovered upon heating samples above their respective A_f temperatures. A slight recovery overlap existed, however, between the two higher temperature laser processed NiTi samples which requires further characterization to determine the impact on microgripper performance.

Table 5.1: Phase transformation temperatures of the NiTi BM and laser processed microgripper components ($^\circ$C).

Sample	M_s	M_f	A_s	A_f
as-received BM	19.1	-28.8	-25.9	19.7
annealed BM	-19.7	-30.3	-9.2	2.7
1st segment	20.2	-6.1	20.6	44.9
2nd segment	52.1	15.0	47.9	88.8
3rd segment	63.4	33.4	70.5	95.1
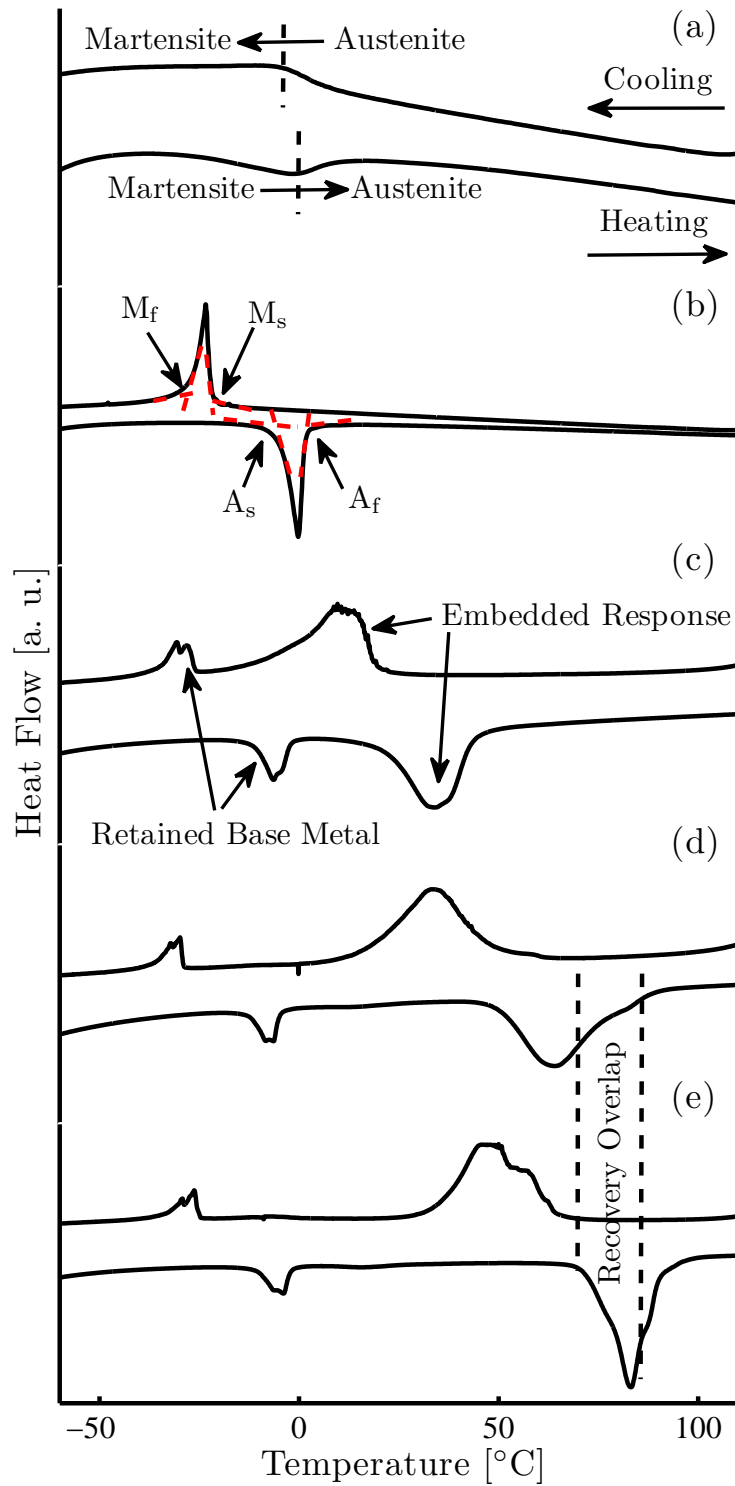
Figure 5.2: DSC scans of the (a) as-received BM, (b) BM heat treated at 800 °C for 300 s, and components of the laser processed NiTi microgripper: first segment (c); second segment (d); and microgripper head (e). Figure reprinted from [114] with permission from Sage Publications.
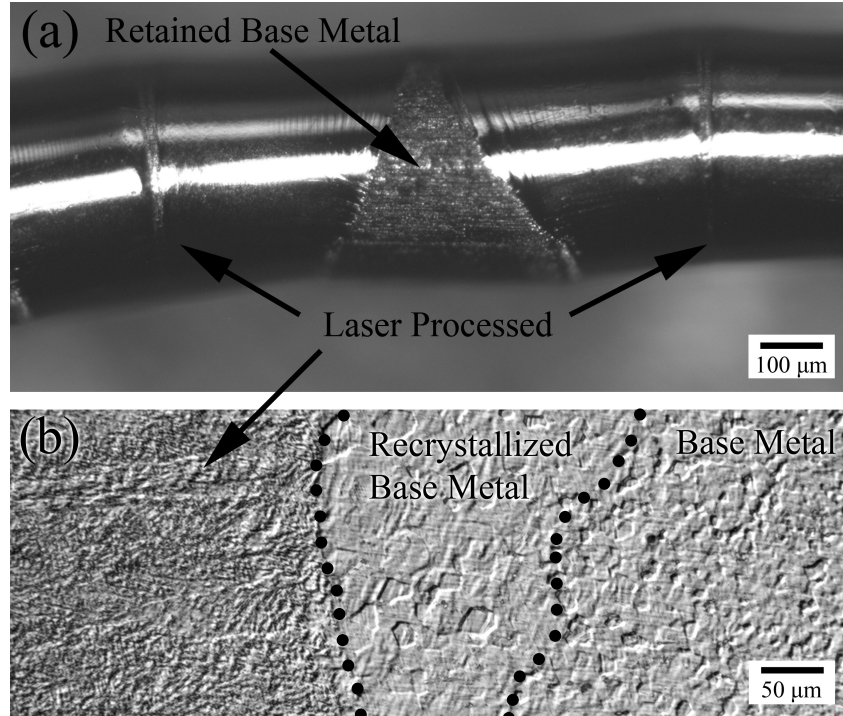
Figure 5.3: Optical micrograph of a typical laser processed NiTi specimen (a) and microstructure of the processing interface (b) for an isolated laser spot. Due to the conical geometry of the processing volume, a relatively small amount of BM was not melted during laser processing operations. Figure reprinted from [114] with permission from Sage Publications.

5.2.2 Shape memory recovery of the laser processed microgripper

Results from tensile testing of individual NiTi microgripper components indicated that, in addition to unique thermal behaviour, the laser embedded material domains possessed different mechanical properties. As shown in Figure 5.4a-c, each of the three active microgripper components exhibited unique stiffening characteristics. As the most thermally stable martensite at room temperature, the microgripper head exhibited the largest resistance to detwinning, which was consistent with trends reported by Miyazaki et al. [103] for solutionized NiTi.

In order to evaluate the combined mechanical responses of microgripper components, a NiTi sample processed to the microgripper dimensions was prepared. As shown in Figure 5.4d, the microgripper underwent a multi-stage detwinning when loaded. At stresses below σ_{Dt_1}, the mechanical response was linear elastic. In the load range of $\sigma_{Dt_1} < \sigma < \sigma_{Dt_2}$, a detwinning of the first microgripper positioning segment occurred. Subsequent detwinning of each of the laser processed microgripper components occurred, which was evident from changing inflections along the microgripper tensile response curve.

Identified by its characteristic serrated Lüders-like mechanical deformation [48], a pseudoelastic response from the retained BM was visible in each of the stress-strain curves
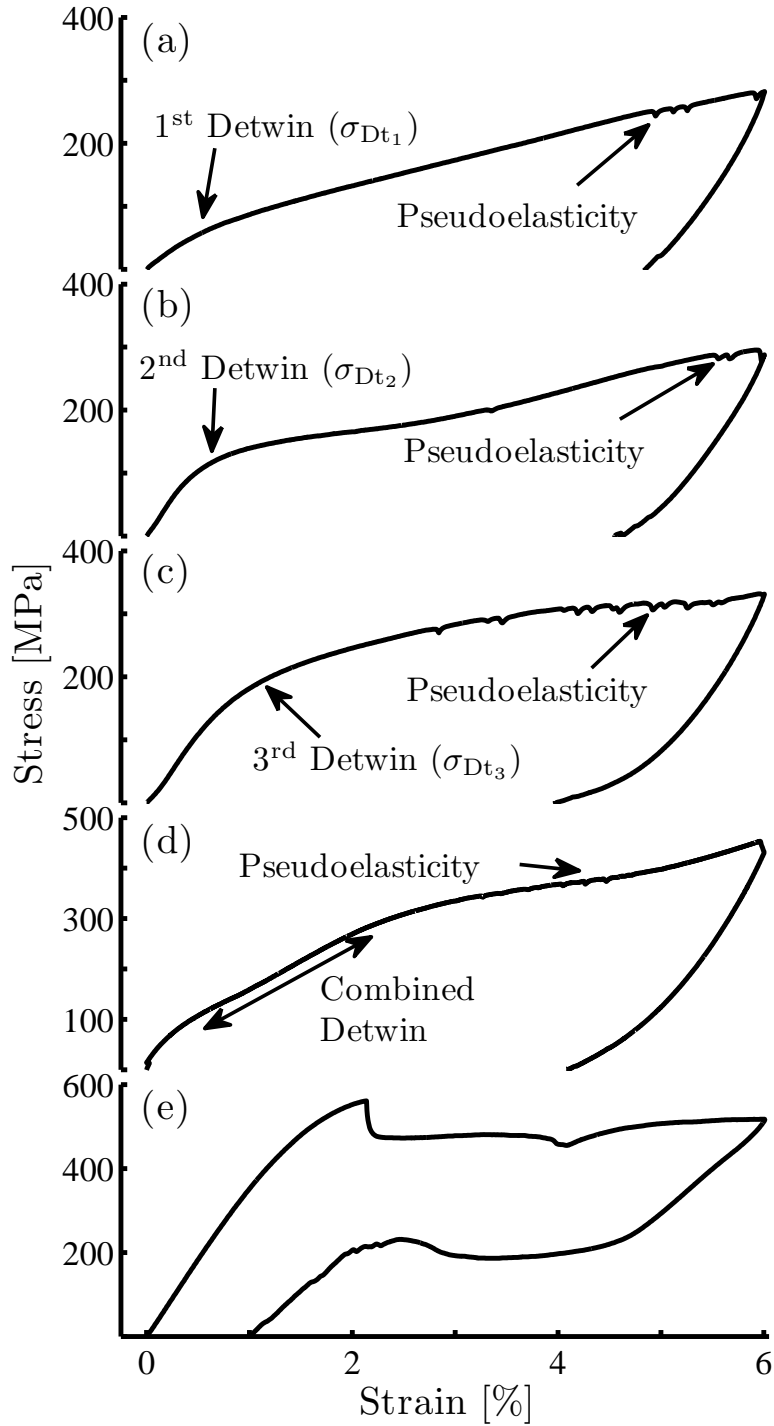
Figure 5.4: Tensile responses of laser processed microgripper components: first segment (a); second segment (b); microgripper head (c); and the as-received BM (e). Mechanical testing of a laser processed specimen incorporating all three microgripper components exhibited a combined response (d). All tensile tests were conducted at room temperature (20 °C). Figure reprinted from [114] with permission from Sage Publications.

presented in Figure 5.4a-d. In comparison to the pseudoelastic behaviour of reference alloy (Figure 5.4e), σ_m for each of the laser processed samples was approximately 100 MPa lower. This reduction in stress was attributed to recrystallization of the BM during laser processing (Figure 5.3b) and has been observed in a previous study by Khan et al. [91]. Although a defined return plateau was not visible in the laser processed samples, according to a study completed by Liu and Galvin [115], martensite variant accommodation can stabilize the stress-induced phase above the A_f temperature. Therefore, the retention of stress-induced martensite upon unloading of laser processed NiTi samples was not unexpected. Further investigation is required, however, to better understand the effects of laser processing on microstructure and corresponding thermomechanical response in retained BM.

Figure 5.5a provides the captured data for the shape memory recoveries of the laser processed tensile specimens presented in Figure 5.4. As predicted by DSC results, each microgripper component exhibited an independent recovery at different temperatures. While there was a slight overlap between recoveries of the second and third shape memory responses, the lower temperature material domain (second microgripper segment) recovered by approximately 90% before activation of the microgripper head. Temperatures corresponding with the onset of shape memory recovery (A_s) correlated very well with the phase transformation onset temperatures determined from DSC testing. The A_f temperatures, however, were slightly higher than anticipated. This discrepancy can be explained by thermal sinking to the tensile grips. A complete recovery was therefore slightly hindered in portions of the laser processed samples that were in close proximity to the gripping point.

As shown in Figure 5.5b, the recovery of the laser processed NiTi microgripper occurred in three stages. Upon heating to temperatures above A_{s_1}, the specimen underwent recovery of the first laser processed positioning segment. Further heating sequentially activated the remaining embedded shape memory behaviours. Actuation of the microgripper head was identified from the data set by the change in inflection of the microgrippers shape memory recovery and comparison to the individual responses provided in Figure 5.5a. In contrast to its individual response, recovery in the laser processed microgripper specimen correlated well with DSC results, which was attributed to the processing dimensions of the tensile specimen (Figure 5.1a). Since the microgripper head segment was not in direct contact with the tensile grips during characterization, thermal sinking did not occur.

It was initially anticipated that the microgripper head would account for 50% of the overall shape memory recovery because of its proportionally larger processing dimensions. Since the amount of detwinned martensite in NiTi determines the magnitude of shape memory recovery [42], and considering the different stiffnesses of laser processed microgripper components, a lessened response from the microgripper head was understandable. In contrast, the shape memory response of the first microgripper segment represented approximately 45% of the overall microgripper recovery, despite being only 25% of its active length. Future studies are planned to further investigate the complex mechanical relationships between laser processed material domains.
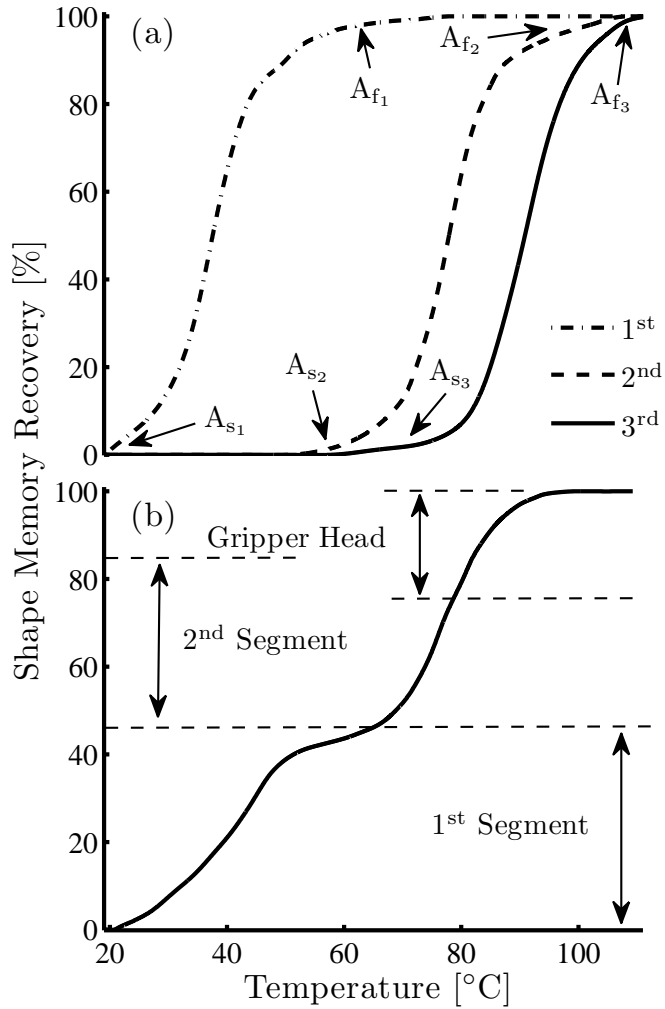
Figure 5.5: Thermomechanical recovery of each microgripper component (a) and the combined recovery of the laser processed NiTi microgripper (b). Figure reprinted from [114] with permission from Sage Publications.

5.2.3 Deployment of the laser processed microgripper

Using the DSC and shape memory recovery results as a guideline, a heating profile was designed to sequentially activate each of the three processed microgripper components. Figure 5.6 provides photographs of each of the four positions achieved by heating the laser processed microgripper along with the measured wire temperature and electrical resistivity profiles. As anticipated, recorded temperatures did not explicitly match with the DSC data because of external loads imposed on the device from fixturing and also from the heat-sinking effects of the temperature sensor. In order to confirm sequential phase transformations in the laser processed NiTi microgripper, optical observations were correlated with in situ resistivity measurements. According to trends reported by Kakeshita et al. [116], sudden increases in the bulk resistance of solution treated NiTi are indicative of a

martensite to austenite phase change. While it was expected that the NiTi material would show some increase in resistivity due to heating, the magnitude of resistance increases in the microgripper could not be explained by joule heating alone. The captured resistivity measurements and photographs therefore confirmed the localized phase changes and sequential activation of embedded shape memory responses in the laser processed microgripper.

While this study has demonstrated the enhanced capabilities of a simple NiTi microgripper, it is anticipated that laser processing can be used to embed added functionality in the more elaborate microgripper designs currently available. Furthermore it is expected that the pseudoelastic response of the retained BM can be exploited to deliver a reversible thermomechanical recovery. A detailed investigation of the energy storage capabilities of retained pseudoelasticity is therefore planned for future research.

5.2.4 Chapter summary

In this study, a novel NiTi microgripper capable of self-positioning was fabricated through the application of laser processing technology. The effects of laser processing removed the prior training of the as-received alloy and considerably altered its thermomechanical characteristics. Results from DSC testing showed three independent material domains with unique austenite onset temperatures of 21, 48 and 71 °C respectively. The three material domains were locally embedded as the active components of a NiTi microgripper. The two lower temperature domains were utilized as the self-positioning microgripper segments, while the higher temperature domain actuated the microgripper head. Mechanical testing revealed three separate thermomechanical behaviours in the laser processed microgripper which corresponded to the independent shape memory recoveries of each embedded material characteristic. Resistive heating of the NiTi microgripper permitted a visual confirmation of the sequential thermal activation of each laser processed microgripper component.
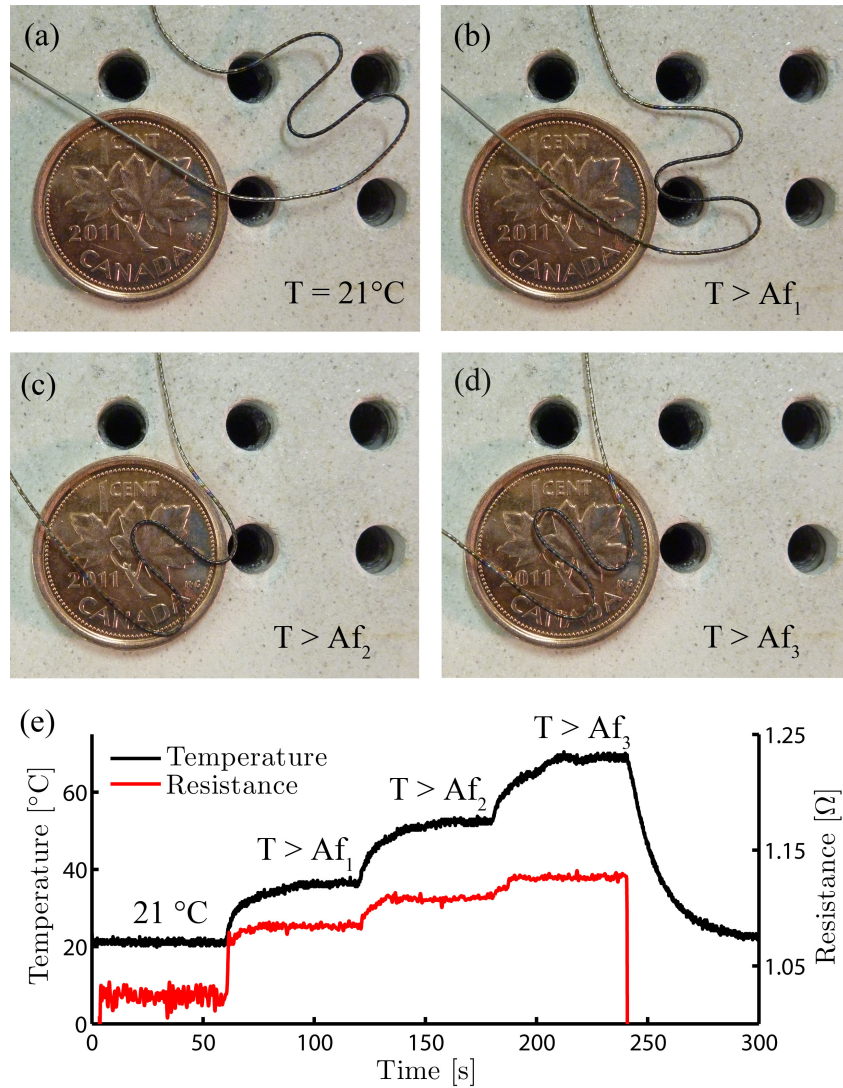
Figure 5.6: Photographs of the laser processed NiTi microgripper during sequential activation of each embedded shape memory response (a)-(d) and collected in situ temperature and resistance measurements (e). Figure reprinted from [114] with permission from Sage Publications.

Chapter 6

Conclusions and recommended future work

In this work, the effects of laser processing on NiTi SMAs have been studied to assess changes in thermomechanical response. Implementation of laser processing was studied in two forms: removal of chemical species through ablation of constituent alloys; and creation of a ternary SMA via laser alloying. In order to demonstrate the improved functionality of processed NiTi SMAs, a novel NiTi microgripper was fabricated through the implementation of laser processing technology. The following summarize the main findings of this study:

1. Laser ablation of NiTi SMA strip induced compositional changes within the LPZ through vaporization of Ni species. Given the sensitivity of phase transformation kinetics to alloy chemistry, composition changes in the LPZ caused shifts in phase transformation onset temperatures and NiTi SMA crystallography. A parametric study of laser pulsing protocol revealed 5 unique sets of phase transformation temperatures which agreed well with reported data. Excessive laser processing, however, resulted in Ti saturation within the SMA microstructure. Further investigation using PIXE is recommended in order to directly correlate laser processed NiTi SMA composition with phase transformation onsets.

2. The localized application of laser energy allowed for additional thermomechanical responses to be embedded within processed NiTi SMAs. Laser processing (at 2 pulses 0% OL) and training of a NiTi SMA wire established a unique shape memory and pseudoelastic response. The laser processed NiTi SMA wire exhibited a shape memory recovery and pseudoelastic plateau at a higher temperature and lower stress than reference alloy. A tensile test of a wire processed with -100% OL revealed the presence of two pseudoelastic plateaus. Laser processing has therefore enhanced the functionality of the NiTi SMA wire. Future work investigating different pulsing protocols is recommended to further exploit the augmented functional capabilities of laser processed NiTi SMAs.

3. Laser processing via localized alloying of Cu was successful in synthesizing the NiTiCu IMC within the LPZ of NiTi SMA strip. Addition of Cu resulted in a shift in phase transformation temperatures and reduction in transformation hysteresis which is desirable for controls applications. As in the laser ablation study, the laser processed NiTi-NiTiCu hybrid SMA possessed two unique shape memory recoveries. Localized alloying of other ternary species is recommended in order to synthesis other hybrid SMAs.

4. Functionality improvements achieved through laser processing can be exploited to create novel smart materials devices. Laser processing of a NiTi SMA wire resulted in the embedment of three unique thermomechanical responses. These material domains also exhibited unique shape memory recoveries and were therefore implemented as the active components of a self-positioning NiTi microgripper. Future work is recommended to investigate the energy storage capabilities of retained BM in laser processed NiTi devices.

References

[1] T. W. Duerig, K. N. Melton, D. Stöckel, and C. M. Wayman, *Engineering Aspects of Shape Memory Alloys.* Butterworth-Heinemann Ltd., 1990.

[2] S. Shabalovskaya, J. Anderegg, and J. Van Humbeeck, "Critical overview of Nitinol surfaces and their modifications for medical applications," *Acta Biomaterialia*, vol. 4, no. 3, pp. 447–467, 2008.

[3] D. J. Hartl and D. C. Lagoudas, "Aerospace applications of shape memory alloys," in *Proceedings of the Institution of Mechanical Engineers, Part G: Journal of Aerospace Engineering*, vol. 221, pp. 535–552, 2007.

[4] T. Duerig, A. Pelton, and D. Stöckel, "An overview of Nitinol medical applications," *Materials Science and Engineering: A*, vol. 273, pp. 149–160, 1999.

[5] M. Kohl, *Shape Memory Microactuators.* Springer Verlag, 2004.

[6] A. R. Pelton, D. Stöckel, and T. W. Duerig, "Medical uses of Nitinol," in *Materials Science Forum*, vol. 327, pp. 63–70, 2000.

[7] D. Stöckel, A. Pelton, and T. Duerig, "Self-expanding Nitinol stents: material and design considerations," *European Radiology*, vol. 14, no. 2, pp. 292–301, 2004.

[8] F. Miura, M. Mogi, Y. Ohura, and H. Hamanaka, "The super-elastic property of the japanese NiTi alloy wire for use in orthodontics," *American Journal of Orthodontics and Dentofacial Orthopedics*, vol. 90, no. 1, pp. 1–10, 1986.

[9] M. Nishida and T. Honma, "All-round shape memory effect in Ni-rich TiNi alloys generated by constrained aging," *Scripta Metallurgica*, vol. 18, no. 11, pp. 1293–1298, 1984.

[10] S. Miyazaki, Y. Igo, and K. Otsuka, "Effect of thermal cycling on the transformation temperatures of Ti—Ni alloys," *Acta Metallurgica*, vol. 34, no. 10, pp. 2045–2051, 1986.

[11] H. C. Lin and S. K. Wu, "Effects of hot rolling on the martensitic transformation of an equiatomic Ti—Ni alloy," *Materials Science and Engineering: A*, vol. 158, no. 1, pp. 87–91, 1992.

[12] C. Grossmann, J. Frenzel, V. Sampath, T. Depka, A. Oppenkowski, C. Somsen, K. Neuking, W. Theisen, and G. Eggeler, "Processing and property assessment of NiTi and NiTiCu shape memory actuator springs," *Materialwissenschaft und Werkstofftechnik*, vol. 39, no. 8, pp. 499–510, 2008.

[13] Y. Shugo, T. Shimizu, K. Morii, T. Yamada, and K. Kusaka, "Effects of heat treatment and thermal cycle on helical spring properties in Ni-Ti-Cu alloy," in *Proceedings of the International Conference on Martensitic Transformations*, pp. 1259–1264, 1992.

[14] X. Liu, Y. Wang, D. Yang, and M. Qi, "The effect of ageing treatment on shape-setting and superelasticity of a Nitinol stent," *Materials Characterization*, vol. 59, no. 4, pp. 402–406, 2008.

[15] W. Tang, "Thermodynamic study of the low-temperature phase B19' and the martensitic transformation in near-equiatomic Ti-Ni shape memory alloys," *Metallurgical and Materials Transactions A*, vol. 28, no. 3, pp. 537–544, 1997.

[16] J. Khalil-Allafi, A. Dlouhy, and G. Eggeler, "Ni_4Ti_3-precipitation during aging of NiTi shape memory alloys and its influence on martensitic phase transformations," *Acta materialia*, vol. 50, no. 17, pp. 4255–4274, 2002.

[17] D. A. Miller and D. C. Lagoudas, "Influence of cold work and heat treatment on the shape memory effect and plastic strain development of NiTi," *Materials Science and Engineering: A*, vol. 308, no. 1-2, pp. 161–175, 2001.

[18] T. Saburi, S. Nenno, Y. Nishimoto, and M. Zeniya, "Effects of thermo-mechanical treatment on the shape memory effect and the pseudoelasticity of Ti–50.2 Ni and Ti-47.5 Ni–2.5 Fe alloys," *Tetsu-to-Hagané (The Iron and Steel Institute of Japan)*, vol. 72, no. 6, pp. 571–578, 1986.

[19] S. Miyazaki, Y. Ohmi, K. Otsuka, and Y. Suzuki, "Characteristics of deformation and transformation pseudoelasticity in Ti-Ni alloys," *Journal de Physique Colloques*, vol. 43, pp. C4 255–260, 1982.

[20] M. I. Khan and Y. Zhou, "Effects of local phase conversion on the tensile loading of pulsed Nd:YAG laser processed Nitinol," *Materials Science and Engineering: A*, vol. 527, no. 23, pp. 6235–6238, 2010.

[21] M. I. Khan, *Pulsed Nd:YAG Laser Processing of Nitinol*. PhD thesis, University of Waterloo, 2011.

[22] B. Tam, M. I. Khan, and Y. Zhou, "Mechanical and functional properties of laser-welded Ti-55.8 wt pct Ni Nitinol wires,"

[23] B. Tam, "Micro-Welding of Nitinol Shape Memory Alloy," Master's thesis, University of Waterloo, 2010.

[24] M. I. Khan and Y. Zhou, "Methods and Systems for Processing Materials, Including Shape Memory Materials," *World Intellectual Property Organization, WO/2011/014962*, 2011.

[25] A. Pequegnat, M. Vlascov, M. Daly, M. I. Khan, and Y. Zhou, "Dynamic actuation of a multiple memory material processed Nitinol linear actuator," in *Proceedings of the ASME Conference on Smart Materials, Adaptive Structures and Intellgient Systems*, 2011 (In Press).

[26] A. Pequegnat, M. Daly, J. Wang, Y. Zhou, and M. I. Khan, "Dynamic actuation of a novel laser processed NiTi linear actuator," *Smart Materials and Structures*, 2012 (Under Review).

[27] G. B. Kauffman and I. Mayo, "The story of Nitinol: the serendipitous discovery of the memory metal and its applications," *The Chemical Educator*, vol. 2, no. 2, pp. 1–21, 1997.

[28] K. Otsuka and X. Ren, "Physical metallurgy of Ti-Ni-based shape memory alloys," *Progress in Materials Science*, vol. 50, no. 5, pp. 511–678, 2005.

[29] C. P. Frick, A. M. Ortega, J. Tyber, A. E. M. Maksound, H. J. Maier, Y. Liu, and K. Gall, "Thermal processing of polycrystalline NiTi shape memory alloys," *Materials Science and Engineering: A*, vol. 405, no. 1-2, pp. 34–49, 2005.

[30] T. B. Massalski, H. Okamoto, P. R. Subramanian, and L. Kacprzak, *Binary Alloy Phase Diagrams.* ASM International, 1990.

[31] K. Otsuka and C. M. Wayman, *Shape Memory Materials.* Cambridge University Press, 1999.

[32] D. C. Lagoudas, *Shape Memory Alloys.* Springer, 2008.

[33] T. V. Philip and P. A. Beck, "CsCl-type ordered structures in binary alloys of transition elements," *Transactaions AIME*, vol. 209, pp. 1269–1271, 1957.

[34] K. Otsuka, T. Sawamura, and K. Shimizu, "Crystal structure and internal defects of equiatomic TiNi martensite," *Physica status solidi (a)*, vol. 5, no. 2, pp. 457–470, 1971.

[35] H. C. Ling and K. Roy, "Stress-induced shape changes and shape memory in the R and martensite transformations in equiatomic NiTi," *Metallurgical and Materials Transactions A*, vol. 12, no. 12, pp. 2101–2111, 1981.

[36] E. Hornbogen, "Surface upheavals, pseudo martensite, and martensite ghosts," *Praktische Metallographie*, vol. 42, no. 9, pp. 445–453, 2005.

[37] K. N. Melton and O. Mercier, "Fatigue of NiTi thermoelastic martensites," *Acta Metallurgica*, vol. 27, no. 1, pp. 137–144, 1979.

[38] H. A. Mohamed and J. Washburn, "Deformation behaviour and shape memory effect of near equi-atomic NiTi alloy," *Journal of Materials Science*, vol. 12, no. 3, pp. 469–480, 1977.

[39] H. A. Mohamed and J. Washburn, "On the mechanism of the shape memory effect in Ni-Ti alloy," *Metallurgical and Materials Transactions A*, vol. 7, no. 7, pp. 1041–1043, 1976.

[40] R. F. Hamilton, H. Sehitoglu, Y. Chumlyakov, and H. J. Maier, "Stress dependence of the hysteresis in single crystal NiTi alloys," *Acta Materialia*, vol. 52, no. 11, pp. 3383–3402, 2004.

[41] K. N. Melton and O. Mercier, "Deformation Behavior of NiTi-Based Alloys," *Metallurgical and Materials Transactions A*, vol. 9A, pp. 1487–1488, 1978.

[42] S. Miyazaki, S. Kimura, K. Otsuka, and Y. Suzuki, "The habit plane and transformation strains associated with the martensitic transformation in Ti-Ni single crystals," *Scripta Metallurgica*, vol. 18, no. 9, pp. 883–888, 1984.

[43] A. Nagasawa, Y. Ishino, K. Enami, Y. Abe, and S. Nenno, "Reversible shape memory effect," *Scripta Metallurgica*, vol. 8, no. 9, pp. 1055–1060, 1974.

[44] T. Fukuda, A. Deguchi, T. Kakeshita, and T. Saburi, "Two-way shape memory properties of a Ni-Rich Ti-Ni alloy aged under tensile-stress," *Materials Transactions*, vol. 38, no. 6, pp. 514–520, 1997.

[45] Y. Liu, Y. Liu, and J. Van Humbeeck, "Two-way shape memory effect developed by martensite deformation in NiTi," *Acta Materialia*, vol. 47, no. 1, pp. 199–209, 1998.

[46] D. Treppmann, E. Hornbogen, and D. Wurzel, "The effect of combined recrystallization and precipitation process on the functional and structural properties in NiTi alloys," *Journal de Physique. IV*, vol. 5, pp. C8 569–574, 1995.

[47] S. Daly, G. Ravichandran, and K. Bhattacharya, "Stress-induced martensitic phase transformation in thin sheets of Nitinol," *Acta Materialia*, vol. 55, no. 10, pp. 3593–3600, 2007.

[48] P. Šittner, Y. Liu, and V. Novák, "On the origin of Lüders-like deformation of NiTi shape memory alloys," *Journal of the Mechanics and Physics of Solids*, vol. 53, no. 8, pp. 1719–1746, 2005.

[49] J. A. Shaw and S. Kyriakides, "On the nucleation and propagation of phase transformation fronts in a NiTi alloy," *Acta Materialia*, vol. 45, no. 2, pp. 683–700, 1997.

[50] J. A. Shaw and S. Kyriakides, "Thermomechanical aspects of NiTi," *Journal of the Mechanics and Physics of Solids*, vol. 43, no. 8, pp. 1243–1281, 1995.

[51] L. C. L. Brinson, I. Schmidt, and R. Lammering, "Stress-induced transformation behavior of a polycrystalline NiTi shape memory alloy: micro and macromechanical investigations via in situ optical microscopy," *Journal of the Mechanics and Physics of Solids*, vol. 52, no. 7, pp. 1549–1571, 2004.

[52] R. Plietsch and K. Ehrlich, "Strength differential effect in pseudoelastic NiTi shape memory alloys," *Acta Materialia*, vol. 45, no. 6, pp. 2417–2424, 1997.

[53] D. A. Porter and K. E. Easterling, *Phase Transformations in Metals and Alloys*. Van Nostrand Reinhold, 1981.

[54] K. Otsuka and K. Shimizu, "Pseudoelasticity and shape memory effects in alloys," *International Metals Reviews*, vol. 31, no. 1, pp. 93–114, 1986.

[55] R. E. Reed-Hill and R. Abbaschian, *Physical Metallurgy Principles: Third Edition*. PWS Publishing Company, 1994.

[56] H. Meier, A. Czechowicz, C. Haberland, and S. Langbein, "Smart control systems for smart materials," *Journal of Materials Engineering and Performance*, pp. 1–5, 2011.

[57] N. Ma, G. Song, and H. J. Lee, "Position control of shape memory alloy actuators with internal electrical resistance feedback using neural networks," *Smart Materials and Structures*, vol. 13, pp. 777–783, 2004.

[58] K. Ikuta, M. Tsukamoto, and S. Hirose, "Shape memory alloy servo actuator system with electric resistance feedback and application for active endoscope," in *Proceedings of the IEEE International Conference on Robotics and Automation*, vol. 1, pp. 427–430, 1988.

[59] S. M. Dutta, F. H. Ghorbel, and J. B. Dabney, "Modeling and control of a shape memory alloy actuator," in *Proceedings of the 2005 IEEE International Symposium on Intelligent Control*, pp. 1007–1012, 2005.

[60] K. H. Eckelmeyer, "The effect of alloying on the shape memory phenomenon in Nitinol," *Scripta Metallurgica*, vol. 10, no. 8, pp. 667–672, 1976.

[61] H. C. Donkersloot and J. H. N. Van Vucht, "Martensitic transformations in gold-titanium, palladium-titanium and platinum-titanium alloys near the equiatomic composition," *Journal of the Less Common Metals*, vol. 20, no. 2, pp. 83–91, 1970.

[62] D. R. Angst, P. E. Thoma, and M. Y. Kao, "The effect of hafnium content on the transformation temperatures of Ni49Ti51- xHfx shape memory alloys," *Journal de Physique. IV*, vol. 5, pp. C8 747–752, 1995.

[63] T. H. Nam, T. Saburi, and K. Shimizu, "Cu-content dependence of shape memory characteristics in Ti-Ni-Cu alloys," *Materials Transactions*, vol. 31, no. 11, pp. 959–967, 1990.

[64] S. Miyazaki, T. Hashinaga, and A. Ishida, "Martensitic transformations in sputter-deposited Ti-Ni-Cu shape memory alloy thin films," *Thin Solid Films*, vol. 281, no. 1-2, pp. 364–367, 1996.

[65] S. M. Russell, "Nitinol melting and fabrication," in *Proceedings of the International Conference on Shape Memory and Superelastic Technologies*, pp. 1–9, 2001.

[66] M. H. Wu, "Fabrication of Nitinol materials and components," in *Materials Science Forum*, vol. 394, pp. 285–292, 2002.

[67] Y. Sekiguchi, K. Funami, and H. Funakubo, "Deposition of TiNi shape memory alloy thin film by vacuum evaporation," in *Proceedings of the 32nd Meeting of the Japanese Society of Materials*, pp. 65–67, 1983.

[68] G. Thomas, H. Mori, H. Fujita, and R. Sinclair, "Electron irradiation induced crystalline amorphous transitions in NiTi alloys," *Scripta Metallurgica*, vol. 16, no. 5, pp. 589–592, 1982.

[69] J. D. Busch, A. D. Johnson, C. H. Lee, and D. A. Stevenson, "Shape-memory properties in Ni-Ti sputter-deposited film," *Journal of applied physics*, vol. 68, pp. 6224–6228, 1990.

[70] J. J. Kim, P. Moine, and D. Stevenson, "Crystallization behavior of amorphous Ni-Ti alloys prepared by sputter deposition," *Scripta Metallurgica*, vol. 20, pp. 243–248, 1986.

[71] S. Miyazaki and A. Ishida, "Martensitic transformation and shape memory behavior in sputter-deposited TiNi-base thin films," *Materials Science and Engineering: A*, vol. 273, pp. 106–133, 1999.

[72] K. Ikuta, H. Fujita, M. Ikeda, and S. Yamashita, "Crystallographic analysis of TiNi shape memory alloy thin film for microactuator," in *Proceedings of the IEEE International Conference on Micro Electro Mechanical Systems*, pp. 38–39, 1990.

[73] K. Kuribayashi, M. Yoshitake, and S. Ogawa, "Reversible SMA actuator for micron sized robot," in *Proceedings of the IEEE International Conference on Micro Electro Mechanical Systems*, pp. 217–221, 1990.

[74] A. Gyobu, Y. Kawamura, H. Horikawa, and T. Saburi, "Martensitic transformations in sputter-deposited shape memory Ti-Ni films," *Materials Transactions*, vol. 37, pp. 697–702, 1996.

[75] D. S. Grummon and T. Lagrange, "Composition of sputtered NiTiX shape-memory and superelastic thin films," *Journal de physique. IV*, vol. 112, pp. 853–856, 2003.

[76] A. Bansiddhi, T. D. Sargeant, S. I. Stupp, and D. C. Dunand, "Porous NiTi for bone implants: A review," *Acta Biomaterialia*, vol. 4, no. 4, pp. 773–782, 2008.

[77] D. C. Lagoudas and E. L. Vandygriff, "Processing and characterization of NiTi porous SMA by elevated pressure sintering," *Journal of Intelligent Material Systems and Structures*, vol. 13, no. 12, pp. 837–850, 2002.

[78] S. M. Green, D. M. Grant, and N. R. Kelly, "Powder metallurgical processing of Ni-Ti shape memory alloy," *Powder Metallurgy*, vol. 40, no. 1, pp. 43–47, 1997.

[79] J. C. Hey and A. P. Jardine, "Shape memory TiNi synthesis from elemental powders," *Materials Science and Engineering: A*, vol. 188, no. 1-2, pp. 291–300, 1994.

[80] S. H. Lee, J. H. Lee, Y. H. Lee, D. Hyuk-Shin, and Y. S. Kim, "Effect of heating rate on the combustion synthesis of intermetallics," *Materials Science and Engineering: A*, vol. 281, no. 1, pp. 275–285, 2000.

[81] A. Biswas, "Porous NiTi by thermal explosion mode of SHS: processing, mechanism and generation of single phase microstructure," *Acta Materialia*, vol. 53, no. 5, pp. 1415–1425, 2005.

[82] M. Whitney, S. F. Corbin, and R. B. Gorbet, "Investigation of the mechanisms of reactive sintering and combustion synthesis of NiTi using differential scanning calorimetry and microstructural analysis," *Acta Materialia*, vol. 56, no. 3, pp. 559–570, 2008.

[83] T. Araki, A. Hirose, and M. Uchihara, "Characteristics and fracture morphology of Ti-Ni type shape memory alloy and its laser weld joint," *Japanese Society of Materials Science*, vol. 38, no. 428, pp. 478–483, 1989.

[84] A. Hirose, M. Uchihara, T. Araki, K. Honda, and M. Kondoh, "Laser welding of Ti–Ni type shape memory alloy," *Journal of the Japan Institute of Metals*, vol. 54, no. 3, pp. 262–269, 1990.

[85] P. Schloßmacher, T. Haas, and A. Schüßler, "Laser welding of Ni-Ti shape memory alloys," in *Proceedings of the First International Conference on Shape Memory and Superelastic Technologies*, pp. 85–90, 1994.

[86] P. Schloßmacher, T. Haas, and A. Schüßler, "Laser-welding of a Ni-rich TiNi shape memory alloy: mechanical behavior," *Journal de Physique. IV*, vol. 7, pp. C5 251–256, 1997.

[87] P. Schloßmacher, T. Haas, and A. Schüßler, "Laser welding of Ni-rich TiNi shape memory alloy: pseudoelastic properties," in *Proceedings of the 2nd International Conference on Shape Memory and Superelastic Technologies*, pp. 137–142, 1997.

[88] A. Falvo, F. M. Furgiuele, and C. Maletta, "Laser welding of a NiTi alloy: mechanical and shape memory behaviour," *Materials Science and Engineering: A*, vol. 412, no. 1, pp. 235–240, 2005.

[89] A. Schüßler, "Laser processing of Nitinol materials," in *Proceedings of the International Conference on Shape Memory and Superelastic Technolgies*, pp. 25–32, 2001.

[90] A. Tuissi, S. Besseghini, T. Ranucci, F. Squatrito, and M. Pozzi, "Effect of Nd-YAG laser welding on the functional properties of the Ni–49.6 at.% Ti," *Materials Science and Engineering: A*, vol. 273, pp. 813–817, 1999.

[91] M. I. Khan, S. K. Panda, and Y. Zhou, "Effects of welding parameters on the mechanical performance of laser welded Nitinol," *Materials Transactions*, vol. 49, no. 11, pp. 2702–2708, 2008.

[92] H. C. Man, Z. D. Cui, and T. M. Yue, "Corrosion properties of laser surface melted NiTi shape memory alloy," *Scripta Materialia*, vol. 45, no. 12, pp. 1447–1453, 2001.

[93] M. Jandaghi, P. Parvin, M. J. Torkamany, and J. Sabbaghzadeh, "Alloying element losses in pulsed Nd: YAG laser welding of stainless steel 316," *Journal of Physics D: Applied Physics*, vol. 41, p. 235503, 2008.

[94] A. P. Lee, D. R. Ciarlo, P. A. Krulevitch, S. Lehew, J. Trevino, and M. A. Northrup, "A practical microgripper by fine alignment, eutectic bonding and SMA actuation," *Sensors and Actuators A: Physical*, vol. 54, no. 1-3, pp. 755–759, 1996.

[95] M. Kohl, E. Just, W. Pfleging, and S. Miyazaki, "SMA microgripper with integrated antagonism," *Sensors and Actuators A: Physical*, vol. 83, no. 1-3, pp. 208–213, 2000.

[96] K. Weinert and V. Petzoldt, "Machining of NiTi based shape memory alloys," *Materials Science and Engineering: A*, vol. 378, no. 1, pp. 180–184, 2004.

[97] A. Undisz, M. Rettenmayr, M. Wilke, and L. Spieß, "Non-martensitic needle-like structures on Ni-Ti alloys-occurrence and origin," in *8th European Symposium on Martensitic Transformations (ESOMAT)*, pp. 2034–2034, 2009.

[98] A. Undisz, K. Reuther, H. Reuther, and M. Rettenmayr, "Occurrence and origin of non-martensitic acicular artifacts on NiTi," *Acta Materialia*, vol. 59, no. 1, pp. 216–224, 2011.

[99] E. L. Semenova and Y. V. Kudryavtsev, "Structural phase transformation and shape memory effect in ZrRh and ZrIr," *Journal of Alloys and Compounds*, vol. 203, pp. 165–168, 1994.

[100] Y. Kudoh, M. Tokonami, S. Miyazaki, and K. Otsuka, "Crystal structure of the martensite in Ti-49.2 at.% Ni alloy analyzed by the single crystal X-ray diffraction method," *Acta Metallurgica*, vol. 33, no. 11, pp. 2049–2056, 1985.

[101] J. Frenzel, Z. Zhang, C. Somsen, K. Neuking, and G. Eggeler, "Influence of carbon on martensitic phase transformations in NiTi shape memory alloys," *Acta Materialia*, vol. 55, no. 4, pp. 1331–1341, 2007.

[102] G. Bianchi and R. Sorrentino, *Electronic Filter Simulation & Design*. McGraw-Hill, 2007.

[103] S. Miyazaki, K. Otsuka, and Y. Suzuki, "Transformation pseudoelasticity and deformation behavior in a Ti- 50.6at.%Ni alloy," *Scripta Metallurgica*, vol. 15, no. 3, pp. 287–292, 1981.

[104] M. A. Iadicola and J. A. Shaw, "The effect of uniaxial cyclic deformation on the evolution of phase transformation fronts in pseudoelastic NiTi wire," *Journal of Intelligent Material Systems and Structures*, vol. 13, no. 2-3, p. 143, 2002.

[105] H. Funakubo and J. B. Kennedy, *Shape Memory Alloys*. 1987.

[106] O. Mercier and K. N. Melton, "The substitution of Cu for Ni in NiTi shape memory alloys," *Metallurgical and Materials Transactions A*, vol. 10, no. 3, pp. 387–389, 1979.

[107] R. H. Bricknell, K. N. Melton, and O. Mercier, "The structure of NiTiCu shape memory alloys," *Metallurgical and Materials Transactions A*, vol. 10, no. 6, pp. 693–697, 1979.

[108] M. Daly, A. Pequegnat, Y. Zhou, and M. I. Khan, "Enhanced thermomechanical functionality of a laser processed hybrid NiTi-NiTiCu shape memory alloy," *Smart Materials and Structures*, 2012 (In Press).

[109] Y. Shugo, F. Hasegawa, and T. Honma, "Effects of copper addition on the martensitic transformation of tini alloy," *Bull. Res. Inst. Min. Dressing Metall. Tohoku Univ.*, vol. 37, no. 1, pp. 79–88, 1981.

[110] W. Ni, Y. T. Cheng, and D. S. Grummon, "Recovery of microindents in a nickel–titanium shape-memory alloy: a self-healing effect," *Applied Physics Letters*, vol. 80, p. 3310, 2002.

[111] Y. Fu, W. Huang, H. Du, X. Huang, J. Tan, and X. Gao, "Characterization of TiNi shape-memory alloy thin films for MEMS applications," *Surface and Coatings Technology*, vol. 145, no. 1-3, pp. 107–112, 2001.

[112] M. Daly, A. Pequegnat, M. I. Khan, and Y. Zhou, "Fabrication of a novel monolithic NiTi based shape memory microgripper via multiple memory material processing," in *Proceedings of the ASME Conference on Smart Materials, Adaptive Structures and Intellgient Systems*, 2011 (In Press).

[113] M. I. Khan and Y. Zhou, "A method to locally modify shape memory and pseudoelastic properties," in *Proceedings of the International Conference on Shape Memory and Superelastic Technologies*, pp. 202–203, 2010.

[114] M. Daly, A. Pequegnat, Y. Zhou, and M. I. Khan, "Fabrication of a novel laser processed NiTi shape memory microgripper with enhanced thermomechanical functionality," *Journal of Intelligent Material Systems and Structures*, 2012 (In Press).

[115] Y. Liu and S. P. Galvin, "Criteria for pseudoelasticity in near-equiatomic NiTi shape memory alloys," *Acta Materialia*, vol. 45, no. 11, pp. 4431–4439, 1997.

[116] T. Kakeshita, T. Fukuda, H. Tetsukawa, T. Saburi, K. Kindo, T. Takeuchi, M. Honda, S. Endo, T. Taniguchi, and Y. Miyako, "Negative temperature coefficient of electrical resistivity in B2-type Ti-Ni alloys," *Japanese Journal of Applied Physics*, vol. 37, pp. 2535–2539, 1998.

[117] R. J. Moffat, "Describing the uncertainties in experimental results," *Experimental thermal and fluid science*, vol. 1, no. 1, pp. 3–17, 1988.

[118] M. S. Van Dusen, "Platinum resistance thermometry at low temperatures," *Journal of the American Chemical Society*, vol. 47, p. 326, 1925.

Appendices

Appendix A

Experimental Uncertainty in Temperature Measurements

In order to assess temperature using the RTD, a number of secondary data acquisition systems were required for sensor powering and load measurements. These systems possessed a degree of uncertainty which must be accounted for when reporting results. Figure A.1 provides the data acquisition elements used to determine temperature, which form the basis of the following uncertainty analysis. Estimates of uncertainty were based on the methodology presented by Moffat [117]. Throughout the analysis, uncertainty is stated at 95% confidence on reported measurements and individual sources of error are combined under an assumption of mutually exclusive contribution. Uncertainty estimates are applicable to Figures 3.18, 4.6 and 5.5.

The data acquisition system used to monitor temperature is divided into three separate devices: a voltmeter, a constant current supply and the RTD device. The voltmeter was used to monitor voltage drop across the RTD device and has an uncertainty of $\pm$ 480 μV. The purpose of the current source is to power the RTD. In order to avoid joule heating of the RTD, a current supply of 1 mA was selected for implementation. Data logging of the current supply using a nano-ammeter showed an average current flow of 0.99658
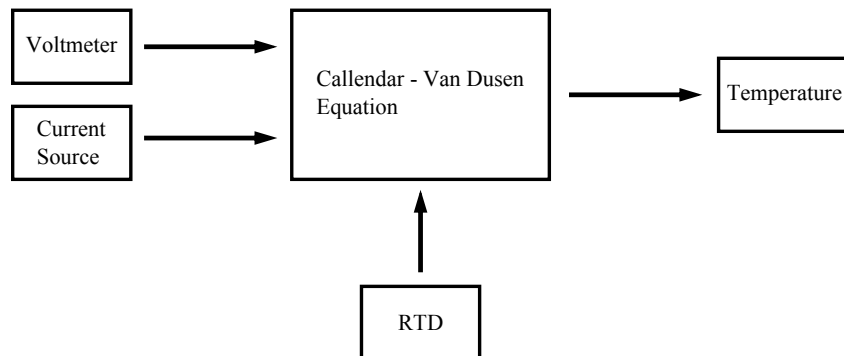
Figure A.1: Block diagram of the data acquisition system used to measure temperature in experiments.

$\pm$ 5.12x10^{-4} mA . Given the comparatively small error associated with the current source, contributions to experimental uncertainty from this element of the data acquisition system were ignored. Together with the measured voltage drop, the supplied current was used to calculate the resistance across the RTD (R_t) by Ohm's law.

The remaining source of error in the temperature measurement system was the RTD itself. RTD devices are designed to deliver a nominal resistance (R_o) of 100 Ω at 0 °C. As reported by the manufacturer, the RTD used in this study possessed an inherent uncertainty of $\pm$ 0.12 Ω. Using the Callendar Van–Dusen equation [118] the actual temperature of the RTD was computed through comparison of R_t and R_o. Following the method of sequential perturbation [117] and using the contributions to uncertainty from R_t and R_o, the total uncertainty in temperature measurements was estimated to be $\pm$ 1.28 °C.

Appendix B

Permission letters

ASM INTERNATIONAL
Everything
Material.
The Materials
Information Society

COPYRIGHT PERMISSION REQUEST

Please complete all contact information:

Name: Matthew Daly

Address: University of Waterloo, 200 University Avenue

West, Waterloo, ON, Canada, N2L 3G1

Title: Graduate Research Assistant

Phone: 1 519 888 4567 ext. 33326

Affiliation: Department of Mechanical and

Mechatronics Engineering, University of Waterloo

Email: m3daly@uwaterloo.ca

1. I am preparing an article/chapter for publication in the following formats (*check as applicable*):

   Print Only _____   Internet Only _____   Print and Electronic Media _x_

2. The information will be used for (*check as applicable*):

   Journal article _____   Internal company records _____   Student course material _____
   Conference presentation _____   Dissertation _x_   Commercial publication* _____

3. Please complete the following:

The article/chapter title will be: Physical Metallurgy of NiTi SMAs
The publication title will be: Thermomechanical response of laser processed nickel-titanium shape memory alloys
Publisher: University of Waterloo
Planned date of publication: April 2012

I hereby request permission for non-exclusive world rights for the above publication and all subsequent editions, revisions, and derivative works in English and foreign translations, in the formats indicated above from the following copyrighted content by ASM International:

Book ISBN: 978-0-87170-403-0   Copyright date: 1990
Book/Publication title: Binary alloy phase diagrams, 2nd edition
Author name(s): Massalski TB, Okamoto H, Subramanian PR, Kacprzak L, editors
Article title: TiNi Phase diagram
Text pages (enclose copy of scan of materials): _____
Figure numbers (with page numbers and copy/scan of figures): p.2874 _____
Table numbers (with page numbers and copy/scan of tables): _____

_____   Matthew Daly   Mar. 1, 2012
Signature   Print Name   Date

FOR ASM INTERNATIONAL USE ONLY:
I (we) grant permission requested above. Please ensure that ASM International receives proper credit as publisher by citing the above ASM publication as a reference and including the following: Reprinted with permission of ASM International. All rights reserved. www.asminternational.org

_____   3/1/2012
Sue Sellers, ASM International   Date

Email: permissions@asminternational.org, Phone: 440-338-5151 x5465

SPRINGER LICENSE
TERMS AND CONDITIONS

Mar 01, 2012

This is a License Agreement between Matthew A Daly ("You") and Springer ("Springer") provided by Copyright Clearance Center ("CCC"). The license consists of your order details, the terms and conditions provided by Springer, and the payment terms and conditions.

All payments must be made in full to CCC. For payment instructions, please see information listed at the bottom of this form.

License Number	2858290232452
License date	Feb 29, 2012
Licensed content publisher	Springer
Licensed content publication	Metallurgical and Materials Transactions A
Licensed content title	Thermodynamic study of the low-temperature phase B19′ and the martensitic transformation in near-equiatomic Ti-Ni shape memory alloys
Licensed content author	Weijia Tang
Licensed content date	Mar 1, 1997
Volume number	28
Issue number	3
Type of Use	Thesis/Dissertation
Portion	Figures
Author of this Springer article	No
Order reference number	None
Title of your thesis / dissertation	Thermomechanical response of laser processed nickel-titanium shape memory alloy
Expected completion date	Apr 2012
Estimated size(pages)	100
Total	**0.00 USD**

Terms and Conditions

If you would like to pay for this license now, please remit this license along with your payment made payable to "COPYRIGHT CLEARANCE CENTER" otherwise you will be invoiced within 48 hours of the license date. Payment should be in the form of a check or money order referencing your account number and this invoice number RLNK500729776. Once you receive your invoice for this order, you may pay your invoice by credit card. Please follow instructions provided at that time.

Make Payment To:
Copyright Clearance Center
Dept 001
P.O. Box 843006
Boston, MA 02284-3006

For suggestions or comments regarding this order, contact RightsLink Customer Support:
customercare@copyright.com **or +1-877-622-5543 (toll free in the US) or +1-978-646-2777.**

Gratis licenses (referencing $0 in the Total field) are free. Please retain this printable license for your reference. No payment is required.

ELSEVIER LICENSE
TERMS AND CONDITIONS

Feb 27, 2012

This is a License Agreement between Matthew A Daly ("You") and Elsevier ("Elsevier") provided by Copyright Clearance Center ("CCC"). The license consists of your order details, the terms and conditions provided by Elsevier, and the payment terms and conditions.

All payments must be made in full to CCC. For payment instructions, please see information listed at the bottom of this form.

Supplier	Elsevier Limited The Boulevard,Langford Lane Kidlington,Oxford,OX5 1GB,UK
Registered Company Number	1982084
Customer name	Matthew A Daly
Customer address	Dept of Mechanical and Mechatronics Eng.
	Waterloo, ON N2L3G1
License number	2857241372353
License date	Feb 27, 2012
Licensed content publisher	Elsevier
Licensed content publication	Materials Science and Engineering: A
Licensed content title	Effect of Nd–YAG laser welding on the functional properties of the Ni–49.6at.%Ti
Licensed content author	A Tuissi,S Besseghini,T Ranucci,F Squatrito,M Pozzi
Licensed content date	15 December 1999
Licensed content volume number	273–275
Licensed content issue number	
Number of pages	5
Start Page	813
End Page	817
Type of Use	reuse in a thesis/dissertation
Portion	figures/tables/illustrations
Number of figures/tables/illustrations	1
Format	electronic
Are you the author of this Elsevier article?	No
Will you be translating?	No

89

Order reference number	
Title of your thesis/dissertation	Thermomechanical response of laser processed nickel-titanium shape memory alloy
Expected completion date	Apr 2012
Estimated size (number of pages)	100
Elsevier VAT number	GB 494 6272 12
Permissions price	0.00 USD
VAT/Local Sales Tax	0.0 USD / 0.0 GBP
Total	0.00 USD

Terms and Conditions

INTRODUCTION

1. The publisher for this copyrighted material is Elsevier. By clicking "accept" in connection with completing this licensing transaction, you agree that the following terms and conditions apply to this transaction (along with the Billing and Payment terms and conditions established by Copyright Clearance Center, Inc. ("CCC"), at the time that you opened your Rightslink account and that are available at any time at http://myaccount.copyright.com).

GENERAL TERMS

2. Elsevier hereby grants you permission to reproduce the aforementioned material subject to the terms and conditions indicated.

3. Acknowledgement: If any part of the material to be used (for example, figures) has appeared in our publication with credit or acknowledgement to another source, permission must also be sought from that source. If such permission is not obtained then that material may not be included in your publication/copies. Suitable acknowledgement to the source must be made, either as a footnote or in a reference list at the end of your publication, as follows:

"Reprinted from Publication title, Vol /edition number, Author(s), Title of article / title of chapter, Pages No., Copyright (Year), with permission from Elsevier [OR APPLICABLE SOCIETY COPYRIGHT OWNER]." Also Lancet special credit - "Reprinted from The Lancet, Vol. number, Author(s), Title of article, Pages No., Copyright (Year), with permission from Elsevier."

4. Reproduction of this material is confined to the purpose and/or media for which permission is hereby given.

5. Altering/Modifying Material: Not Permitted. However figures and illustrations may be altered/adapted minimally to serve your work. Any other abbreviations, additions, deletions and/or any other alterations shall be made only with prior written authorization of Elsevier Ltd. (Please contact Elsevier at permissions@elsevier.com)

6. If the permission fee for the requested use of our material is waived in this instance, please be advised that your future requests for Elsevier materials may attract a fee.

7. Reservation of Rights: Publisher reserves all rights not specifically granted in the combination of (i) the license details provided by you and accepted in the course of this licensing transaction, (ii) these terms and conditions and (iii) CCC's Billing and Payment terms and conditions.

8. License Contingent Upon Payment: While you may exercise the rights licensed immediately upon issuance of the license at the end of the licensing process for the transaction, provided that you have disclosed complete and accurate details of your proposed use, no license is finally effective unless and until full payment is received from you (either by publisher or by CCC) as provided in CCC's Billing and Payment terms and conditions. If full payment is not received on a timely basis, then any license preliminarily granted shall be deemed automatically revoked and shall be void as if never granted. Further, in the event that you breach any of these terms and conditions or any of CCC's Billing and Payment terms and conditions, the license is automatically revoked and shall be void as if never granted. Use of materials as described in a revoked license, as well as any use of the materials beyond the scope of an unrevoked license, may constitute copyright infringement and publisher reserves the right to take any and all action to protect its copyright in the materials.

9. Warranties: Publisher makes no representations or warranties with respect to the licensed material.

10. Indemnity: You hereby indemnify and agree to hold harmless publisher and CCC, and their respective officers, directors, employees and agents, from and against any and all claims arising out of your use of the licensed material other than as specifically authorized pursuant to this license.

11. No Transfer of License: This license is personal to you and may not be sublicensed, assigned, or transferred by you to any other person without publisher's written permission.

12. No Amendment Except in Writing: This license may not be amended except in a writing signed by both parties (or, in the case of publisher, by CCC on publisher's behalf).

13. Objection to Contrary Terms: Publisher hereby objects to any terms contained in any purchase order, acknowledgment, check endorsement or other writing prepared by you, which terms are inconsistent with these terms and conditions or CCC's Billing and Payment terms and conditions. These terms and conditions, together with CCC's Billing and Payment terms and conditions (which are incorporated herein), comprise the entire agreement between you and publisher (and CCC) concerning this licensing transaction. In the event of any conflict between your obligations established by these terms and conditions and those established by CCC's Billing and Payment terms and conditions, these terms and conditions shall control.

14. Revocation: Elsevier or Copyright Clearance Center may deny the permissions described in this License at their sole discretion, for any reason or no reason, with a full refund payable to you. Notice of such denial will be made using the contact information provided by you. Failure to receive such notice will not alter or invalidate the denial. In no event will Elsevier or Copyright Clearance Center be responsible or liable for any costs, expenses or damage incurred by you as a result of a denial of your permission request, other than a refund of the amount(s) paid by you to Elsevier and/or Copyright Clearance Center for denied permissions.

LIMITED LICENSE

91

The following terms and conditions apply only to specific license types:

15. **Translation**: This permission is granted for non-exclusive world **English** rights only unless your license was granted for translation rights. If you licensed translation rights you may only translate this content into the languages you requested. A professional translator must perform all translations and reproduce the content word for word preserving the integrity of the article. If this license is to re-use 1 or 2 figures then permission is granted for non-exclusive world rights in all languages.

16. **Website**: The following terms and conditions apply to electronic reserve and author websites:
Electronic reserve: If licensed material is to be posted to website, the web site is to be password-protected and made available only to bona fide students registered on a relevant course if:
This license was made in connection with a course,
This permission is granted for 1 year only. You may obtain a license for future website posting,
All content posted to the web site must maintain the copyright information line on the bottom of each image,
A hyper-text must be included to the Homepage of the journal from which you are licensing at http://www.sciencedirect.com/science/journal/xxxxx or the Elsevier homepage for books at http://www.elsevier.com , and
Central Storage: This license does not include permission for a scanned version of the material to be stored in a central repository such as that provided by Heron/XanEdu.

17. **Author website** for journals with the following additional clauses:

All content posted to the web site must maintain the copyright information line on the bottom of each image, and
he permission granted is limited to the personal version of your paper. You are not allowed to download and post the published electronic version of your article (whether PDF or HTML, proof or final version), nor may you scan the printed edition to create an electronic version,
A hyper-text must be included to the Homepage of the journal from which you are licensing at http://www.sciencedirect.com/science/journal/xxxxx , As part of our normal production process, you will receive an e-mail notice when your article appears on Elsevier's online service ScienceDirect (www.sciencedirect.com). That e-mail will include the article's Digital Object Identifier (DOI). This number provides the electronic link to the published article and should be included in the posting of your personal version. We ask that you wait until you receive this e-mail and have the DOI to do any posting.
Central Storage: This license does not include permission for a scanned version of the material to be stored in a central repository such as that provided by Heron/XanEdu.

18. **Author website** for books with the following additional clauses:
Authors are permitted to place a brief summary of their work online only.
A hyper-text must be included to the Elsevier homepage at http://www.elsevier.com

All content posted to the web site must maintain the copyright information line on the bottom of each image
You not allowed to download and post the published electronic version of your chapter, nor

may you scan the printed edition to create an electronic version.
Central Storage: This license does not include permission for a scanned version of the material to be stored in a central repository such as that provided by Heron/XanEdu.

19. **Website** (regular and for author): A hyper-text must be included to the Homepage of the journal from which you are licensing at http://www.sciencedirect.com/science/journal/xxxxx. or for books to the Elsevier homepage at http://www.elsevier.com

20. **Thesis/Dissertation**: If your license is for use in a thesis/dissertation your thesis may be submitted to your institution in either print or electronic form. Should your thesis be published commercially, please reapply for permission. These requirements include permission for the Library and Archives of Canada to supply single copies, on demand, of the complete thesis and include permission for UMI to supply single copies, on demand, of the complete thesis. Should your thesis be published commercially, please reapply for permission.

21. **Other Conditions**:

v1.6

93

To : Japan Institute of Metals

Request for Permission to Reproduce Copyrighted Material

Dear

    I am preparing an article entitled: Thermomechanical response of laser processed nickel-titanium shape memory alloy

to appear in : Thesis work

which is published by : University of Waterloo .

Expected publication date : April 2012

Language : English

    I wish to have your permission to include in my article the following material(s):

Title of Publication : Materials Transactions

Author(s) : M. I. Khan*, S. K. Panda and Y. Zhou

Title of Selection : Effects of Welding Parameters on the Mechanical Performance of Laser Welded Nitinol

Year : 2008   Vol : 49   No.: 11   Page : 2702 to 2708

Figure(s)/Table(s): Figure 7

    If permission is granted for the use of this material, the author(s) and your publication will be credited as the source. If you would like the credit line to take any special form, please let me know what this should be.

    I should be greatly appreciate if you would indicate your agreement by signing and returning this form. Thank you for your cooperation.

Sincerely yours,

Name : Matthew Daly

Affiliation : Graduate Student, Dept. of Mech. Eng., University of Waterloo

Address : 200 University Ave. West, Waterloo, Ontario, Canada, N2L 3G1

E-mail : m3daly@uwaterloo.ca

TEL : 1-519-888-4567 ext. 33326   FAX :

****

I/We hereby grant permission for the use of the material requested above.

Date   Feb. 29, 2012

Signed   Y. Kajiwara

Copyright Holder : THE JAPAN INSTITUTE OF METALS
8-14-32, ICHIBANCHO, AOBA-KU SENDAI 980-8544, JAPAN

ELSEVIER LICENSE
TERMS AND CONDITIONS

Feb 27, 2012

This is a License Agreement between Matthew A Daly ("You") and Elsevier ("Elsevier") provided by Copyright Clearance Center ("CCC"). The license consists of your order details, the terms and conditions provided by Elsevier, and the payment terms and conditions.

All payments must be made in full to CCC. For payment instructions, please see information listed at the bottom of this form.

Supplier	Elsevier Limited The Boulevard,Langford Lane Kidlington,Oxford,OX5 1GB,UK
Registered Company Number	1982084
Customer name	Matthew A Daly
Customer address	Dept of Mechanical and Mechatronics Eng.
	Waterloo, ON N2L3G1
License number	2857260051598
License date	Feb 27, 2012
Licensed content publisher	Elsevier
Licensed content publication	Materials Science and Engineering: A
Licensed content title	Effects of local phase conversion on the tensile loading of pulsed Nd:YAG laser processed Nitinol
Licensed content author	M.I. Khan,Y. Zhou
Licensed content date	15 September 2010
Licensed content volume number	527
Licensed content issue number	23
Number of pages	4
Start Page	6235
End Page	6238
Type of Use	reuse in a thesis/dissertation
Intended publisher of new work	other
Portion	figures/tables/illustrations
Number of figures/tables/illustrations	3
Format	electronic
Are you the author of this Elsevier article?	No

Will you be translating?	No
Order reference number	
Title of your thesis/dissertation	Thermomechanical response of laser processed nickel-titanium shape memory alloy
Expected completion date	Apr 2012
Estimated size (number of pages)	100
Elsevier VAT number	GB 494 6272 12
Permissions price	0.00 USD
VAT/Local Sales Tax	0.0 USD / 0.0 GBP
Total	0.00 USD

Terms and Conditions

INTRODUCTION

1. The publisher for this copyrighted material is Elsevier. By clicking "accept" in connection with completing this licensing transaction, you agree that the following terms and conditions apply to this transaction (along with the Billing and Payment terms and conditions established by Copyright Clearance Center, Inc. ("CCC"), at the time that you opened your Rightslink account and that are available at any time at http://myaccount.copyright.com).

GENERAL TERMS

2. Elsevier hereby grants you permission to reproduce the aforementioned material subject to the terms and conditions indicated.

3. Acknowledgement: If any part of the material to be used (for example, figures) has appeared in our publication with credit or acknowledgement to another source, permission must also be sought from that source. If such permission is not obtained then that material may not be included in your publication/copies. Suitable acknowledgement to the source must be made, either as a footnote or in a reference list at the end of your publication, as follows:

"Reprinted from Publication title, Vol /edition number, Author(s), Title of article / title of chapter, Pages No., Copyright (Year), with permission from Elsevier [OR APPLICABLE SOCIETY COPYRIGHT OWNER]." Also Lancet special credit - "Reprinted from The Lancet, Vol. number, Author(s), Title of article, Pages No., Copyright (Year), with permission from Elsevier."

4. Reproduction of this material is confined to the purpose and/or media for which permission is hereby given.

5. Altering/Modifying Material: Not Permitted. However figures and illustrations may be altered/adapted minimally to serve your work. Any other abbreviations, additions, deletions and/or any other alterations shall be made only with prior written authorization of Elsevier Ltd. (Please contact Elsevier at permissions@elsevier.com)

6. If the permission fee for the requested use of our material is waived in this instance, please be advised that your future requests for Elsevier materials may attract a fee.

7. Reservation of Rights: Publisher reserves all rights not specifically granted in the combination of (i) the license details provided by you and accepted in the course of this licensing transaction, (ii) these terms and conditions and (iii) CCC's Billing and Payment terms and conditions.

8. License Contingent Upon Payment: While you may exercise the rights licensed immediately upon issuance of the license at the end of the licensing process for the transaction, provided that you have disclosed complete and accurate details of your proposed use, no license is finally effective unless and until full payment is received from you (either by publisher or by CCC) as provided in CCC's Billing and Payment terms and conditions. If full payment is not received on a timely basis, then any license preliminarily granted shall be deemed automatically revoked and shall be void as if never granted. Further, in the event that you breach any of these terms and conditions or any of CCC's Billing and Payment terms and conditions, the license is automatically revoked and shall be void as if never granted. Use of materials as described in a revoked license, as well as any use of the materials beyond the scope of an unrevoked license, may constitute copyright infringement and publisher reserves the right to take any and all action to protect its copyright in the materials.

9. Warranties: Publisher makes no representations or warranties with respect to the licensed material.

10. Indemnity: You hereby indemnify and agree to hold harmless publisher and CCC, and their respective officers, directors, employees and agents, from and against any and all claims arising out of your use of the licensed material other than as specifically authorized pursuant to this license.

11. No Transfer of License: This license is personal to you and may not be sublicensed, assigned, or transferred by you to any other person without publisher's written permission.

12. No Amendment Except in Writing: This license may not be amended except in a writing signed by both parties (or, in the case of publisher, by CCC on publisher's behalf).

13. Objection to Contrary Terms: Publisher hereby objects to any terms contained in any purchase order, acknowledgment, check endorsement or other writing prepared by you, which terms are inconsistent with these terms and conditions or CCC's Billing and Payment terms and conditions. These terms and conditions, together with CCC's Billing and Payment terms and conditions (which are incorporated herein), comprise the entire agreement between you and publisher (and CCC) concerning this licensing transaction. In the event of any conflict between your obligations established by these terms and conditions and those established by CCC's Billing and Payment terms and conditions, these terms and conditions shall control.

14. Revocation: Elsevier or Copyright Clearance Center may deny the permissions described in this License at their sole discretion, for any reason or no reason, with a full refund payable to you. Notice of such denial will be made using the contact information provided by you. Failure to receive such notice will not alter or invalidate the denial. In no event will Elsevier or Copyright Clearance Center be responsible or liable for any costs, expenses or damage incurred by you as a result of a denial of your permission request, other than a refund of the amount(s) paid by you to Elsevier and/or Copyright Clearance Center for denied permissions.

LIMITED LICENSE

The following terms and conditions apply only to specific license types:

15. **Translation**: This permission is granted for non-exclusive world **English** rights only unless your license was granted for translation rights. If you licensed translation rights you may only translate this content into the languages you requested. A professional translator must perform all translations and reproduce the content word for word preserving the integrity of the article. If this license is to re-use 1 or 2 figures then permission is granted for non-exclusive world rights in all languages.

16. **Website**: The following terms and conditions apply to electronic reserve and author websites:
Electronic reserve: If licensed material is to be posted to website, the web site is to be password-protected and made available only to bona fide students registered on a relevant course if:
This license was made in connection with a course,
This permission is granted for 1 year only. You may obtain a license for future website posting,
All content posted to the web site must maintain the copyright information line on the bottom of each image,
A hyper-text must be included to the Homepage of the journal from which you are licensing at http://www.sciencedirect.com/science/journal/xxxxx or the Elsevier homepage for books at http://www.elsevier.com , and
Central Storage: This license does not include permission for a scanned version of the material to be stored in a central repository such as that provided by Heron/XanEdu.

17. **Author website** for journals with the following additional clauses:

All content posted to the web site must maintain the copyright information line on the bottom of each image, and
he permission granted is limited to the personal version of your paper. You are not allowed to download and post the published electronic version of your article (whether PDF or HTML, proof or final version), nor may you scan the printed edition to create an electronic version,
A hyper-text must be included to the Homepage of the journal from which you are licensing at http://www.sciencedirect.com/science/journal/xxxxx , As part of our normal production process, you will receive an e-mail notice when your article appears on Elsevier's online service ScienceDirect (www.sciencedirect.com). That e-mail will include the article's Digital Object Identifier (DOI). This number provides the electronic link to the published article and should be included in the posting of your personal version. We ask that you wait until you receive this e-mail and have the DOI to do any posting.
Central Storage: This license does not include permission for a scanned version of the material to be stored in a central repository such as that provided by Heron/XanEdu.

18. **Author website** for books with the following additional clauses:
Authors are permitted to place a brief summary of their work online only.
A hyper-text must be included to the Elsevier homepage at http://www.elsevier.com

All content posted to the web site must maintain the copyright information line on the bottom of each image
    You are not allowed to download and post the published electronic version of your chapter, nor

may you scan the printed edition to create an electronic version.

Central Storage: This license does not include permission for a scanned version of the material to be stored in a central repository such as that provided by Heron/XanEdu.

19. **Website** (regular and for author): A hyper-text must be included to the Homepage of the journal from which you are licensing at http://www.sciencedirect.com/science/journal/xxxxx. or for books to the Elsevier homepage at http://www.elsevier.com

20. **Thesis/Dissertation**: If your license is for use in a thesis/dissertation your thesis may be submitted to your institution in either print or electronic form. Should your thesis be published commercially, please reapply for permission. These requirements include permission for the Library and Archives of Canada to supply single copies, on demand, of the complete thesis and include permission for UMI to supply single copies, on demand, of the complete thesis. Should your thesis be published commercially, please reapply for permission.

21. **Other Conditions**:

v1.6

Dear Sarah Ryder,

Thank you for your prompt reply. I would like to reprint Figures 1-6 and table 1 in my thesis dissertation. Please let me know if there are any further questions and thank you again for your kind consideration.

Regards,

Matt

On 28/02/2012 8:08 AM, Permissions wrote:

> Dear Matthew Daly
>
> Thank you for your permission request to the IOP. We however require more information of the content you wish to reproduce - Will you be using figures/tables and if so which ones?
>
> Please can you reply to the following email address with further details, so that your request can be processed.
>
> Best Wishes
>
> Sarah Ryder
>
> Publishing Administrator
> Email: permissions@iop.org
>
>
> From: Matthew Daly <m3daly@uwaterloo.ca>
> To: permissions@iop.org,
> Date: 27/02/2012 22:27
> Subject: Request for permission to reprint article
>
>
> To whom it may concern:
>
> I am seeking permission to reprint elements of my paper "Enhanced thermomechanical functionality of a laser processed hybrid NiTi-NiTiCu shape memory alloy" (SMS/414239/PAP) which is currently under consideration for publication in the Smart materials and Structures Journal.
>
> The purpose of this reprint will be for my thesis dissertation. The
>
> material will not be reprinted for commercial purpose. Please advise in
> writing as soon as possible.

Thank you for your kind consideration.

Regards,

Matthew Daly

--
Matthew Daly
MASc Candidate
Center for Advanced Materials Joining
Mechanical and Mechatronics Engineering
University of Waterloo
200 University Avenue West
Waterloo, ON, N2L 3G1, Canada
Phone: 1 519 888 4567 ext. 33326

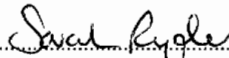PERMISSION TO REPRODUCE AS REQUESTED IS GIVEN PROVIDED THAT:

(a) the consent of the author(s) is obtained
(b) the source of the material including author, title of article, title of journal, volume number, issue number (if relevant), page range (or first page if this is the only information available), date and publisher is acknowledged.
(c) for material being published electronically, a link back to the original article should be provided (via DOI).

IOP Publishing Ltd
Temple Circus
Temple Way
BRISTOL   29/02/2012   ⟋Sarah Ryde⟍
BS1 6BE   Date   Rights & Permissions

Subject: Request for permission to reprint
From: "Bernard, Valerie" <valerie.bernard@sagepub.co.uk>
Date: 07/03/2012 7:47 AM
To: "m3daly@uwaterloo.ca" <m3daly@uwaterloo.ca>

Dear Matthew

Thank you for your request.

You are very welcome to reuse figures 1-6 and table 1 from your paper on "Fabrication of a Novel Laser Processed NiTi Shape Memory Microgripper with Enhanced Thermomechanical Functionality" in your thesis dissertation.

Please consider this email as written permission and make sure to include full academic referencing to the original paper.

I hope this helps,

Kind regards,

Jo

Jo Davies
Permissions Temp
SAGE Publications Ltd
1 Oliver's Yard, 55 City Road
London, EC1Y 1SP
UK
Tel: +44 (0) 207 336 9146
Fax: +44 (0) 207 324 8600
www.sagepub.co.uk
SAGE Publications Ltd, Registered in England No.1017514
Los Angeles | London | New Delhi
Singapore | Washington DC

-----Original Message-----
From: Matthew Daly [mailto:m3daly@uwaterloo.ca]
Sent: 28 February 2012 16:18
To: Bernard, Valerie
Subject: Request for permission to reprint

To whom it may concern:

I am seeking permission to reprint elements of my paper "Fabrication of a Novel Laser Processed NiTi Shape Memory Microgripper with Enhanced Thermomechanical Functionality" (JIM-11-347.R1) which is currently under consideration for publication in the Journal of Intelligent Material Systems and Structures.

The reprinted material consists of figures 1-6 and table 1. The purpose of this reprint will be for my thesis dissertation. The material will not be reprinted for commercial purpose. Please advise in writing as soon as possible.

Thank you for your kind consideration.

Regards,

Matthew Daly

--
Matthew Daly
MASc Candidate
Center for Advanced Materials Joining
Mechanical and Mechatronics Engineering

Request for permission to reprint

```
University of Waterloo
200 University Avenue West
Waterloo, ON, N2L 3G1, Canada
Phone: 1 519 888 4567 ext. 33326
```